GEOSCIENCE AUSTRALIA

Record 2003/12

# Geological framework of the central Great Australian Bight and adjacent areas

*Sayers, J., Bernardel, G. & Parums, R.*

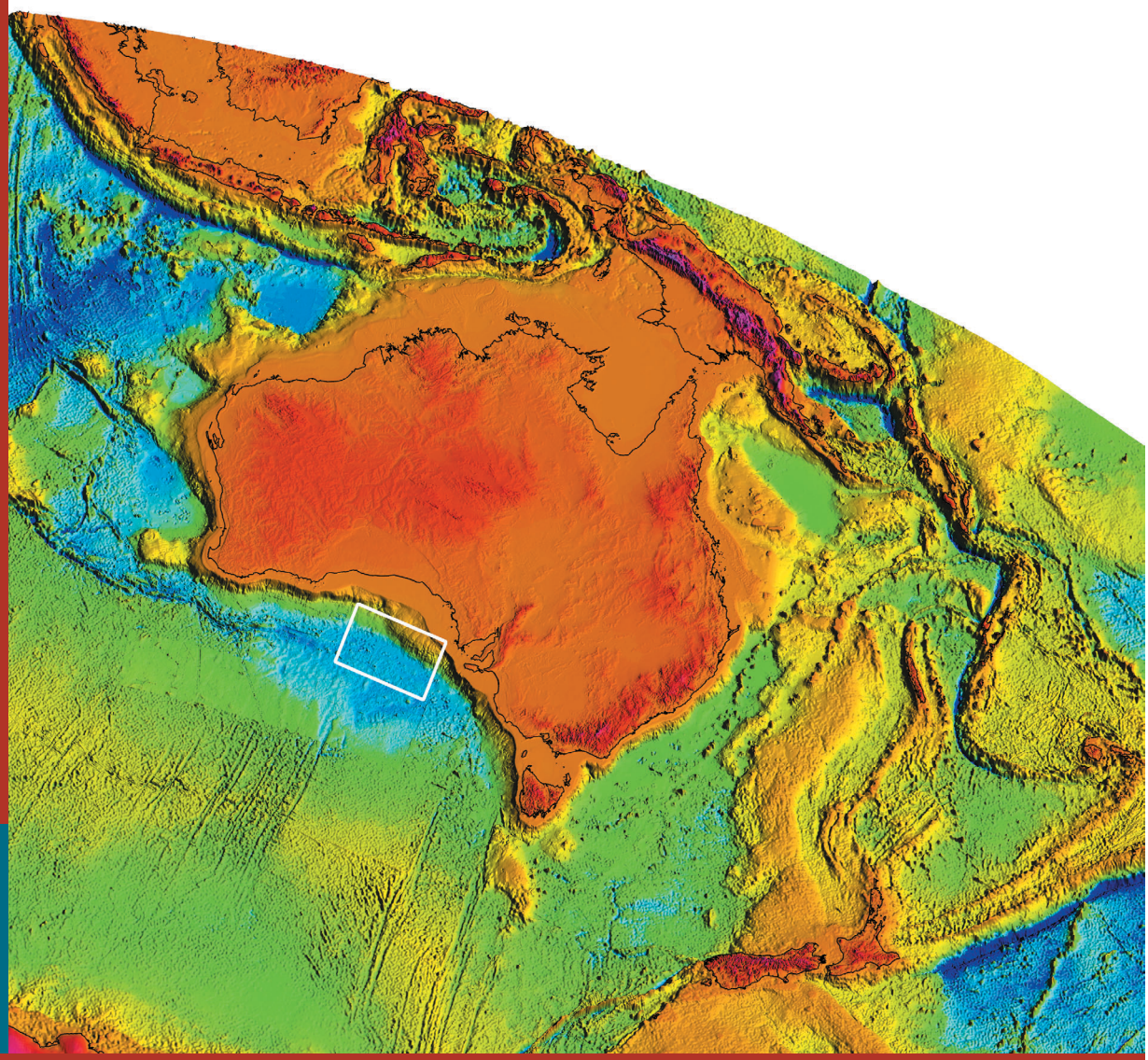

GEOSCIENCE AUSTRALIA

SPATIAL INFORMATION FOR THE NATION

GEOSCIENCE AUSTRALIA

DEPARTMENT OF INDUSTRY, TOURISM & RESOURCES

Geoscience Australia Record 2003/12

# GEOLOGICAL FRAMEWORK OF THE CENTRAL GREAT AUSTRALIAN BIGHT AND ADJACENT AREAS

J. SAYERS, G. BERNARDEL & R. PARUMS

**Petroleum & Marine Division, Geoscience Australia,**

**GPO Box 378, Canberra, ACT 2601**

**CANBERRA 2003**

**Department of Industry, Tourism & Resources**

Minister for Industry, Tourism & Resources: Senator The Hon. Ian McFarlane, MP
Parliamentary Secretary: The Hon. Warren Entsch, MP

Geoscience Australia

Chief Executive Officer: Neil Williams



**ISSN: 1039-0073**
**ISBN: 0 642 46769 2**

Bibliographic reference: Sayers, J., Bernardel, G. & Parums, R., 2003. Geological framework of the central Great Australian Bight and adjacent areas. *Geoscience Australia, Record 2003/12*

# CONTENTS

The data, and the interpretations based on that data, contained in this report are not necessarily indicative or representative of the final information that might be used by Australia to support the location of the outer limit of the continental shelf beyond 200 nautical miles.

# EXECUTIVE SUMMARY

This report summarises the geological framework of the central Great Australian Bight (GAB), including the geology of the lower continental slope, continent–ocean transition zone (COT) and adjacent abyssal plain. The study was carried out within Geoscience Australia's Law of the Sea Project and aims to provide supporting background information to assist Australia's definition in this area of the outer limit of Australia's continental shelf under the terms of the 1982 United Nations Convention on the Law of the Sea (UNCLOS).

Deep seismic reflection data, together with seismic refraction and gravity and magnetic data were specifically acquired by Geoscience Australia in 1997 over the central GAB targeting the lower continental slope and COT zones. These data also included two transects of the complete margin, from the shelf to the abyssal plain.

The study reported here provides a number of key scientific findings that are relevant to the geological evolution for the southern margin of Australia. Specifically:

- The deep-water area of the central GAB can be divided into a number of tectono-magmatic provinces including, from distal to proximal: (1) the ocean basin; (2) a COT interpreted as largely continental in nature, but heavily intruded and probably altered; (3) an extensive basement ridge mostly igneous in nature; and (4) extended continental crust and overlying syn-rift and post-rift sediments.
- Our interpretation suggests that the COT is largely continental in origin so that we now interpret the continent–ocean boundary (COB) as being 80 km oceanward of its previously determined location.
- The thickness of the crust and sediments determined from seismic refraction data is about 13–17 km under the lower continental slope, 12–16 km in the COT, and >6km under the abyssal plain.
- The thickness of post-breakup sediments (*c*. 83 Ma, early Campanian to Recent) is of the order of 2 km or less in the COT, reducing to about a 1 km or less over oceanic crust. The interpretation of sequences below the breakup unconformity indicates the presence of an older sedimentary section, and these seismic sequences may represent pre-breakup sediments that are possibly as old as Palaeozoic.
- The modelling of magnetic profiles and associated chrons, together with the new interpretation for the COB, now suggest that the breakup age on the southern continental margin of Australia is early Campanian (*c*. 83 Ma), rather than Cenomanian (*c*. 95 Ma), as previously interpreted.
- We have interpreted the upper crust and upper mantle as brittle, and the lower crust and lower lithosphere mantle as ductile, similar to the model of Brun & Beslier (1996). We do not see evidence for lithosphere-scale detachments, but instead propose extension using a pure shear model, and interpret the extensive basement ridge as resulting from upwelled mantle.

# 1. INTRODUCTION

The 1982 United Nations Convention on the Law of the Sea (UNCLOS) defines a nation's seabed and subsoil jurisdiction as extending throughout its Continental Shelf (Appendix 1). Where the continental margin of a nation extends beyond 200 nautical miles, the outer limit of this 'Legal' Continental Shelf[1] (LCS) is defined by a series of rules contained within Article 76 of UNCLOS. The rules require definition of the foot of the continental slope, knowledge of sediment thickness and good bathymetric information defining the 2500 m bathymetric contour. In areas of complex or unusual bathymetry, geological considerations, such as structure and crustal characteristics, may be used to support the definition of the outer limit.

A preliminary analysis of the extent of Australia's legal Continental Shelf under UNCLOS (Symonds & Willcox, 1989) indicated that it could be at least 12 million km$^2$ in area[2] — nearly one and a half times the area of the continental landmass, and one of the world's largest. Nine areas of Continental Shelf extend beyond the 200 nautical mile Australian Exclusive Economic Zone (AEEZ). Geoscience Australia has the responsibility for ensuring that Australia has the necessary technical information to fully define its Continental Shelf under UNCLOS. In planning for surveys to acquire this information, Geoscience Australia decided to adopt a 'safe minimum' approach to Continental Shelf definition, in which bathymetric and seismic data are generally acquired, or compiled, on profiles spaced about 30 nautical miles apart over areas of margin extending beyond the AEEZ. Internal Geoscience Australia assessments indicated that further data collection and analysis were needed in about six of the nine areas extending beyond the AEEZ. One of the areas requiring such analysis was the segment of continental margin in the central Great Australian Bight (GAB) off southern Australia (Figure 1), the subject of this report.

The GAB region forms part of Australia's southern continental margin. It can be taken broadly to extend from the SW tip of Australia to Kangaroo Island (located just east of the project area (Figure 1a), an area of approximately 1 million km$^2$. It contains a number of primarily Mesozoic to Cainozoic sedimentary basins, ranging in area from 5000 to 180 000 km$^2$, with depocentres containing 5 to 12 km of sedimentary rocks and lying in water depths of 60–5500 m.

The maps in this report cover that part of the central GAB between longitudes 125.5°E and 134.5°E, and latitudes 31°S and 40°S (i.e. project area in Figure 2) although the study focussed on an area significantly smaller in size (i.e. 127–134 °E, 34.5–38 °S, study area). Morphologically, the project area is defined by the broad shallow Eucla Shelf in the north, the mid-slope Ceduna

[1] The 'legal' Continental Shelf (LCS), as defined by a complex series of rules or formulae, is quite distinct from the geomorphic continental shelf as understood by a marine scientist. The LCS most likely includes the geomorphic continental shelf, the continental slope, marginal plateaus and, occasionally, the continental rise and inboard edge of deep ocean basins.
[2] This area is 14.8 million km$^2$ if the EEZ around the Australian Antarctic Territory is included.

and Eyre Terraces, a continental slope that is broad in the west and narrow in the east, and the abyssal plain to the south. The project area includes four main depocentres (Figure 3):

- the Eyre Sub-basin, part of the Bight Basin and underlying the Eyre Terrace. The sub-basin is a small E–W elongate extensional basin;
- the Ceduna Sub-basin, part of the Bight Basin and underlying the Ceduna Terrace. The sub-basin is a broad thick, lobe-like sedimentary basin extending from the edge of the continental shelf to beneath the inner edge of the abyssal plain;
- the Recherche Sub-basin, part of the Bight Basin. The sub-basin is a thick, flat-lying sedimentary succession, deposited in a broad depression on the lower continental slope, and extending southwards from the base of the Eyre Terrace; and
- the Australian–Antarctic Basin, which forms a post-breakup veneer of sediments deposited on oceanic crust, and underlying the abyssal plain.

In essence, this report interprets the geological framework and data relevant to the extended continental shelf in the central GAB immediately beyond the Ceduna and Eyre Terraces and associated lower slope province. Analogies are also made with the more-extensively studied Grand Banks-Iberian/Galician conjugate margins.

Note: the authors of this report had the following roles. Jacques Sayers was group leader for the GAB study, providing technical leadership and determining its overall content. He was responsible for the final report, and interpreted the seismic reflection data including all pre-breakup sequences and horizons. He developed a method for processing, interpreting and modelling the seismic refraction data, and modelled most of that data. George Bernardel interpreted the seismic reflection data including the post-breakup seismic sequences and horizons, reviewed the literature, produced some of the images, and wrote parts of Chapters 3, 5 and 7. Robert Parums assisted Jacques Sayers in modelling the refraction data and wrote Appendix 3A.

# 2. DATASETS

## 2.1 Introduction

The interpretation contained in this report is based on a range of geophysical and geological datasets collected over a number of years by both Geoscience Australia and other organisations. These datasets include reflection and refraction seismic, bathymetry, potential field (gravity and magnetic) and heatflow data, as well as geological samples acquired from scientific and petroleum exploration drilling, dredging and shallow sediment coring. This chapter briefly summarises the most-important of the datasets.

## 2.2 Bathymetry Data

Whilst bathymetric data have been routinely acquired on all research cruises and surveys in the region, the density of coverage is highly variable, ranging from high on parts of the shelf to sparse over parts of the abyssal plain. The bathymetric data presented in this report have been integrated from all available sources, including conventional 2-D bathymetric profiling, 3-D multi-beam swath-mapping and, where ship data are very sparse, satellite-predicted bathymetry of Sandwell & Smith (1997). A regional bathymetry image (from Petkovic et al., 1999; Petkovic & Buchanan, 2002) is shown in Figure 2, and GEBCO bathymetry contours (Jones et al., 1997) are shown as a backdrop in Plates 1 and 2, and Figures 2 and 4.

## 2.3 Seismic Reflection Data

Figure 4 shows the location of surveys in the central GAB while Plate 1 shows shot point locations for individual lines. The interpretation contained here is based mainly on Geoscience Australia's Survey 199, although conventional seismic data acquired on Surveys 65 and 169, together with the industry surveys Shell Roving Reconnaissance N and JA90 were examined to assist the interpretation and synthesis (Plates 3–4).

The Shell Survey 'Roving Reconnaissance N' is often referred to in literature as the Shell Petrel Survey (after the vessel "*MV Petrel*" contracted by Shell for the work) and is referred to as such in this report. 'AGSO' refers to the Australian Geological Survey Organisation and 'BMR' refers to the Bureau of Mineral Resources, both previous names for Geoscience Australia. Details of the seismic surveys and associated acquisition parameters are given in Appendix 2, and summarised below.

- **Survey 199** (Geoscience Australia, 1997): 3448 km of 40-fold data were collected in the central GAB, comprising ten lines recorded specifically for the Law of the Sea Project and including two major transects of over 600 km length from the shelf to the abyssal plain (Ramsay – pers. comm. 1999: Figure 4). The seismic data show excellent penetration and resolution, with clear imaging of the reflection Moho in places.

- **Survey 65** (Geoscience Australia, 1986): 3574 km of data were acquired

over the Eyre and Ceduna Terraces, and the Polda Trough (Willcox et al. 1988). Of these data, some 3070 km of 24-fold were collected with a 2400 m streamer over the Eyre and western Ceduna Terraces and adjacent slope, while the remaining 504 km of 6-fold data were collected with a 600 m streamer over the Polda Trough. Five lines from the survey were used to aid this study's seismic horizon identification and correlation (i.e. lines 65/1, 65/3, 65/4, 65/14 and 65/15).

- **Survey 169** (Geoscience Australia, 1996): 1803 km of data were collected as a multi-site survey for ODP Leg 182 (Feary, 1993), mainly on the continental shelf and slope. The data were collected on a number of tight grids at proposed well locations with tie-lines shot between these grids to aid in seismic horizon correlation. Only line 169/8 intersecting ODP Site 1128 was interpreted as part of this study.

- **Survey Shell Petrel (or Shell Roving Reconnaissance Survey N)** (Shell International, 1972): several lines from the Shell Petrel Survey were used. These lines, N404–N407, traverse a range of water depths, mainly on the continental slope.

- **Survey JA90** (Japanese National Oil Corporation, 1990): A N–S/E–W orientated grid was recorded by JNOC in the NW central GAB, mostly on the shelf and Eyre Terrace. Several lines were examined as part of the current study.

- **Survey DWGAB** (Seismic Australia, 1998) covers the Ceduna Sub-basin with a grid of NW–SE/NE–SW orientated lines. These data were acquired in December 1998, processed by August 1999 but, because of their commercial nature, were not available to this study. An interpretation partly based on these data is contained in Totterdell et al. (2000).

- **Survey HRGAB** (Seismic Australia, 1998) include lines shot in an E–W/N–S grid between the Potoroo-1 well and the Eyre Sub-basin, as well as several lines on the outer shelf tieing wells Apollo-1 and Platypus-1. An interpretation partly based on these data is contained in Totterdell et al. (2000).

## 2.4 Velocity Data

Refraction-based velocity data were recorded using sonobuoys in 1972 and 1976 by the Lamont-Doherty Geological Observatory on *Eltanin* Cruise 55, and *Vema* Cruise 33, and in 1997 during Survey 199 (Ramsay – pers. comm., 1999). Key publications addressing the interpretation of the refraction data from *Eltanin* Cruise 55 and *Vema* Cruise 33 are those of König & Talwani (1977) and Talwani et al. (1978), respectively.

A total of 15, 37 and 17 sonobuoy stations were occupied on the Southern Margin during *Eltanin* Cruise 55, *Vema* Cruise 33 and Survey 199, respectively. Forty-four of these stations were located within the project area (Plates 1–2) and 35 were used in this study to aid in the interpretation of the structure of the deep crust. Data from 15 of the Survey 199 sonobuoy stations

were modelled, specifically to obtain sediment thicknesses and to estimate the likely crustal geology based on the velocities (Appendix 3A & 3B). Data from sonobuoys 17 and 18, located on the continental shelf, were modelled separately by Brown (1999). Thicknesses and velocities were also calculated by König & Talwani (1977) and Talwani et al. (1978) from the *Eltanin* and *Vema* cruises, and are listed in Appendix 3C. The geological interpretation resulting from the use of the refraction data is covered in Chapter 6.

## 2.5 Potential Field Data

Gravity and magnetic data are routinely acquired on most marine geophysical surveys. In the past, analysis of shipboard magnetic profiles has provided the basis for plate kinematic interpretations between Australia and Antarctica; these literature reviews are summarised in Chapter 4. The magnetic data also provide information on seafloor ages and spreading rates. Interpretations of the magnetic lineations, based on the work of Cande & Mutter (1982) and Tikku & Cande (1999) are presented in Figure 5.

Since the 1980s, shipboard gravity data have been supplemented by high-resolution satellite-derived free-air gravity datasets (Sandwell & Smith, 1997). This has resulted in a re-direction of gravity studies from 2-D profile-based modelling to regional analysis of gridded datasets which are particularly valuable in studies of plate kinematics. The gravity images in Figures 3 and 5 are from the work of Petkovic et al. (1999) who used the concepts of Sandwell & Smith (1995) to create a regional grid of Free-Air Gravity.

## 2.6 Geological Samples

Geological samples come from three main sources: petroleum exploration wells, scientific drilling, and direct seabed sampling through dredging and coring. Locations of wells and sample stations are shown in Figure 6 and Plates 1–2; sample descriptions are listed in Appendix 4.

The stratigraphy of the central GAB (Figure 7) is mainly interpreted from the few petroleum exploration wells that have been drilled in the Eyre and Ceduna Sub-basins. The wells of most relevance to this study are Jerboa-1 and Potoroo-1. Digital log data for these wells are displayed in Figures 8 and 10. Seismic sections showing the supersequence boundaries at these wells are displayed in Figures 9 and 11.

Scientific drilling carried out during Ocean Drilling Program (ODP) Leg 182 in 1998 (Feary et al., 1999) has provided information critical to sequence dating of the Cainozoic stratigraphy on the continental slope. Lithological and other data for ODP Site 1128 are displayed in Plate 5 and results published in the preliminary report of the drilling leg (Feary et al., 1999).

Geoscience Australia Survey 66 dredged rocks from the GAB region at several sites on the lower continental slope south of the Eyre and Ceduna Terraces (Willcox et al. 1988). A suite of gravity cores was collected at sites along a SW-trending transect over the Ceduna Terrace on the same survey (Figure 6; Plate 2). This survey was augmented by a second, more regional, sampling survey by Geoscience Australia (Survey 102; see Feary, 1993),

which included dredging on the abyssal plain and the slope below the Ceduna Terrace.

## 2.7 Heatflow Data

Geoscience Australia Research Cruises 10 & 11 (Willcox et al. 1988) collected heatflow data (Appendix 5) from the Eyre and Ceduna Terraces (Plate 2). Heatflow data were not, however, used in this study.

# 3. PREVIOUS WORK*

## 3.1 Introduction

Exploration on the southern margin of Australia by both scientific and industry agencies dates back to the 1960s. Peaks of industry activity including seismic acquisition and petroleum exploration drilling occurred in the early 1970s, early 1980s and currently. The region has also been of considerable scientific interest, particularly in terms of the rifting, breakup and spreading history between Australia and Antarctica.

This section summarises the historical aspects of petroleum exploration and continental margin research in the region. Detailed discussion of the continental margin setting and the hydrocarbon potential will be presented in later sections of this report.

## 3.2 Petroleum Exploration

Petroleum exploration in the GAB began in 1954 when Oil Exploration License (OEL) 7 was granted to R. F. Bristowe and Santos Ltd for the South Australian portion of the GAB. The first exploration drilling took place in 1972, and drilling occurred sporadically until 1986, when, as a result of decreasing world oil prices, exploration activity effectively ceased. BHP drilled three wells in the Duntroon Sub-basin in the early 1990s. Exploration was virtually dormant until 1999 when the Commonwealth Government released large areas for competitive exploration bidding (Department of Industry, Science and Resources, 1999). The exploration history of the GAB region is summarised below. The location of wells, basins and sub-basins can be found in Plates 1–2 and Figure 3.

- In 1961, a reconnaissance aeromagnetic survey was flown by Haematite Exploration Pty Ltd over the continental shelf south of Kangaroo Island.

- From 1961 to 1966, several Oil Exploration Leases (OEL's) were awarded over inboard areas of the GAB to Haematite Exploration, Beach Petroleum, Blacker/Brady & Turner, Outback Oil Company NL and Shell Development (Australia) Pty Ltd. The largest of these (OEL 38), which covered an area of approximately 114,000 square km of the Eyre, Ceduna and Duntroon Sub-basins, was awarded to Shell Development (Australia) Pty Ltd. In 1968/69, OEL 38 was re-gazetted as three separate Exploration Petroleum Permits (EPP 5, EPP 6 and EPP 7) with Shell as operator. During this period, Hematite Petroleum Pty Ltd and Outback Oil Company NL continued to operate permits EPP 1,2, 3 and 4 (formerly OEL 26 and 33) in the Bight Basin and Duntroon Sub-basin.

- In 1966, a regional aeromagnetic survey was flown over the Eucla and Denman Basins, Duntroon Sub-basin, and Polda Trough.

* Part of this chapter was contributed by Barry Willcox of Geoscience Australia

- In 1967, Tenneco conducted the first seismic survey on the Western Australian side of the GAB with the acquisition of some 2060 km of reflection data in the offshore Eucla Basin.

- From 1969 to 1976, Shell carried out ten reflection seismic surveys, totalling 23 172 km of data, over the Ceduna and Duntroon Sub-basins. Shell's exploration program during these years is summarised in Whyte (1978).

- In 1970 and 1971, Bridge Oil NL recorded 2133 km of reflection seismic data over the Polda Trough and northern Ceduna Sub-basin. Further to the west, Coastal Petroleum acquired 1641 km of reflection seismic data over the Eucla Basin.

- In 1972, drilling activity commenced with the Platypus-1 and Echidna-1 wells (Shell Development Company) in the Duntroon Sub-basin. To the north, 3194 km of reflection seismic data were acquired by Outback Oil Co. Ltd, over the Denman Basin. In the Western Australian side of the GAB, Continental Oil acquired 957 km of reflection seismic data over its permit WA-47P on the continental shelf. The data indicated a thin sedimentary section, and the permit was relinquished in 1973.

- In 1974, Esso acquired 2224 km of reflection seismic data in its permits WA-50P and WA-51P over the Bremer Sub-basin, west of the GAB. The data showed that the basin was highly-structured and has a thick sedimentary section. The permits were relinquished in 1977.

- In 1975 drilling activity peaked with Potoroo-1 (Shell) on the northern structural margin of the Ceduna Sub-basin, Apollo-1 (Outback Oil NL) in the Denman Basin, and Gemini-1 (Outback Oil NL) in the Polda Trough.

- In 1978, a detailed aeromagnetic survey was flown by Outback Oil NL to re-assess the basement structure around Gemini-1. The data indicated several kms of sedimentary section below the total depth of the well.

- From 1979 to 1983, Esso Australia held leases WA-135P and WA-126P over the Eyre Sub-basin. A total of 4073 km of reflection seismic data was acquired on both regional and semi-detailed grids.

- In 1981, in response to the re-evaluation of the basement structure beneath Gemini-1, an additional 3214 km of reflection seismic data were recorded by the operator (Outback Oil NL).

- In 1982, Mercury-1 and Columbia-1 were drilled in the Polda Trough (Australia Oxidental Petroleum) while Jerboa-1 (Esso Australia) tested a tilted basement block in the Eyre Sub-basin. Oil fluorescence inclusions were identified in Jerboa-1. All three wells were plugged and abandoned as dry.

- From 1981 to 1984, several small seismic surveys were acquired in the Duntroon Sub-basin by BP Petroleum Development Ltd, resulting in the drilling of Duntroon-1 in 1986.

- After an exploration hiatus in the late 1980s, BHP Petroleum instigated a resurgence of activity in 1993 with the drilling of Borda-1, Greenly-1 and Vivonne-1 in the Duntroon Sub-basin.

- In late 1998 – early 1999 Seismic Australia, in joint venture with Geoscience Australia, acquired approximately 8500 km of reflection seismic data in two surveys. Survey DWGAB recorded data down to 10 sec TWT and Survey HRGAB recorded data down to 4 sec TWT.

- In April 1999, eleven offshore areas in the GAB region were gazetted for exploration by the Australian Government (Department of Industry, Science and Resources, 1999): W99-35 to 37 in West Australian waters; and S99-1 to 8 in South Australian waters. These areas were focused on the Ceduna, Eyre and Duntroon Sub-basins.

- In April 2000, three exploration permits were awarded to a consortium comprising Woodside Energy Ltd, Anadarko Australia Company Pty Ltd and PanCanadian Petroleum Ltd (i.e. now EnCana). The 3-year work program includes the drilling of an exploration well.

Results from the petroleum exploration work are discussed in 'Chapter 7 – Resource Potential'.

## 3.3 Continental Margin Research

The present understanding of the regional geology of the GAB and the wider Southern Margin of Australia comes from a number of sources. These sources are outlined below; their findings are discussed in more detail in later sections of this report.

Several papers have discussed the plate kinematic and structural history of the GAB. Boeuf & Doust (1975) were amongst the first authors to identify the Southern Margin as an Atlantic-type continental margin, and, along with Deighton et al. (1976), place it in a tectono-stratigraphic setting. König & Talwani (1977), Talwani et al. (1978) and Williamson et al. (1989) proposed various breakup models to account for the anomalous 'Magnetic Quiet Zone' (MQZ), located landward of the last identifiable seafloor magnetic lineation. Hegarty et al. (1988) derived subsidence histories from well data to model rift phases for the Otway Basin to GAB region, and to support shearing along a lithospheric detachment system. Stagg et al. (1989) and Willcox (1990) examined filtered magnetic profiles and interpreted gravity maps, to interpret the geometry of pre-breakup lithospheric extension. Phases of oblique extension were proposed by Willcox & Stagg (1990) for the incipient Australia–Antarctic margin and by Middleton (1991) for the Bremer and Eyre Sub-basins. Stagg & Willcox (1992) interpreted the tectono-stratigraphic framework of the Eyre and Recherche Sub-basins to support an early Neocomian breakup. Seismic and potential field-based studies of the Ceduna

and Eyre Sub-basins, were undertaken by Fraser & Tilbury (1979) and Bein & Taylor, (1981), respectively. More recently, Totterdell et al. (2000) presented an up-dated chronostratigraphic framework for the Bight Basin, linking the sequence stratigraphy and subsidence history of the basin. This work incorporated the interpretation of a large amount of 1990s vintage seismic data.

Early attempts at morphological fits between the Australian and Antarctic margins were made by Sproll & Dietz (1969), Smith & Hallam (1970) and Veevers (1982). Veevers & Eittreim (1988) examined bathymetry, seismic and magnetic data on both margins, and proposed the onset of rifting in the Middle Jurassic and breakup in the middle Cretaceous. The story is complicated somewhat by several factors. Firstly, until recently there were relatively few data across the Australian-Antarctic Basin and, in particular, the Antarctic margin. Secondly, the nature of the crust underlying the MQZ is unknown. Thirdly, it is difficult to interpret in the highly tectonised Diamantina Zone, located at the southwestern tip of Western Australia.

A number of papers have discussed seafloor spreading reconstructions, and have attempted to match the pattern of magnetic lineations across parallel to sub-parallel profiles and across the proposed conjugate margin positions of Antarctica and Australia. The various interpretations of seafloor spreading history and magnetic anomalies include Weissel & Hayes (1972), Cande & Mutter (1982), Mutter et al. (1985), Veevers (1986), Veevers et al. (1990) and Tikku & Cande (1999). The spreading model of Tikku & Cande (1999) is used as the reference model in this report.

Several papers have discussed the general setting of rifted (passive) continental margins and their evolution, based largely on seismic reflection profiling, as well as both seabed and subsoil sampling data. Lister et al. (1986) and Lister et al. (1991) built on the ideas of Wernicke & Burchfiel (1982) and Wernicke (1985) and revised extensional models for upper-plate/lower-plate conjugate margin separation via a lithosphere-scale detachment. The highly-sampled and studied Galician/Iberian Margin (Portugal/Spain) is studied in Boillot et al. (1980) and Boillot et al. (1989). Their interpretations as well as those of Brun & Beslier (1996), Whitmarsh et al. (1996), and Whitmarsh et al. (1998), help resolve issues with upper mantle involvement and upwelling of the asthenosphere along an incipient breakup axis in continental crust. The idea of mantle involvement has also been considered by Froitzheim & Manatschal (1996) for the origin of nappe structures in the western European Alps. These results help in the understanding of rifted margin evolution processes.

Several reports have discussed the results of scientific drilling by the Ocean Drilling Program (ODP) and other seabed sampling surveys in the region. Nicholls et al. (1981) examined ultramafic dredge samples from the Diamantina Zone, south of the Naturaliste Plateau. Willcox et al. (1988) and Davies et al. (1989) discussed dredge, gravity core and heatflow results from BMR research cruises 10 and 11 in the GAB, while Feary (1993) presented results of similar sampling activities in Survey 102 over a larger sampling

region of the GAB. The principal results from ODP Leg 182, and ODP Site 1128, in particular, are useful (see Feary et al. 1999) for resolving the early Eocene to Recent chronostratigraphy.

# 4. REGIONAL SETTING

## 4.1 Physiography

The physiography of the central GAB region was described initially by Conolly & von der Borch (1967), Conolly et al. (1970) and Willcox (1978), with Fraser & Tilbury (1979) describing the Ceduna Terrace in greater detail. Most recently, Rollet et al. (2001) mapped the geomorphology and seabed character of the GAB using 3.5 KHz echo-sounding records and high-resolution profiles.

The continental shelf slopes gently out to the shelf break at approximately 200 m depth where the gradient increases significantly. The shelf is up to 200 km in width north of the Ceduna Sub-basin, and up to 100 km north of the Eyre Sub-basin, and trends E–W in a broad arcuate fashion (Figure 2).
The continental slope varies in width and gradient along the margin, and is marked by two major upper/mid-slope terraces (i.e. the Ceduna and Eyre Terraces) and numerous canyons. The upper/mid slope descends steeply south of the Eyre Terrace and Kangaroo Island, but is more gentle across the Ceduna Terrace (Figure 2).

The Eyre Terrace is an E–W-trending elongate upper slope terrace with a maximum width of about 70 km. It occurs in water depths of 200 to 2000 m. Below the terrace, the mid and lower slope is made up of two provinces – the Eyre Slope and the Recherche Lower Slope. The Eyre Slope is a conventional slope province with gradients up to 4 degrees that extend to a depth of 3500m. The Recherche Lower Slope is a very broad (up to 200km wide) province with gradients between 0.5 and 0.9 degree. True rise development in this area is negligible.

The Ceduna Terrace is a WNW–ESE trending lobate-like mid-slope terrace (Figure 2). It is up to 200 km wide and extends from water depths of 200 to 3000 m. The lower continental slope S and SE of the Ceduna Terrace is very narrow. Beyond the lower continental slope, the abyssal plain lies at water depths of 5500–6000 m.

## 4.2 Regional Evolution

### Breakup phase – Santonian to Early Campanian

Breakup of East Gonwana commenced with the separation of Greater India in the Valanginian, which was followed by the Australian–Antarctic breakup in the Santonian (Fullerton et al. 1989; Veevers et al. 1991; Müeller et al. 1998).

Magnetic lineations in the Southern Ocean were first identified and mapped by Weissel & Hayes (1972). They concluded that the oldest magnetic anomaly that could be identified was A22**,** and that breakup between Australia and Antarctica occurred at about 55 Ma in the early Eocene, with seafloor spreading approximately on a N–S azimuth.

In a major re-interpretation of the oldest part of the magnetic anomaly series, Cande & Mutter (1982) found that the magnetic anomalies originally identified as 19–22 could be better modelled as 20–34 using a very slow half-rate (~4.5 mm/yr). On this basis, Cande & Mutter (1982) estimated that breakup of Australia and Antarctica took place at some time in the interval 110–90 Ma. This revised interpretation was considered to account for the roughness of the Diamantina Zone in the western GAB, which was attributed to the slow spreading. It also solved some of the previous difficulties in identifying the older magnetic anomalies, and the period of rapid basin subsidence prior to 90 Ma on the Southern Margin (Falvey & Mutter, 1981).

Veevers (1986) and Veevers & Eittreim (1988) further refined the estimate of breakup age to 95+/–5 Ma (Cenomanian–Turonian). By extrapolating the 4.5 mm/yr spreading rate, they proposed that Cande and Mutter's magnetic anomaly 34 was a COB edge-effect anomaly. Veevers et al. (1991) interpreted a major reorganisation of plates at the end of the Santonian (i.e. equivalent to magnetic anomaly 34y time, 85 Ma). These authors showed breakup occurring along the eastern margin of Australia in the Tasman Sea and Pacific Ocean, and along the Southern Margin from west of the Naturaliste Plateau to south of the South Tasman Rise. This breakup phase was also correlated with a change in plate motion in the Indian Ocean from E–W to more N–S, with Greater India moving northwards.

Tikku & Cande (1999) re-examined existing and additional magnetic data between Australia and Antarctica. They confirmed the presence of magnetic anomaly 34y and modelled breakup at 95Ma. However, Tikku & Cande (1999) also highlighted potential problems with the revised anomaly identifications, which resulted in significant continental overlap in reconstructions in the east.

Sayers et al. (2001) interpreted magnetic anomaly 34y as overlying the seismically defined COT that has a continental origin. This suggests that the origin of magnetic anomaly 34y is not related to seafloor spreading. Downlapping sequences independently interpreted as post-early Campanian overlie the COT where magnetic anomaly 34y (i.e. 83–115 Ma) is interpreted. Downlapping seismic sequences post-date chron 34 thus providing independent support for the interpretation of magnetic anomaly 34y. In this study, the workers interpreted the oldest identifiable seafloor spreading anomaly to be 33o overlying unambiguous seismically-interpreted oceanic crust. If this is correct, then the breakup along the Southern Margin would have commenced in the early Campanian (~ 83 Ma) — a highly significant result, with ramifications for understanding the period leading up to continental breakup, as is discussed later (Chapter 8).The period Santonian–early Campanian is characterised by substantial syn-rift sedimentation deposition, magma extrusions and significant thinning of the crust leading to breakup.

### Post-breakup phase – Early Campanian to Recent

The early Campanian–early Eocene is characterised by ultra-slow seafloor spreading and a basin sag phase. The spreading rate then increased from chron C18, in the early Eocene (~ 40 Ma, Veevers et al. 1990; Tikku & Cande,

1999). A change in the spreading direction, from NW–SE to N–S, is interpreted to have commenced at chron C18 time (Veevers et al. 1991), in the post-middle Eocene. Restricted marine conditions persisted until the middle Oligocene. The change to open marine conditions occurred when Antarctica cleared SE Tasmania along the trace of the Tasman Fracture Zone, allowing circum-circular ocean currents to flow around Australia (Exon et al. 1999). This was followed by a continuing sag phase and margin subsidence, with hemipelagic to pelagic sedimentation being deposited.

## 4.3 Regional Basin Distribution

### Introduction

The basins of the Southern Margin are largely the product of a protracted episode of Mesozoic extension in eastern Gondwana which led to the development of the 'Southern Rift System' (Stagg et al. 1990), and the breakup of Australia and Antarctica. The Southern Rift System extends for some 4000 km, from Broken Ridge at the SW tip of Australia to the South Tasman Rise in the SE, and includes, from west to east, the Bight (i.e. that includes the Eyre, Recherche, Ceduna, Bremer and Duntroon Sub-basins), and Otway and Sorell Basins. This report focuses on sedimentary basins located in the central part of the Great Australian Bight including the Recherche, Ceduna and Eyre Sub-basins of the Bight Basin (Figure 3).

### Ceduna Sub-basin

The Ceduna Sub-basin comprises the major sediment accumulation, is approximately 90 000 $km^2$ in area, and contains more than 10 000 m of sediment. It underlies the Ceduna Terrace in water depths ranging from 200 to >4000 m (Figure 3). The main depocentre lies in water depths of 600–2000 m.

The Ceduna Sub-basin can be divided into three major structural elements. From NE to SW, these are the:

- NW-trending Ceduna Monocline — comprising the most rapidly thickening part of the basin between the edge of the continental shelf and the Ceduna Sub-basin. The monocline varies from 40–50 km in width and the sedimentary section thickens from less than 2000 m to probably more than 10 000 m thick. All sequences, except the Cainozoic, thicken across this zone. Faulting within the sedimentary section is relatively minor.
- Central Ceduna Depositional Axis — a broad depositional trough containing Lower and Upper Cretaceous sections extending for some 350 km beneath the central Ceduna Terrace. The trough is some 80–100 km in width and the axis appears to migrate oceanwards up the section. This area is characterised by extensional planar faulting and listric growth faults.
- Outer Margin High — a 15–40 km wide zone of uplifted section (or section which has remained high relative to the central axis) extending along the SW flank of the Ceduna Sub-basin beneath the outer flank of the Ceduna Terrace. The section within the Outer Margin High is elevated by as much

as 1.5 s TWT (>2000 m) relative to the depocentre.

### Eyre Sub-basin

The Eyre Sub-basin forms a 'perched' extensional basin underlying the Eyre Terrace (Figure 3), is approximately 8000 km$^2$ in area and contains up to 4000–5000 m of section. While the Eyre Sub-basin is bounded by basement highs to the north, south and west, part of its sedimentary fill is contiguous with the Ceduna and Recherche Sub-basins.

In broad terms, the Eyre Sub-basin comprises two half-grabens, previously interpeted as sitting on a major crustal detachment fault (Etheridge et al. 1989). While the northern margin of the sub-basin has a gross E–W trend, Stagg et al. (1990) and Willcox & Stagg (1990) showed NW–SE offsets at interpreted transfer faults or relay ramps. It is apparent from the structural elements of the Recherche and Ceduna Sub-basins that the extensional direction was NW–SE to NNW–SSE, while being co-linear on the northern margins of the Eyre Sub-basin and Polda Trough. A high-standing, ENE-trending eroded basement block forms the southern flank of the Eyre Sub-basin. The seaward flank of this block, interpreted to be the head-wall fault of the Recherche Sub-basin underlying the lower continental slope, has been postulated to be a fundamental branch of the main detachment fault (Lister et al. 1986, 1991).

### Recherche Sub-basin

The Recherche Sub-basin comprises that part of the Bight Basin underlying the broad lower continental slope (Recherche Lower Slope) in water depths ranging from 3000 to >5000 m (Figure 3) and contains up to 8000 m of sedimentary section. The Recherche Sub-basin is bounded to the north by the outer basement block of the Eyre Sub-basin, and appears partly contiguous with the Ceduna Sub-basin to the east. The southern limit of the Recherche Sub-basin was originally taken as the COB, as defined by Veevers (1986) at about 35°30'S; the sub-basin continues to the southwestern tip of Australia (Rollet et al. 2001). Sayers et al. (2001) have redefined the COB to be 80 km further south of the previous interpretation by Veevers et al. (1991) extending the basin further southward where it is onlapped by younger (post-breakup) sediments of the Australian-Antarctic Basin.

The half-graben geometry of the Eyre Sub-basin is not replicated in the Recherche Sub-basin. The pre-breakup basinal fill of the Recherche Sub-basin consists of multiple, concordant seismic sequences, more typical of sag phase sequences than syn-rift. This may suggest that accommodation space and subsequent basin fill may have been controlled dominantly by subsidence associated with deep thinning, and less so by mid-upper crustal mechanical extension. These seismic sequences overlie an unconformable surface, highly irregular in profile, and probably Tithonian. Poor seismic reflectivity below this unconformable surface prevents an accurate interpretation of the basinal architecture below the rift-fill.

# 5. STRATIGRAPHY

## 5.1 Sequence Stratigraphic Framework of the Bight Basin*

### Introduction

As described in section 4.3, the Bight Basin is divided into three major depocentres — the Eyre, Recherche and Ceduna Sub-basins — and is continuous with the Duntroon Sub-basin to the east (Figure 3). These basins developed during a period of extension and subsidence that took place along Australia's Southern Margin from the Late Jurassic to Cainozoic.

Deposition in the Bight Basin and Duntroon Sub-basin commenced in the Late Jurassic during a period of lithospheric-scale extension. Fluvial and lacustrine clastic sediments filled half graben systems. These syn-rift sediments were then overlain by widespread fluvio-lacustrine, deltaic and marginal marine sediments deposited during the subsequent phase of thermal subsidence in the Berriasian to middle Albian.

A period of accelerated subsidence during the middle Albian to late Santonian, which preceded the onset of seafloor spreading in the early Campanian (see Chapter 8), was accompanied by the accumulation of thick marine to marginal marine deposits in the Bight Basin, and by major fault reactivation and ductile shale tectonism. A further phase of thermal subsidence took place from the late Santonian onwards. Progradation and aggradation of massive shelf margin delta complexes occurred in the late Santonian to Maastrichtian, particularly in the Ceduna Sub-basin, where up to 5000 m of sediment accumulated.

An overall transgressive phase of sedimentation in the early Cainozoic was followed by the establishment of widespread, open-marine carbonate shelf conditions as a result of accelerated seafloor spreading from the early Eocene onward.

### Sequence Stratigraphy

A sequence stratigraphic framework for the central GAB has been devised by Geoscience Australia's Southern Margin Frontiers Project (Figures 7–11), based on the interpretation of petroleum exploration wells in the Bight Basin and Duntroon Sub-basin, and a grid of new and older, largely reprocessed, seismic data in the Bight Basin (Figure 4). This sequence framework and the implications for petroleum prospectivity are addressed in detail by Totterdell et al. (2000), Blevin et al. (2000) and Krassay & Totterdell (In press). This chapter summarises their work and discusses the Late Jurassic to Cainozoic sediments of the Bight Basin and Duntroon Sub-basin upon which much of the sediments of the deeper water areas is based on.

* Section 5.1 was contributed by Jennifer Totterdell, Barry Bradshaw and Jane Blevin (Southern Margin Frontiers Project, Geoscience Australia)

The two wells drilled in the Bight Basin — Jerboa-1 in the Eyre Sub-basin (Figure 8) and Potoroo-1 in the Ceduna Sub-basin (Figure 10) — provide key reference sections for tying with the seismic data (Figures 9 & 11). Many of the features described in the following section are illustrated in these figures.

To avoid the confusion often caused by naming sequences after existing formation equivalents, a new set of sequence names (based on marine fauna) was introduced by Totterdell et al. (2000; Figure 7). The sequence units are largely 2$^{nd}$-order scale supersequences.

### Late Jurassic Extensional Phase

The oldest supersequence identified in wells is the Callovian–Kimmeridgian age (*M. florida* assemblage zone) **Sea Lion** supersequence. The supersequence was deposited in a series of half graben in the Eyre and Recherche Sub-basins, and was intersected in the Jerboa-1 well. The Sea Lion supersequence consists dominantly of fluvial-lacustrine sandstone and mudstone, and generally shows considerable growth into the half graben-bounding faults. It forms a generally low-amplitude seismic package above a set of high-amplitude basal reflections.

The overlying **Minke** supersequence is Tithonian–early Berriasian in age (*R. watherooensis*–Lower *C. australiensis* assemblage zones). It has been intersected in the Eyre Sub-basin and is interpreted to be present in the Recherche Sub-basin, and in grabens and half grabens adjacent to Potoroo-1 in the Ceduna Sub-basin. This succession shows some growth into the half graben-bounding faults, and it accumulated during either a very late rift or an early thermal subsidence stage. In Jerboa-1, the Minke supersequence consists mainly of lacustrine mudstone. In the Recherche Sub-basin, the supersequence contains relatively continuous, parallel reflections that onlap faulted basement and the Callovian–Kimmeridgian half graben.

### Thermal Subsidence Phase 1 (Pre-Breakup)

The **Southern Right** supersequence is Berriasian in age (*C. australiensis*), and has been penetrated in the Eyre Sub-basin and Duntroon Sub-basin. The supersequence is also interpreted in the Recherche Sub-basin and in grabens in the inner Ceduna Sub-basin. The supersequence consists dominantly of fluvio-lacustrine mudstone, siltstone and sandstone. In Echidna-1 in the Duntroon Sub-basin, the supersequence is over 800 m thick and consists of aggradational mudstone and siltstone, which is overpressured near the base of the well. In the Eyre Sub-basin, variations in seismic character, from high- to moderate-amplitude relatively continuous reflections, to dominantly low-amplitude sections, imply significant changes in lithofacies. High-amplitude, relatively continuous reflections within the supersequence may indicate the presence of coal. The geometry of the succession in the Eyre Sub-basin suggests that accommodation was created largely by thermal subsidence and compaction.

The **Bronze Whaler** supersequence is of Valanginian–middle Albian (Upper *C. australiensis* –Lower *C. paradoxus*) age. In the wells, the supersequence is an aggradational succession of fluvial and lacustrine sediments. In Echidna-1,

in the Duntroon Sub-basin, the Bronze Whaler supersequence consists of over 1700 m of fluvial channel and floodplain deposits. An intermittent marine influence in the upper part of the supersequence is indicated by the presence of dinoflagellates in some wells in the Duntroon Sub-basin. In the Eyre Sub-basin, deposition of the supersequence appears to have been concentrated above the half-grabens, and thickness variations may be due to compaction of the underlying rift-fill. The supersequence has a relatively uniform distribution in the Recherche Sub-basin. In the Eyre Sub-basin, the Bronze Whaler supersequence is characterised by low-moderate amplitude reflections; higher amplitude reflections near the top of the supersequence may be caused by coal.

The middle Albian–Cenomanian (Lower *C. paradoxus – P. pannosus;* upper *C. denticulata*-lower *D. multispinum)* **Blue Whale** supersequence reflects the first major marine flooding event in the Bight Basin, and was deposited at the start of a phase of accelerated subsidence. This supersequence is present throughout the basin and where intersected in wells it consists generally of nearshore or restricted marine siltstones. The section is sandier in Duntroon-1 and glauconitic in Potoroo-1. In the Eyre Sub-basin, the basal Blue Whale sequence boundary truncates, and incises into, the underlying Bronze Whaler supersequence. These incised valleys contain laterally prograding strata that onlap the sequence boundary and represent the fluvial lowstand systems tract of the supersequence. The transgressive and highstand systems tracts of the Blue Whale supersequence extend beyond the older half graben system and overlie basement on the shelf. The presence of an incised valley system, which is interpreted to be part of the Blue Whale lowstand systems tract, on the edge of the shelf indicates the development of a shelf break morphology, with some relief between the Eyre and Recherche depositional systems. Further basinward, in the Ceduna and Recherche Sub-basins, the supersequence appears to consist mainly of ductile, overpressured mudstone and is seismically transparent. Cenomanian and younger growth faults and toe-thrusts sole out on the base of the supersequence.

The **White Pointer** supersequence is of Cenomanian age (*A. distocarinatus;* upper *D. multispinum – P. infusoroides)*. In the wells, it generally consists of fluvial to lagoonal siltstone and mudstone, although sandier, high-energy fluvial facies are present in Platypus-1. The upper part of the White Pointer supersequence is characterised by growth strata associated with a series of listric faults that sole out in underlying ductile shales of the Blue Whale supersequence. The growth faulting is accompanied, further downslope, by compressional deformation in the form of tight folds and toe-thrusts. In the Recherche Sub-basin, the lower part of the supersequence is not affected by growth faulting. Rapid deposition of this section may have caused the underlying mud to become overpressured and ductile, resulting in the gravity-driven growth faulting and deformation. This period of growth faulting was coincident with both a high rate of tectonic subsidence and high global sea levels (Figure 7). The White Pointer supersequence has a generally high-amplitude, high-continuity seismic reflection character, particularly in the growth section.

Well intersections of the Turonian–Santonian (*P. mawsonii* – intra *T. apoxyexinus*/intra *I. cretaceum)* **Tiger** supersequence consist predominantly of aggradational marine mudstones. A sandier, progradational (highstand systems tract) section is present in the upper part of the supersequence at Potoroo-1. The supersequence is characterised by continuous, high- to moderate-amplitude seismic reflections, typical of interbedded marine shales and sandstones or siltstones. The base of the supersequence is strongly erosional in places, and on some seismic lines in the Recherche Sub-basin, it truncates the Cenomanian growth strata. In the Ceduna Sub-basin, the supersequence is extensively faulted, due to reactivation of older faults and continuing movement of the underlying Albian–Cenomanian ductile shale system.

**Thermal Subsidence Phase 2 (Post-Breakup)**

The late Santonian–Maastrichtian (intra *T. apoxyexinus* – Upper *T. longus*; intra *I. cretaceum* – intra *M. druggii*) **Hammerhead** supersequence marks an influx of deltaic sediments into the basin. In the wells that have penetrated this supersequence, it consists of interbedded sandstone and mudstone, and massive mudstone units deposited in delta plain to prodelta environments. The base of the supersequence is strongly erosional in places and the up-dip portion of the basal sequence boundary is characterised by marked incision. Much of the faulting within the underlying succession pre-dates deposition of the Hammerhead supersequence.

Seismic data reveals that the Hammerhead supersequence contains at least three third-order sequences and has an overall progradational–aggradational character. Each of the third-order sequences contains a number of higher order sequences, as suggested by the numerous incision surfaces that can be seen in the seismic data. The lowermost third-order sequence has a strongly progradational seismic character. The sequence boundary at the base of the second sequence records a drop in relative sea level below the previous shelf edge (defined by the edge of the prograding shelf clinoforms of the first sequence). The succession onlaps this sequence boundary well back onto the shelf towards Potoroo-1, before eventually prograding basinward beyond the previous shelf margin. The overlying sequence is dominantly aggradational in character. On strike, or oblique-strike lines, this sequence has a very incoherent seismic character, consisting of variable amplitude, extremely discontinuous reflections. This seismic character is consistent with poorly-interconnected channel sandstones within a mudstone-dominated floodplain succession. The distal portions of the first two sequences probably contain ductile shales, as the basal sequence boundaries are seen to be décollement surfaces on some lines. In the southwestern part of the basin, rapid progradation during the Campanian resulted in slope instability, growth-faulting and load-induced collapse of the shelf margin (Totterdell et al. 2000).

There is some seismic evidence of igneous rocks within the Hammerhead supersequence. Very high-amplitude reflections of limited lateral extent can be seen on several seismic lines in the Ceduna Sub-basin. These reflections exhibit both bed-parallel and cross-cutting geometries, and are interpreted to be caused by igneous sills and dykes. In some cases, they are associated

with mounds, possibly volcanic in origin, which have developed on the Cretaceous–Cainozoic unconformity.

The **Wobbegong** supersequence is of Paleocene–early Eocene age (Lower *L. balmei* – Upper *M. diversus/M. crater*). It consists of marginal marine to deltaic sandstone and minor siltstone. The supersequence is generally thin and unconformably overlies the Cretaceous section. In the Ceduna Sub-basin, near the present-day shelfbreak, the supersequence is characterised by prograding highstand wedges. Lowstand wedge successions within incised canyons and basin-floor fans are situated further basinward. The basin-floor fans have a relatively transparent seismic character, reflecting lithological homogeneity, and contain low amplitude, low-angle prograding reflections.

The middle Eocene (Lower *N. asperus*) to Pleistocene **Dugong** supersequence generally consists of a coarse basal sand overlain by a monotonous carbonate succession, representing deposition on a progradational–aggradational cool-water carbonate shelf. The basal sequence boundary is erosional, and the Dugong supersequence overlies probable Turonian age rocks in Jerboa-1. The sequence boundary forms a major onlap surface, especially at the base of the continental slope, indicating that the margin subsided during the middle Eocene, possibly as a result of the increase in the rate of seafloor spreading.

## 5.2 Seismic Stratigraphy of the Deep Water Great Australian Bight

### Introduction

In this study, the seismic sequence nomenclature (Section 5.1; Figure 7) used by Geoscience Australia's Great Australian Bight regional basin study for the main depocentres of the Bight Basin (Totterdell et al. 2000) was extended into the deep-water areas, in particular the distal portions of the Ceduna and Recherche Sub-basins. These distal areas lie well away from the stratigraphic control provided by the drilling at Jerboa-1 and Potoroo-1 located on the continental shelf and upper slope, and may be characterised by significantly different facies assemblages and hiatuses. Particular horizons have been identified in the deep-water areas, in addition to sequence boundaries identified in upper shelf and slope sub-basins (Figure 12a). Horizons interpreted in the deep-water areas include:

- horizons in the Cainozoic section (i.e. *lmio*, *eoli*, *leoc*, *meo2*, *meo1*, *ter2*, *ter1*) of the Australian–Antarctic Basin;
- horizons at ODP Site 1128 (i.e. *1128.1*, *1128.2*, *1128.3*, *1128.4*);
- horizons in the continent-ocean transition zone (COT) (i.e. *ter2*, *ter1*, *Hammerhead*, *tran*); and
- top of oceanic crust (i.e. *ocea*), top of lower crust and Moho (i.e. *lcru*, *Moho*).

Table 1 lists the sequences and sequence boundaries in the proximal portions of the Ceduna & Recherche Sub-basins and those identified within the deep-

water part of the Bight Basin and overlying Australian-Antarctic Basin. Part of the post-Eocene stratigraphy is based on ties made from ODP well 1128 (Feary et al., 1999) via seismic line 169-08 (Figure 12b).

A full listing of interpreted supersequence boundaries/horizons with reference to type-sections is summarised in Appendix 6.

Table 1: comparison of supersequences interpreted in the Eyre/Ceduna /Recherche Sub-basins (Totterdell et al. 2000) with supersequence boundaries/horizons interpreted in the deep-water areas (this study).

| **Age** | **Supersequences – Eyre/Ceduna/ Recherche Sub-basins** | **Supersequence boundaries Eyre/Ceduna/ Recherche Sub-basins** | **Horizons interpreted in the deep-water areas** |
|---|---|---|---|
| Pleistocene | | Water bottom | Water bottom |
| Pliocene? | | | |
| | | | *1128.1* |
| Late Miocene | | | |
| | | | *1128.2/lmio* |
| Early Oligocene | | | |
| | | | *1128.3/eoli* |
| Early Oligocene | | | |
| | | | *1128.4/leoc* |
| | *Dugong* | | |
| Middle Eocene | | *Base Dugong* | *meo2* (upper boundary) *meo1* (lower boundary) |
| | *Wobbegong* | | |
| Maastrichtian/ Paleocene | | *Base Wobbegong* | *ter2* (upper near-base Cainozoic); *ter1* (lower near-base Cainozoic) |
| | *Hammerhead* | | |
| Santonian/ Campanian | | *Base Hammerhead* | *Base Hammerhead, tran* |
| | *Tiger* | | |
| Cenomanian | | *Base Tiger* | *Base Tiger* |
| | *White Pointer* | | |
| Cenomanian | | *Base White Pointer* | *Base White Pointer* |
| | *Blue Whale* | | |
| Albian | | *Base Blue Whale* | *Base Blue Whale* |
| | *Bronze Whaler* | | |
| Berriasian | | *Base Bronze Whaler* | *Base Bronze Whaler* |
| | *Southern Right* | | |
| Berriasian | | *Base Southern Right* | *Base Southern Right* |
| | *Minke* | | |
| Kimmerigian | | *Base Minke* | *Base Minke* |
| | *Sea Lion* | | |
| Callovian? | | *Base Sea Lion* | *Base Sea Lion* |
| | | | Lower crust |
| | | | Moho |

### Seismic horizon definition at ODP Site 1128

ODP Site 1128 (i.e. Leg 182) is located on the upper continental slope (water depth 3800 m), seaward of the Eyre Terrace (Figure 6, Plate 1). ODP Site 1128 sampled approximately 452 m of early–middle Eocene to Pleistocene pelagic to siliceous sediments (Plate 5); the lithostratigraphy and

biostratigaphy are extracted from Feary et al. (1999). The Cainozoic stratigraphy at ODP Site 1128 (Feary et al. 1999), and correlative seismic picks on seismic line 169/08 (D.A.Feary, pers. comm., 1999), were examined, and provided reliable ties to post Eocene horizons (i.e. 1128.1, 1128.2, 1128.3, 1128.4, Figure 12b). The above horizons could not be interpreted unambiguously into the Recherche Sub-basin and study area. Nevertheless, based on jump-tie correlations, changes in sedimentation rates and sampled hiatus depths, age-control on horizons 1128.1, 1128.2, 1128.3, 1128.4 has helped to infer ages for other horizons interpreted in the Australian–Antarctic Basin.

**Seismic interpretation of the Continent–Ocean Transition Zone (COT)**

The COT is an E–W-trending zone which is taken here as extending oceanward from the end of unambiguous continental crust to the first unequivocally identified oceanic crust. Within the COT, we have interpreted a number of horizons beneath the Tertiary sediments of the Australian-Antarctic Basin (i.e. *meo1*), and overlying the breakup unconformity (i.e. near base *Hammerhead*), equivalent in places to the top of highly-altered transitional crust (i.e. *tran*). Seismic horizons interpreted in the COT with tentatively assigned ages are:

- *tran* (top of transitional crust), approximately Santonian or older;
- *base Hammerhead* (near top Santonian);
- *ter1* (?near base Cainozoic, older horizon); and
- *ter2* (?near base Cainozoic, younger horizon).

Horizon *tran* defines the top, time-transgressive boundary, of interpreted contorted and faulted pre- and syn-rift strata that also includes igneous intrusions. In places, horizon *tran* forms the top of blocks of probable continental crust (Plate 3; Figure 13), while elsewhere it appears to be the boundary between largely igneous rocks and overlying strata which commonly downlap and onlap onto it.

The base *Hammerhead* supersequence boundary has been carried through from the Ceduna and Recherche Sub-basins (Figure 12b). Its character varies in the COT probably because of a changing depositional regime, and the masking effects of volcanics interpreted in the sequences above.

Horizon *ter1* was identified initially on line 65/01 as a high-amplitude reflection and is a major onlap surface on line 199/01 (Plate 3). In the COT it is generally a strong reflection defined by both onlap and downlap, and separates an overlying package of mostly low-amplitude and continuous reflections from an underlying package of higher amplitude and lower continuity (Figure 12a). To the east it becomes more erosional in nature, as on line 199/11, whereas to the north, it has been interpreted as the eroded top of a toe-thrust zone.

Horizon *ter2* is identified as an onlap surface to the north on lines 199/01 and 65/01 (Plate 3), where it has been carried beyond the faulted southern edge of the Recherche Sub-basin. It is a downlap surface to the south. It is interpreted

on Survey 199 lines to the east on the basis of a seismic character-tie.

### Seismic interpretation of the Australian–Antarctic Basin

The Australian–Antarctic Basin sedimentary succession underlies the abyssal plain and its base is characterised by a strong onlap surface (i.e. *meo1*, Figure 12a). The Australian–Antarctic Basin succession was deposited during a mostly continuous period of sedimentation in an open marine environment, after the onset of fast seafloor-spreading in the middle Eocene. Horizons range from middle Eocene to present. The Australian-Antarctic Basin succession onlaps sediments of the Recherche Sub-basin within the COT along the base of the lower continental slope. There is no continental rise development, and in many places the lower continental slope is an erosional surface.

Horizon *meo1* defines the base of the Australian–Antarctic Basin succession. In places it onlaps the earlier Cainozoic section of the Recherche Sub-basin or oceanic crust, but is generally concordant with underlying older strata, where they are present. Where the Australian–Antarctic Basin sedimentary package thins, above the COT, horizon *meo1* is generally carried through to the pinch-out point (Figure 12a). The sequence above is characterised by sub-parallel reflectors of moderate continuity and variable amplitude.

Horizon *meo2* and the overlying sequence onlaps horizon *meo1*; this horizon may mark a change in lithostratigraphy in the middle Eocene. Seismic amplitude strength weakens significantly in the sequence above.

Horizon *leoc* marks the lower boundary of a package of parallel reflectors characterised by high-amplitude and continuity. A wavy reflection character in some areas reflects differential compaction above basement highs. Horizon *leoc* is tentatively assigned a late Eocene age, but may correlate with horizon *1128.4* at ODP Site 1128, which was interpreted by Feary et al. (1999) to mark the Eocene/Oligocene boundary.

Horizon *eoli* is the next stratigraphically higher onlap surface, and marks a transition from an underlying sequence of high-amplitude, parallel and continuous reflections to an overlying sequence with lower amplitude and continuity. This character change implies a change in lithofacies, perhaps to more pelagic sediments. Horizon *eoli* is assigned a probable early Oligocene age.

Horizon *lmio* is the shallowest reflection event that exhibits onlap in the Australian–Antarctic Basin. The overlying seismic facies is characterised by parallel reflections with moderate amplitude and high continuity, implying laterally consistent rates of sedimentation in an abyssal environment. Horizon *lmio* has been correlated with horizon *1128.2* present at ODP Site 1128 (Plate 5), and assigned a late Miocene age (Feary et al. 1999). This event is likely to represent a depositional hiatus, or change in sedimentation rate in the deeper waters and more distal regions of the Australian–Antarctic Basin, rather than an erosional break.

In places faults are identified in the sedimentary section over basement highs in the Australian–Antarctic Basin, probably largely as a result of differential compaction. Approximately 30–40% of these faults coincide with basement faults while the remainder terminate in the sedimentary section. Faulting may affect the upper Miocene sediments and may extend up to the Pliocene in places (Figure 14b).

**Igneous Units**

A number of horizons were designated in this study to mark the top of non-sedimentary (i.e. igneous) units (see Plates 3–4). These are:

- *ocea* (top oceanic crust);
- *buil* (top volcanic buildup);
- *oflo* (top ?volcanic flows overlying oceanic basement);
- *ovol* (?volcaniclastics/flows overlying oceanic basement);
- *intr* (top of intrusions in continental crust);
- *brid* (top basement ridge);
- *lcru* (top lower continental crust); and
- *Moho* (top ?Moho).

Horizon *ocea* defines top of oceanic crust, and does not extend landward of the continent-ocean boundary at seafloor-spreading anomaly 33o. *Ocea* is characterised as a high-amplitude reflection but is discontinuous due to probable faulting and variable relief. Where oceanic crust is characterised by large-scale, high-relief buildups protruding above the seafloor, these are defined as horizon *buil*.

Seismic facies with a chaotic character have been identified on the landward edges of possible faulted/uplifted oceanic blocks, and the top is defined as horizon *oflo*. The seismic facies contain discontinuous, low-amplitude reflections, and may represent syn-tectonic lava flows on the outward-facing scarps of grabens flanking the former spreading axis (Macdonald et al. 1996). Similar seismic facies but more transparent in character have been identified in similar locations. The top of these seismic facies is defined as *ovol*, and these facies probably represent possible volcanic flows and/or volcaniclastics. Top of possible intrusions in continental crust is identified as horizon *intr* (Plate 3, line 199/01).

Horizon *brid* is used to define an extensive basement ridge feature that is interpreted on the inner (landward) flank of the COT (Plates 3–4; Figure 13). This ridge is thought to be composed of a combination of serpentinised peridotites and mafic intrusions or extrusions (Sayers et al., 2001).

Horizon *lcru* defines top of lower continental crust. Modelled velocities from refraction events have helped to confirm this boundary which is also marked by a significant change in seismic character (Figure 13).

A deep (10–12 s) reflection event, present below the landward flank of the COT has been interpreted as reflection Moho (base of crust) and designated horizon *Moho* (Plate 3, lines 199/04 and 199/05). The Moho has not been

recognised below oceanic crust or in the COT. Where identified, *Moho* is characterised by a very high amplitude and continuity.

# 6. MAJOR CRUSTAL PROVINCES

## 6.1 Introduction

This chapter is based on the following datasets, listed here in their order of importance:

- reflection seismic data from Survey 199;
- modelled refraction velocities and thicknesses based on data from sonobuoy stations acquired during Survey 199;
- refraction velocities and thicknesses modelled and interpreted by König & Talwani (1977) and Talwani et al. (1978);
- magnetic lineations initially defined from magnetic anomaly picks of Cande & Mutter (1982), and redefined by Tikku & Cande (1999); and
- dredge hauls undertaken by Geoscience Australia (Feary, 1993).

The *Eltanin* Cruise 55 sonobuoy data were acquired in 1973, and the models derived from these data are summarised in König & Talwani (1977). The sonobuoy data from the *Vema* Cruise 33 were acquired in 1976, and the models derived from these data are summarised in Talwani et al. (1978).

Appendix 3A summarises procedures used in the processing of Survey 199 sonobuoy-data (i.e. ray tracing and production of final refraction-based models). The modelled refraction data from Survey 199, *Eltanin* Cruise 55 and *Vema* Cruise 33 are presented in a number of formats (Appendix 3B & 3C).

The magnetic lineations in Figure 5 and Plate 1 are based on the interpretations of magnetic anomalies by Cande & Mutter (1982) and Tikku & Cande (1999). Tikku & Cande (1999) interpret magnetic lineations 33o–24o (83–56 Ma) as being offset, or missing, in the eastern part of the study area (Figure 5), implying a possible crustal offset in the form of a transform fault that may form on the oceanic extension of the accommodation zone of Willcox & Stagg (1990). The location of this transform fault agrees with offsets interpreted in the E–W-trending basement ridge (Figure 15, Plate 1). The fault zone may have been active up to around chron M23 (52.5 Ma, Figure 5), when extensional tectonism took on a secondary role and gave way to seafloor spreading along this part of the margin, that is , true breakup may have occurred somewhat later in the east of the study area.

Outputs based on the above interpretations include:

- a crustal/structural province map (Figure 15, Plate 1). We identify four major provinces: oceanic crust, COT, basement ridge and extended continental crust.
- interpreted seismic sections and profiles (Plates 3–4, Figure 16).
- profiles compiled from 1-D depth–velocity models across each crustal province (Figures 17–20).

## 6.2 Oceanic Crust

The oceanic crust is readily identified by its strong acoustic response, general reflection character, location beneath the abyssal plain, and relatively shallow depth beneath the seafloor. The very slow-spreading oceanic crust immediately adjacent to the COB has a generally rough basement surface related to submarine volcanic buildups and tilt blocks. The term 'buildup' is used here to define large volcanic constructions that formed (Figure 21b, Plates 3–4) during seafloor spreading. The volcanic buildups are irregular in shape, vary in width from less than 1 km to more than 10 km, and protrude through the sedimentary cover, in places to as much as 1500 m above the surrounding abyssal plain. It has not been possible to ascertain whether these buildups form ridges, principally because of the large (average of 90 km) seismic line spacing. However, ridge formation is likely in places as some volcanic buildups appear to correspond to episodes of extremely slow spreading (e.g. half rate of 1.5 mm/yr between anomalies 24o and 31o; Tikku & Cande 1999), and could have formed elongate features during periods of slow movement between Australia and Antarctica.

The second type of oceanic basement high tends to be asymmetric and block faulted (Figure 14b; lines 199/02 and 199/10 in Plates 3,4). The longer limbs of the fault blocks dip landward, and are generally overlain by a thin, seismically transparent layer (up to 0.3 km thick) that commonly thickens slightly towards the adjacent block. The transparent layer is onlapped by strongly reflecting sediments, and the nature of the intervening sequence boundary may imply a continuation of faulting and block rotation (amagmatic extension) of oceanic crust for some time after its initial formation. Fault planes associated with the rotated oceanic basement highs are generally poorly imaged at depth.

Nine sonobuoy stations are located over oceanic crust (Plate 1), including five stations from Survey 199, three from *Vema* Cruise 33, and one from *Eltanin* Cruise 55. Velocities modelled from *Vema* Cruise 33 sonobuoy data and corresponding to post-breakup sediments are assumed, whilst velocities derived from Survey 199 sonobuoy data are based on seismic processing velocities, and range from 1.7–3.0 km/s.

Only two of the five Survey 199 stations had data that permitted modelling of the entire oceanic crust down to Moho (Figure 17). The two 1-D models (i.e. 199-02, 199-05) give oceanic crust thicknesses of 7.3 and 9.5 km. The modelled mantle velocity of 7.9 km/s is constrained by two to five traces, making the thickness estimates statistically unreliable. Modelling of *Vema* Cruise 33 data produced two-layer 1-D models for the oceanic crust; an upper layer with velocities ranging from 4.75–5.0 km/s, and a lower layer with velocities ranging from 6.6–7.1 km/s (Figure 17). The thickness of oceanic crust based on these data ranges from 4.95–6.01 km. The 1-D model obtained at station V33-08 assumes a velocity of 4.8 km/s for the upper layer, whilst the thickness at station V33-16 is poorly determined. The thickness of oceanic crust modelled from Survey 199 sonobuoy data is significantly greater than the estimates given for the *Vema* Cruise 33 sonobuoy data; the reason for this is unclear.

Some information on the petrology of oceanic crust along Australia's Southern margin is provided by dredging operations undertaken by Geoscience Australia in 1991 (Feary, 1993). Dredge hauls from sites 102DR09 and -13 are located near relatively young oceanic crust (Figure 5). These sites are coinciding with magnetic anomalies 24 (53 Ma) and 29 (66 Ma), respectively, which are characterised by a seafloor spreading rate of approximately 1.5 mm/y (Tikku & Cande, 1999). The dredges sampled igneous buildups exposed on the seafloor. The recovery from site 102DR09 included 10% basalt, which was subdivided petrographically into three main types of basalt (Feary, 1993). The basalts are described as vesicular quenched, plaglioclase-phyric and porphyritic, and are typical ocean-floor basalts. Dredge 102DR09 targeted basalts that had erupted prior to ~ 45 Ma, during a period of ultra-slow seafloor spreading between Australia and Antarctica (<10 mm/year).

The dredge at site 102DR13 (Figure 5) recovered 60% igneous rocks. These rocks consisted of 5% gabbro with crosscutting bands of fine-grained basalt, 10% porphyritic, mafic rock type with late-stage chloritic and K-feldspar veining, and 25% basalt with late-stage felsic veining, described petrographically as aphyric dolerite. Another 5% of the haul comprised basalts, lacking felsic veining, subdivided as either equigranular or fine grained, and 10% of the recovery included coarse-grained gabbro, whilst another 5% was a speckled grey basalt rock.

Dredge hauls from sites 102DR10 and -11 overlie oceanic crust coinciding with magnetic anomalies 12–13 (i.e. 36 Ma) (Figure 5). Dredge 102DR10 recovered 75% coarse-grained igneous rocks which are described as possible serpentinised gabbros (Feary, 1993). The samples have been described as olivine-clinopyroxene-plaglioclase gabbro, greenshist facies, metagabbros and altered basalts. The basalts have been subdivided into five main categories; two of these include a mafic, porphyritic rock and greenshist, plaglioclase-phyric and porphyritic dolerite. Ten percent of the recovery from site 102DR11 included material consisting of two types of basalt. The basalts are described as glomeroporphyritic, plagioclase-clinopyroxene-phyric, and porphyritic plagioclase-phyric. More details on the samples can be found in Feary (1993).

## 6.3 Continent-Ocean Transition Zone

Crust within the COT exhibits neither typically oceanic nor continental seismic reflection characteristics. This crust lies between the very slow-spreading oceanic crust to the south (Anomaly 33 onwards; Figure 15), and the basement ridge complex to the north (see next section), as well as the extended continental crust of the outer Recherche and Ceduna Sub-basins.

Crust underlying pre-breakup sediments within the COT has an irregular upper surface, partly resulting from localised block faulting. The seismic characteristics of this layer are similar to those of the interpreted lower continental crust north (inboard) of the basement ridge complex (Sayers et al. 2001). We use the term lower crust to refer to crystalline crust found in the lower 15 km of 'normal' thickness continental crust. Both the upper and lower crystalline continental crust are present beneath the continental shelf of the

central GAB; however, the upper crystalline crust has been largely removed by extension beneath the outer continental slope, and may form a significant component of the conjugate Antarctic margin (Etheridge et al. 1989). Within the COT, the upper crystalline crust appears to be largely absent, and the lower crust is highly extended and directly overlain by probable Mesozoic sediments. Refraction-derived velocities have also helped in establishing the presence of crystalline continental crust within the COT (velocity of 5.9–6.7 km/s), by comparison with the area north of the basement ridge (velocity of 5.9–6.8 km/s) where the crust is better imaged by seismic reflection data (see section 6.4).

Pre-breakup sediments interpreted in the COT consist of relatively thick sedimentary sequences that exhibit several phases and styles of deformation and intrusion (Figure 16), and have similar seismic characteristics to sequences occurring in the outer Ceduna Sub-basin to the north of the basement ridge complex (Figure 22). Evidence of possible volcanism within the COT is seen on seismic sections (Figures 21c & 21d).

Sediments deposited during the post-breakup thermal sag phase can be divided into those deposited during the slow seafloor spreading phase (Early Campanian – middle Eocene), and those deposited during the fast seafloor spreading phase (Mid-Eocene–Recent). The later sediments constitute a southward-thickening wedge of onlapping sediments that forms part of the Australian-Antarctic Basin. High-amplitude, chaotic seismic facies present within the older sediments, are interpreted as lava flows and/or volcaniclastics, resulting from restricted and episodic volcanic activity during the Campanian to early Cainozoic (Figure 21a).

Eleven sonobuoy stations are located within the COT including four stations from the *Eltanin* Cruise 55, two from the *Vema* Cruise 33, and five from Survey 199 (Plate 1). The lower crust may be at least 1–2 km thick although estimates of crustal thickness are generally unreliable, due to the base of the lower crust being rarely resolved in the refraction data. The lower crust has also been highly extended and varies substantially in thickness throughout the project area. Thickness of crystalline upper crust ranges from being absent in the west to potentially up to 4 km thick in the east (e.g. sonobuoy199-26, Figure 18).

Velocities in relation to the interpreted nature of crust and sediments require further explanation. Collins (1988) showed that velocities of up to 5.9 km/s can be representative of Proterozoic rocks of the Kimberley region of Western Australia. The Collins' measurements are well constrained by geology so that, in the absence of accurate ground-truthing on the Southern Margin, 5.9 km/s has been taken to indicate a high-end cut-off for Phanerozoic sediments. In general, velocities ranging between 5.9 and 6.2 km/s have been taken as representative of crystalline upper crust, whilst velocities of 6.4 to 6.8 km/s are believed to be more representative of lower crust. Overlaying refraction-based velocity-depth models on seismic reflection data also helped in making this differentiation. Velocities representative of either underplated or intruded lower crust, or serpentinised upper mantle, are generally taken as 7.0–7.5 km/s

(Eldholm et al. 1989; Pérez-Gussinyé et al. 2001), while mantle velocities, range between 7.9–8.5 km/s (Appendix 3B & 3C).

Models derived from the *Eltanin* Cruise 55 and *Vema* Cruise 33 data did not differentiate between pre- and post-breakup sediments (König & Talwani, 1977; Talwani et al. 1978; Figure 18). In contrast to the above velocity-depth models, the Survey 199 data (i.e. combined seismic reflection and refraction data) suggest that velocities less than 3.0 km/s are generally characteristic of post-breakup sediments although a few exceptions occur due to varying depth of burial. It has also been shown from the Survey 199 data that velocities of up to 5.7 km/s can be modelled in Mesozoic sediments, given sufficient burial (e.g. station 199-19 in Appendix 3B. König & Talwani, 1977 and Talwani et al. (1978) would interpret such a velocity as Palaeozoic suggesting that their identification of sediment and crustal type may be, at least in part, outdated.

The minimum thicknesses of pre- and post-breakup sediments based on 1-D models derived from Survey 199 sonobuoy stations ranges from 0.63–1.97 km and 1.32–2.85 km, respectively (Figure 18).

## 6.4 Basement Ridge Complex

An east–west-trending basement ridge complex has been interpreted landward of anomaly 34y (Figure 16, Plate 1). It extends along strike for at least 500 km, and averages 20 km in width where it protrudes through pre-breakup sediments (i.e. pre-Early Campanian) and broadens to about 60 km at depth. The exact shape of the basement ridge is difficult to map at depth although its general form and continuity, as illustrated in Figure 15, is supported by the dimensions of the associated gravity and magnetic anomaly highs, at least as far east as line 199/06 (Sayers et al. 2001). In detail the basement ridge is a complex feature, in width, relief, seismic character and probably composition. Sayers et al. (2001) interpret the ridge to be composed of a combination of serpentinised peridotites and mafic intrusions or extrusions derived by mantle upwelling and partial melting. The ridge appears to be segmented (Figure 15), and in places may consist of two or more coalescing ridges or peaks (Figure 16, line 199/01). The general structural position of the basement ridge between the extended crust of the outer Recherche and Ceduna Sub-basins to the north, and the highly deformed and intruded crust and sediments of the COT to the south, is maintained along its full strike-length (Figure 16); however, other characteristics vary, particularly to the east. In the west, the basement ridge is associated with a shallowing of mantle; uplift and deformation of pre-breakup sediments and crust above its northern flank (Figure 16); and more localised culminations at its crest. These features begin to disappear between lines 199/06 and 199/07, and to the east the ridge appears to be underlain by a very poorly defined reflection Moho. The Moho in the east is interpreted to have a consistent northerly dip based on the geometry of the overlying crust. This northerly dip may be offset by seaward-dipping faults. To the east the ridge has a more transparent seismic character typical of the lower continental crust to the north, and its top has a characteristic strongly reflecting, chaotic appearance (e.g. line 199/10 in Plate 4). East of the apparent dextral offset in the COB (Plate 1, line 199/11) at the edge of our study area, the basement ridge complex is difficult to map, and its

character changes significantly. The upper surface of the basement ridge retains its chaotic reflection character, but here may be underpinned by thicker, transparent lower crust. In this location, the ridge, and possible large tilt blocks within and adjacent to the COT, appear to be bounded by southward-dipping, low-angle normal faults.

Planar normal faults are interpreted at Moho level, trending E–W, and located inboard and beneath the basement ridge. Offsets at Moho level have been interpreted as faults on lines 199/03 to 199/05 (Plate 1), but these may continue as far west as line 199/01. Fault throws vary from a few hundred metres to about 6 km on line 199/04. Fault plane dips decrease westwards from approximately 30° on line 199/04, to 15° on line 199/03. Most of these faults die out within the lower crust and do not penetrate the upper crust, although a few (e.g. line 199/04 in Plate 3) extend into overlying sediments of the *Tiger* supersequence.

Three sonobuoy stations are located directly over or adjacent to the basement ridge (Plates 1–2). Modelling of sonobuoy refraction data was necessary to estimate p-wave velocities through the basement ridge, thus providing information on which to base an estimate of its composition (Figure 19).

Station 199-02 straddles the zone between the basement ridge and oceanic crust, and refracted raypaths may have sampled the southern flank of the basement ridge or extended continental crust from the COT. Velocities obtained for the deeper layer at station 199-02 range from 5.9–6.4 km/s, and are significantly lower than at stations 199-13 and 199-22 (Figure 19). Refracted raypaths from station 199-13 are interpreted to have passed through both the base of the basement ridge, and sections of altered and intruded continental crust. Station 199-22 is the only station where raypaths passed through the apex, middle and deeper sections of the basement ridge. A 3-layer 1-D model was obtained: 5.2 km/s at the apex of the basement ridge, 6.2 km/s in mid-section, and 7.2 km/s at the base. The 7.2 km/s velocity layer is significantly faster than adjacent upper/lower crustal velocities in the COT that range from 5.9–6.8 km/s.

Two other 1-D models may be representative of the basement ridge; one at station V33-36 where a velocity of 7.4 km/s was modelled, and one at station V33-13 where velocities range from 6.7–7.3 km/s. The high 7.4 km/s velocity modelled at station V33-36 was interpreted by Talwani et al. (1978) as being representative of continental crust. This interpretation was based solely, at the time, on refraction data. Reflection seismic data from Shell-*Petrel* line 407 located adjacent to station V33-36 (Plate 4), shows uplifted lower crust and mantle. We interpret this 7.4 km/s velocity layer as sampling the northern limb of the basement ridge. Implications of the results are discussed in Chapter 8 and in Sayers et al. (2001).

## 6.5 Extended Continental Crust

Extended continental crust immediately inboard of the basement ridge roughly coincides with the Magnetic Quiet Zone (MQZ) (Talwani et al. 1978; Williamson et al. 1989). Over the years this zone has been variously

described as the product of seafloor spreading within a magnetic quiet period (Veevers, 1986; Veevers & Eittreim, 1988; Veevers et al. 1990) or crustal extension through detachment faulting (Lister et al. 1986, 1991).

Similar to the crust underlying the COT, the upper crust in this province has been thinned by extension beneath the outer continental slope. The lower crust has also been attenuated, probably in a ductile manner (i.e. 7 km to less than 2 km under the lower continental slope north of the basement ridge). The relative absence of penetrative faulting (Figure 16) supports the interpretation that the lower crust may have behaved in a ductile manner. An initial brittle/ductile transition at the top of the lower crust may have acted as a deep shear zone, or possibly extensional detachment beneath the outer margins to the north of the basement ridge. We suggest that movement along both the gravity-driven décollements and possible extensional detachment, and associated faulting and deformation, peaked in the late Cenomanian (approximately 10 Ma before breakup). A second phase of extension leading to breakup, was characterised by further ductile deformation and thinning of the lower crust.

With regards to post-Jurassic sediments, unequivocal evidence of a Jurassic rifting event is documented in the Eyre Sub-basin, where the geometry of faulted basement tilt blocks indicates that extension took place in a generally NW–SE direction (Etheridge et al. 1989). Jurassic sediments are interpreted to be highly attenuated in the Recherche Sub-basin, and under the COT where remnant blocks are thought to be present (Figure 16, line 199/07). The presence of older sediments is possible although difficult to substantiate from seismic data. It is probable that faulting of crystalline upper crust during the pre-rift/rift phase leading to breakup involved re-activation of Jurassic rift faults.

A major décollement surface within the mid-Albian of the Ceduna Sub-basin (Totterdell et al. 2000) extends under the continental slope where gravity-driven listric growth faults, and associated toe-thrusts, sole onto it (Figure 14a). The décollement, growth faults and associated deformation are interpreted to have been active during the Cenomanian following deposition of Albian-Cenomanian marine shales (Totterdell et al. 2000).

Fourteen refraction stations are located over extended continental crust (Plates 1–2) and 1-D depth–velocity models from these sites are shown in Figure 20. The crystalline upper crust thickness ranges from 0.83–8.67 km (i.e. stations 199-09 & V33-39, Figure 20); lower crustal thickness estimates range from 2.55–6.67 km (i.e. stations V33-12 & 199-09). It is difficult to establish clear thickness trends due to poor refraction constraint of the lower crust, although the lower crust is expected to thicken under the upper continental slope, attaining a more uniform thickness under the continental shelf. The lower crust is, however, well constrained from seismic reflection data where it takes on a transparent character (Figure 23).

The minimum thickness of Phanerozoic sediments, based on data from *Vema* Cruise 33 (Talwani et al. 1978) ranges from 2.12 km at station V33-36 to

8.49 km at station V33-38. Thickness of Phanerozoic sediments can be seen to increase to the east and in the Ceduna Sub-basin (Figure 20). A sedimentary section can be seen on seismic data in the Recherche Sub-basin (Plate 3, line 199/09), between the breakup unconformity (i.e. early Campanian) and an older unconformity (i.e. Tithonian). These sediments were modelled to have a thickness of 6.63 km (Appendix 3B) at sonobuoy 199-19, and correlate with Mesozoic sediment when tieing with reflection seismic data. This estimate, based on Survey 199 data differs from estimates using *Vema* Cruise 33 data. This indicates the following: (1) König & Talwani (1977) and Talwani et al. (1978) did not differentiate between pre- and post-breakup sediments; and (2) crystalline crust interpreted by Talwani et al. (1978) and König & Talwani (1977) is clearly shown to be sediments based on our evaluation of the data; this explains the large discrepancies in thickness (see Figure 20).

# 7. RESOURCE POTENTIAL

## 7.1 Introduction

Symonds & Willcox (1989) identified the GAB area as an area where Australia could possibly claim an extra 90 000 km$^2$ of 'legal' Continental Shelf beyond the AEEZ. This extended area may be of importance in the future because of the presence of potential petroleum systems. A petroleum system can be defined as a mature source rock and all its generated hydrocarbon accumulations (Magoon & Dow, 1991). This includes all the appropriate facies for source, reservoir and seal, geometries for entrapment, overburden for maturation and both faulting and permeability for migration.

Twelve petroleum exploration wells (Table 2) have been drilled within the GAB. These wells are Duntroon-1, Echidna-1, Platypus-1, Borda-1, Greenly-1 and Vivonne-1 in the Duntroon Sub-basin; Gemini-1, Mercury-1 and Columbia-1 in the Polda Trough; Apollo-1 in the Denman Basin; Jerboa-1 in the Eyre Sub-basin; and Potoroo-1 on the northern margin of the Ceduna Sub-basin (see Figure 3, Plates 1–2 for location). Considering the wide geographic expanse and substantial sedimentary accumulations in these basins, this region is under-explored by world standards, and is classified as a frontier region. The deep-water setting of the GAB and the distance to infrastructure, coupled with concerns about the distribution of source rocks and the presence of an active petroleum system, have tendered to hind exploration. However, following regional work undertaken by Geoscience Australia, and the award of exploration permits in the central GAB in July 2000, plans are currently underway for the drilling of a deep-water well in the Ceduna Sub-basin during 2003 (Bruins et al. 2001; Longley, 2003).

This chapter presents an overview of the resource potential of the GAB region together with some play concepts derived from the interpretation of Survey 199 seismic data. A more comprehensive analysis, supported by the recent acquisition of a large reflection seismic dataset over the central Bight Basin, has been undertaken by the Southern Margin Frontiers Project group at Geoscience Australia (Totterdell et al. 2000).

## 7.2 Discoveries and Shows

To date, there have been no economic hydrocarbon discoveries in the GAB although there were oil shows in Greenly-1 in the Duntroon Sub-basin. Geochemical analyses of potential source rock intervals show that the majority of sediments drilled are at a low level of maturity. However, the sedimentary column in the Bight Basin has not been adequately sampled, and the drilling generally targeted shallow fault-controlled basement structures. Furthermore, it should also be noted that no well has sampled the substantial sedimentary section in the deep-water areas of the Ceduna and Recherche Sub-basins.

Messent (1998) summarises exploration drilling in the Bight Basin and

addresses reasons for failure; Table 2 summarises the drilling results to date.

Table 2: Summary of wells drilled in the GAB (WD – water depth, TD – total drill-depth).

| Well | WD (m) | TD (m) | Primary target | Status Discovery / Show Fm | Comment |
|---|---|---|---|---|---|
| Echidna-1 | 13 | 3832 | Mobile shale mass on faulted high | Dry, no shows | Hydrocarbons may have migrated |
| Platypus-1 | 158 | 3893 | Broad rollover structure over mobile sediments | Dry, no shows | Very bottom section in oil window |
| Apollo-1 | 75 | 877 | Interpreted sedimentary dome | Dry, no shows | Mis-interpretation of shallow basement high |
| Gemini-1 | 68 | 894 | Anticlinal closure over salt pillow | Dry, no shows | Terminated before proposed TD |
| Potoroo-1 | 252 | 2924 | Fault-dip closure over basement hinge | Dry, no shows | Section above basement near onset of hydrocarbon generation |
| Jerboa-1 | 771 | 2537 | Closure over faulted and rotated basement block | Dry, fluorescence found in L. Jurassic – Neocomian base | Indication of oil migration through sediments |
| Mercury-1 | 77 | 3251 | Anticlinal closure over salt pillow | Dry, minor gas detected in rafted block | *in-situ* sediments had no shows |
| Columbia-1 | 74 | 2168 | Closure on a horst structure | Dry, no shows | Generally immature section |
| Duntroon-1 | 144 | 3515 | Closure over mobilised shale layer | Dry, no shows | No evidence of hydrocarbon migration |
| Borda-1 | 157 | 2800 | Structural high | Dry, no shows | |
| Greenly-1 | 181 | 4860 | Closure over down-faulted block | Dry, show in Wigunda and Platypus Fms | Shows evident over 1800 m of section |
| Vivonne-1 | 137 | 3000 | Closure over tilted fault block | Dry, no shows | |

## 7.3 Source Rocks and Maturity

Only limited source rock and maturity information is available in the GAB region.

### Ceduna Sub-basin

Source rock and maturity characteristics for the Ceduna Sub-basin, based on Potoroo-1 indicate that the Upper Cretaceous section is essentially immature, while the Lower Cretaceous Blue Whale and Bronze Whaler supersequences are presently in the oil window (Struckmeyer et al. 2001). In terms of source richness, the overall level of organic carbon content in the Cretaceous section of Potoroo-1 is moderate. The sediments at Potoroo-1 are, however, thermally immature. Basinward of Potoroo-1, the thicker and deeper buried sequences and greater sediment overburden have likely placed the Blue Whale supersequence and younger units into the oil and gas generation windows (Struckmeyer et al. 2001).

### Eyre Sub-basin

In the Eyre Sub-basin, total organic carbon content (TOC) values show that

the shaly sequences throughout Jerboa-1 are organic rich, particularly in the Late Jurassic Sea Lion supersequence (Ruble et al. 2001). The kerogens in the deeper shales are dominantly amorphous, and are rich in extractable hydrocarbons, suggesting that they have a high potential for oil generation (Burns, 1981). Biomarker interpretations (Edwards et al. 1999) suggest that the organic matter is derived from land plants and algal matter, deposited under anoxic conditions in a fluvial-lacustrine environment. Vitrinite reflectance data indicate that the entire section is thermally immature. However, it is likely that the shales in the flanking half-grabens are thermally more mature. This is supported by recent fluorescence studies that show an early phase of oil generation in the vicinity of Jerboa-1.

### Duntroon Sub-basin

The shale and coal facies of the Cretaceous sequences in the Duntroon Sub-basin have good potential for generating hydrocarbons, as shown by significant oil shows in the Wigunda and Platypus Formations of Greenly-1 (see Figure 7 for correlation of lithostratigraphic and sequence stratigraphy units). Thermal maturity markers demonstrate that the basal Ceduna Formation of Platypus-1 is near the threshold of maximum oil generation (McKirdy, 1984). Re-interpretation of geochemical analyses (Cockshell, 1990) from Echidna-1, Platypus-1 and Duntroon-1 identified the deeper Upper Borda Formation (see Figure 7 for correlation of lithostratigraphic and sequence stratigraphy units), and its coals in particular, as the richest, most oil-prone and volumetrically most significant source interval. Generally, the Upper Cretaceous and Cainozoic section is immature, while erosion of the Upper Cretaceous at Echidna-1 has probably contributed to the lack of mature source rocks in the Lower Cretaceous.

### Polda Trough

Stagg et al. (1992) described the source rock and maturity characteristics for the Polda Trough sequences based on the geochemistry at Mercury-1 and Columbia-1. The Proterozoic red bed section is heavily oxidised, and, therefore, has low source potential. However, total organic carbon measurements for Mercury-1 indicate that the Jurassic Polda Formation has good source potential (see Figure 7 for correlation of lithostratigraphic and sequence stratigraphy units). Thermal gradients suggest that the basin is relatively ‘cold’ at drilling depths. Nevertheless, deeper burial may place the Upper Jurassic section in a more favourable setting for hydrocarbon generation.

## 7.4 Reservoir Rocks and Seals

As was the case with source and maturity, only very limited information is available on reservoir properties and seal quality.

### Ceduna Sub-basin

For the Ceduna Sub-basin, reservoir and seal rock characteristics are largely inferred from Potoroo-1. The Hammerhead and Wobbegong supersequences, with their thick unconsolidated sandstones, have excellent porosities (Totterdell et al. 2000), and the Minke supersequence has sandstones of

moderate porosity, while the reservoir potential of the fluvial to upper delta plain sandstone interbeds of the White Pointer supersequence is possibly reduced by increased shale content. It is expected that these characteristics would also be found further south in the main depocentre and the stronger influence of marine conditions could increase the sorting of the sandy facies. The development of major progradational–aggradational shelf margin complexes within the Hammerhead supersequence has probably provided the potential for stratigraphic plays within its interfingering shale and sand layers. The marine shales of the thick Tiger supersequence gives it potential as a regional seal. This is also expected to be the case along the southern boundary of the basin, where shales cover the anticlinal crests of the toe-thrust complexes. The Southern Right supersequence, or equivalent may act as additional seals; although thin at Potoroo-1, they are thicker in the main part of the basin.

### Eyre Sub-basin

Reservoir and seal rock characteristics for the Eyre Sub-basin were determined from Jerboa-1. In the well, a number of good quality reservoirs were identified at the base of the Minke supersequence, with some excellent porosities (Totterdell et al. 2000). Higher in the section, thin prograding shelf-edge sands of the Wobbergong supersequence, or equivalent, may have suitable porosities. Regional seals could be provided by the thick claystones of the Southern Right supersequence, or equivalent.

### Duntroon Sub-basin

In the Duntroon Sub-basin, fluvial to paralic sandstones of the Cretaceous Potoroo to Echidna Formations and marine sands of the Cainozoic Pidinga Formation have excellent reservoir potential (Stagg et al. 1990), see Figure 7 for correlation of lithostratigraphic and sequence stratigraphy units). In Platypus-1, the sandstones of the Ceduna and Platypus Formations are highly porous. Prodelta claystones of the Wigunda Formation may provide effective regional seals, while thick shales are expected to act as seals in the Borda and Neptune Formations (Stagg et al. 1990).

### Polda Trough

Stagg et al. (1992) described the fluviatile sediments of the Polda Formation to be highly porous and permeable (see Figure 7 for correlation of lithostratigraphic and sequence stratigraphy units). This sequence is too shallow in the wells to provide an effective reservoir, but may do so with deeper burial in other parts of the basin. In Columbia-1 and Mercury-1, good reservoir potential was found for sands in the upper part of the Proterozoic Kilroo Formation. Claystones of the Polda Formation might provide localised seals.

## 7.5 Petroleum Play Types

An overview of the hydrocarbon play types targeted by the GAB exploration drilling effort to date on the shelf and upper slope can be found in Stagg et al. (1990) and Blevin et al. (2000). A discussion of potential petroleum systems further offshore in deeper water must consider the substantial sedimentary packages and structural styles developed in the deep-water Recherche and

Ceduna Sub-basins. The evaluation in this report is only superficial, due to the large distances between drill holes, limited seismic coverage, and the report's focus on a broad geological framework setting.

In this section we concentrate on the potential for trap development and presence of petroleum systems along the southern flank of the Ceduna Sub-basin extending into the Recherche Sub-basin. It should be noted that water depths in these areas are generally much greater than the current limit on petroleum production anywhere in the world.

### Upper Cretaceous – Palaeogene sedimentary apron

The 1–2 s TWT thick sedimentary apron containing Upper Cretaceous to Palaeogene siliciclastic sediments extends seawards from the base of the Ceduna Terrace, across the Recherche Sub-basin, and thins as it downlaps/onlaps onto the underlying blocks of the COT. Seismic interpretation has identified mostly sediments of the *Hammerhead* and *Tiger* supersequences (i.e. ~ Potoroo Formation and Wigunda Formation equivalents, see Figure 7). In these, marine shale facies are likely to provide source potential, as they were laid down in probable warmer waters of a restricted-marine to open-marine setting, prior to the establishment of a colder Circum-Antarctic current in the Oligocene. Prograding sands and turbidite facies, eroded off the uplifted and exposed continental shelf/Ceduna Terrace, are possible reservoirs. The postulated upwelling asthenosphere at the time of breakup may have provided additional heat input to generate hydrocarbons from organic material in the shale facies and from the deeper, more consolidated sediments of continental blocks within the COT. Extensional faulting could have provided migration pathways. Play types include structural closure over faulted and uplifted continental blocks and stratigraphic traps, such as turbidite facies within deep marine shale facies.

### Toe-thrust play

The identification of possible seismic flatspots in the toe-thrusts on the flanks of the Ceduna Sub-basin (Figure 24) may highlight this WNW to ESE-trending complex as an area of some future (very long-term) petroleum potential. The underlying mobile zone and fold-belt may represent overpressured shales of the Lower Cretaceous *Blue Whale* supersequence (or equivalent), though salt mobilisation, which is associated with possible play types in the Polda Trough (Stagg et al. 1992), is also possible. The *White Pointer* supersequence could contain folded and sealed sandy facies in the anticlinal crests of the individual thrust sheets. Similar exploration targets such as salt-driven structures are present in the Perdido Fold Belt of the Gulf of Mexico (Trudgill et al. 1999). Internal décollements and fracturing parallel to the thrust planes could provide a migration pathway between potential source rocks and reservoirs. These plays are high risk due to the water depths involved (>3000 m).

## 7.6 Mineral Resources

Exploration and exploitation of marine minerals, other than hydrocarbons, is in its infancy. In the case of the deep-water GAB region, the only resource of any potential economic interest is manganese nodules and crusts so that economic benefits are also small at present. The principal minerals that have

economic interest in the medium to long-term are construction materials (e.g. sand and aggregate), alluvial diamonds, and manganese nodules and crusts, which include nickel, copper and cobalt. For these, exploration and exploitation of construction materials and diamonds are confined to shallow waters and, hence, are unlikely ever to be relevant to the extended Continental Shelf.

In the western GAB, the Cape Leeuwin nodule field south of the Diamantina Zone contains the richest manganese nodule deposits in Australian waters (Exon et al., 1990). Although not dredged or cored on BMR research cruises 10 and 11 (Willcox et al. 1988), manganese nodules and crusts were extensively sampled in the project area by Survey 102 (Feary, 1993; see Appendix 4). Phosphate, which is of some immediate economic interest, was dredged from a depth of approximately 3000 m on BMR research cruises 10 and 11 (Exon et al. 1990). In all cases, the deep-water marine minerals recovered off Australia are of low grade, and are unlikely to have any economic value, even in the long term.

# 8. GENERAL SCIENTIFIC OUTCOMES AND DISCUSSION

## 8.1 Introduction

The Southern Margin is classified as non-volcanic in origin (Symonds et al. 1998b; Sayers et al. 2001). This study has concentrated on understanding the characteristics of this margin, investigating the nature of the COT, and reaching some understanding of the crustal processes involved in the breakup process. This chapter focuses on the nature and processes of margin breakup by making a comparison between the Southern Margin and the Iberia Margin, off western Portugal. Four models that have been proposed for breakup of the Iberia Margin (Whitmarsh & Miles, 1995; Krawczyk et al. 1996; Brun & Beslier, 1996; Whitmarsh & Sawyer, 1996) based on the results of ODP Legs 103 and 149, and other geophysical data. These models are examined and assessed for relevance to the Southern Margin. Later models and interpretations of the Iberia Margin based largely on the results of ODP Leg 173 and recent studies of Alpine extensional geology are published in Wilson et al. (2001) and Whitmarsh et al. (2001). These later results were unavailable during the initial preparation of this report, and are only briefly mentioned in the following discussion.

## 8.2 Breakup Models — Iberia Margin

### Combined tectonism and magmatism model

The combined tectono-magmatic model of Whitmarsh & Miles (1995) proposes that the COT in a rifted margin setting was formed by both tectonic and magmatic disruption of continental crust (Figure 25a & b). The model describes four zones: (1) crust with normal thickness; (2) continental crust thinned by upper crustal extension; (3) transitional crust consisting of blocks of faulted continental crust and a zone of high density intrusives, which are orientated parallel to the seafloor spreading anomalies; and (4) oceanic crust, produced by seafloor spreading, bounded landward by mantle ultramafic rocks forming a peridotite ridge.

The absence of magnetic lineations within the COT as observed by Whitmarsh & Miles (1995), implies that the COT may be continental in origin. The magnetic anomalies present immediately east of the peridotite ridge are interpreted to result from syn-rift intrusions in the lower crust under the same stress regime that later determined the direction and nature of seafloor spreading within the oceanic crust. By contrast, magnetic anomalies over thinned continental crust are attributed to an earlier amagmatic or extension episode. This model fits the magnetic anomaly data more convincingly than the ultra-slow seafloor spreading model of Whitmarsh & Sawyer (1996) where the anomalies could not be modelled adequately.

The principal petrological evidence for substantiating a combined tectonic and magmatic model is the range of Nd values (6.3–10.3), that is indicative of

some mixing of parental source from both oceanic and continental crust. Additionally, the gabbro from ODP Site 900 (i.e. drilled within the COT) has transitional mid ocean ridge basalts (MORB) to alkaline affinities; these affinities do not strongly support the idea of a widespread MORB-like oceanic crust under the COT. Other petrological evidence presented in Whitmarsh & Miles (1995) is not unique to the dual tectonism/magmatism model.

### Ultra-slow seafloor spreading model

Whitmarsh & Sawyer (1996) interpreted data from the non-volcanic rifted Iberia Margin, and made observations that are characteristic of an ultra-slow seafloor spreading model, that may be relevant to the Southern Margin. Evidence was obtained from magnetic profiles, refraction and reflection data together with petrological analyses of dredged and cored samples. Observations from the above data sources can be interpreted in a number of ways.

The refraction data indicate that transitional crust in the COT ranges in thickness from 3.0–6.0 km (Figure 25c–d; Whitmarsh & Sawyer, 1996). Oceanic crust ranges in thickness from 3–5 km seaward of the peridotite ridge. Upper mantle velocities range from 7.4–7.55 km/s in the COT, and from 7.0–7.6 km/s seaward of the peridotite ridge. A thin oceanic crust, and velocities interpreted as being representative of serpentinised peridotite, support ultra-slow seafloor spreading. These velocities are unlikely to be representative of underplating as this would imply anomalously high asthenospheric temperatures and outpouring of large basalt flows. Large basalt flows have, as yet, not been interpreted on the Iberia Margin.

The Iberia Margin was relatively well sampled during ODP Leg 149, and petrological data play a key role in assessing models. The petrological data have all come from dredge and core samples, and ODP Sites 897, 899 and 900.

There is, from west to east across the Iberia Margin, a 10-fold reduction in the bulk magnetization of the crust (Sibuet et al. (1995) in Whitmarsh & Sawyer (1996)). However, igneous samples from ODP Site 899, within the COT, are on average five times more strongly magnetised than those from ODP Site 897 at the outboard edge of the COT, these sites being 20 km apart. Whitmarsh & Miles (1995, in Whitmarsh & Sawyer, 1996) were, however, unable to match the magnetic anomalies within the COT using very slow spreading rates even though low amplitude, linear magnetic anomalies are consistent with ultra-slow seafloor spreading. Despite this, Whitmarsh & Sawyer (1996) concluded that the Iberia Margin COT is underlain by oceanic lithosphere, with a crust formed by ultra-slow spreading, and with peridotite and gabbro exposed at the seafloor by extensive faulting.

### Detachment fault model

The model put forward by Krawczyk et al. (1996) encompasses a large-scale detachment fault ‘H’ (Figure 26a), and possibly others as yet unidentified. It is proposed that deep lithospheric levels were tectonically unroofed (Figure 26b) as a result of conjugate, lithospheric shear zone activity during rifting (Beslier

et al. (1995) in Krawczyk et al. (1996)), of which detachment fault 'H' would be part. The consequences of progressive extension and unroofing of the lower plate resulted in:

- a bowing of the overlying crust, possibly rendering some detachment faults, like 'H', inactive;
- a number of faulting phases as indicated by normal faults cutting the original detachment 'H'; therefore, these faults may also have been tectonically active at a later stage than fault 'H'. Wedge-shaped blocks were also rotated during a later phase of faulting and extension; and
- a cross-section with a basement consisting, from east to west, of upper crust, lower crust and upper mantle — observations that are supported by petrological analyses from ODP sites.

Krawczyk et al. (1996) state that the model is broadly consistent with the observations from the conjugate Newfoundland Margin (Reid, 1994), with only a few exceptions. Firstly, the east-cutting normal faults on the conjugate margin, for example, do not appear to cut down into the mantle, but rather detach at a lower crustal level. Secondly, the Moho dips westward under the upper continental slope appearing to truncate the lower crust. The Moho reflector is not imaged unambiguously under the Iberia Margin, as on the Newfoundland Margin, which prevents a thorough comparison.

The model proposed by Krawczyk et al. (1996) has different implications for evolution depending on whether the crust under the Iberia Margin could be a piece of the upper plate, or whether it is largely part of the lower plate, as is proposed above. These uncertainties are caused by ambiguities in linking and resolving seismic detachments, and listric and normal faults at depth.

**Multiple shear zone model**

Brun & Beslier (1996) experimented with sand-box models to recreate the evolution of rifting on a passive margin. In their model experiments, they have made the mid-crust and upper part of the lithosphere mantle high-strength layers (brittle), and the lower crust and lower part of the lithosphere mantle low-strength (ductile) layers (Figure 26c). On extension, the sand-box model experiment showed that internal asymmetry of structures can develop in a model undergoing bulk pure shear. For example, the brittle mid-crust evolves into a series of tilted blocks while the ductile crust becomes highly attenuated. Similarly, the high-strength layer in the sub-Moho mantle undergoes faulting and boudinage. The lower crust is attenuated, and acts as a décollement fault, within which boudinaged blocks of the upper mantle intermix. In effect, conjugate shear zones within the ductile lower crust and mantle, cross-cut each other in the ductile lower crust and in the widest zone of the upper mantle, and form boudins. Due to the brittle nature of the upper mantle further extension has the effect of allowing the lower part of the mantle lithosphere to rise, a process attributed solely to isostacy. Thus, the mantle lithosphere progressively becomes exhumed as a result of extreme crustal thinning during extension.

Brun & Beslier (1996) propose that the tectonic contact between the upper

crust and the mantle, on the Iberian Margin, does not result from a flat-lying detachment fault cross-cutting the whole lithosphere, as proposed by Krawczyk et al. (1996). Instead, conjugate shear zones developing in the lower crust and sub-Moho mantle will eventually merge. One ramification of this model is that extension on the Iberia Margin did not occur wholly as a result of a simple shear process. Overall, the lithosphere necking on a broad scale largely corresponds to a pure shear process, with only localised simple shear zones. In contrast to models that use simple shear, asymmetry of extensional structures does not necessarily demonstrate that extension involved simple shear on a lithospheric scale (Brun & Beslier, 1996).

The results of the sand box model experiments have been compared to the non-volcanic rifted Iberia Margin to associate the model observations with those seen on an actual margin. Evidence of flat-lying, normal sense shear zones is seen within peridotite and flazer gabbros that display various stages of ductile shearing up to the formation of ultramylonites, as seen in the ultra-slow oceanic seafloor spreading model of Whitmarsh & Sawyer (1996). Evidence of microscopic shear seen in petrofabric data shows a normal sense of shear.

Whitmarsh et al. (2001) combined aspects of some of the above models, as well as the results of ODP Leg 173 and studies of the margins of the former Tethyan ocean as now exposed in the Alps, to develop a new conceptual model that focuses on the final stage of continental extension and rifting. This model predicts and explains a wide range of observations from non-volcanic rifted margins, particularly in the North Atlantic, such as: low-angle detachments in continental crust; a zone of exhumed continental mantle that evolves oceanward into seafloor spreading; a systematic oceanward increase in syn-kinematic extrusives/intrusives across the zone of exhumed mantle; and a systematic trend from shallow to deeper exhumation of subcontinental mantle towards the locus of breakup. Some of these observations, and parts of the model, may be relevant to the Southern Margin.

## 8.3 Comparison between the Southern and Iberia Margins

### Structure

The structure of the Iberia and Southern Margins has both similarities and dissimilarities. A comparison of similarities and dissimilarities allows some degree of speculation to be made on the characteristics of the Southern Margin; for example, the Iberia Margin is much more heavily sampled than the Southern Margin thus bringing petrological evidence to bear on understanding the rocks in the COT.

- The amount of unroofing of the mantle is less extensive in the COT of the central GAB than on the Iberia Margin. The lower crust was exhumed during the Upper Cretaceous, on the landward side of the basement ridge, but has not generally been exhumed oceanward (Figure 16). This differs from the Iberia Margin where the upper and lower crust have both become progressively exhumed and removed oceanward.
- The lower crust/sediment interface is clearly resolved from seismic data

within and adjacent to the COT of the central GAB (Figure 23), but is obscured under the Iberia Margin. Rifted crust and sediments are also observed in the COT of the central GAB, and the layers are more stratified, as opposed to models involving a regional ramp as is the case on the Iberia Margin (Krawczyk et al. 1996; Figure 26a & b). Faulted continental blocks within the COT of the central GAB can be correlated with good confidence to upper crustal blocks on the northern side of the basement ridge (Figures 22 & 27).

- Basement ridges of probable peridotite composition are identified adjacent to the COB on the Iberia Margin, but are absent adjacent to the COB of the central GAB.
- Large-scale detachment faults may be present in the central GAB, as proposed by Etheridge et al. (1989), Lister et al. (1986, 1991), but have not been resolved in this study. Therefore, such faults may not play as significant a role on the Southern Margin as may be the case on the Iberia Margin (Whitmarsh & Miles, 1995; Krawczyk et al. 1996). Décollement 'faults' interpreted within sediments of the Ceduna Sub-basin and at the top of the lower crust (Figure 14a) may play a role not too dissimilar to the detachment faults (Sayers et al. 2001).
- Synthetic–antithetic fault sets, growth faults, toe-thrusts and localised décollement faults are interpreted in the sediments of the Ceduna Sub-basin, and under the continental slope oceanward of it. Planar faults are interpreted to be present in pre-Tithonian sediments of the Recherche Sub-basin, while synthetic–antithetic fault sets are present in the Eyre Sub-basin. In contrast, planar and detachment faults have been interpreted on the Iberia Margin (Krawczyk et al. 1996).
- Faulted Moho has been interpreted under the lower continental slope and suggesting a brittle upper mantle (Plate 1). The presence of faulted Moho has been implied on the Newfoundland Margin (Reid, 1994) but has not been identified, as yet, under the Iberia Margin.
- Faults in the mid-crust and sediments of the central GAB rarely penetrate into the lower crust, suggesting that the lower crust may have been ductile in nature. In comparison, a listric fault, low-angle planar fault, and sizeable fault blocks have been observed on the Iberia Margin (Krawczyk et al. 1996), implying more-brittle characteristics.
- Brittle fault sets occur in oceanic crust of the Southern Margin (Figure 14b) and similar fault sets have also been interpreted on the Iberia Margin (Whitmarsh & Miles, 1995).

### Oceanic crust

The thickness of the oceanic crust on the Iberian Margin has been shown to be approximately 6 km (see 'Ultra-slow seafloor spreading model'). In contrast, the oceanic crust appears to be further attenuated on the conjugate margin off Newfoundland, being 4 km thick in one location. The thickness of oceanic crust in the central GAB, as calculated by König & Talwani (1977) and Talwani et al. (1978; see Chapter 6) is in the range 5–6 km. The data modelled in this study (i.e. sonobuoys 199-02 and 199-05) are not

unambiguously constrained by first break arrivals from an oceanic Moho, but modelling suggests a minimum thickness of 6 km, and possibly as thick as 9 km (Figure 17). Potential field modelling of line 199/05 suggests an oceanic crust ranging in thickness from 6–10 km adjacent to the COB (Figure 27). It would, therefore, appear that thickness of oceanic crust on both margins is comparable (i.e. 5 – 10 km), although control on these measurements is very limited.

Ultra-slow seafloor spreading (defined when the seafloor spreading rate is less than 10 mm/yr) produces anomalously thin crust. Tikku & Cande (1999) suggest that this is the case for the Southern Margin between magnetic anomaly magnetic anomaly 34o (120 Ma) and 18o (40.1 Ma). Rates of less than 10 mm/yr, using the arguments of Whitmarsh & Sawyer (1996) and White et al. (1992 in Whitmarsh & Sawyer, 1996) should produce an oceanic crust in the order of 4 km in thickness, caused as a result of insufficient magma produced by decompression melting of the asthenosphere. This argument is not supported unambiguously by the estimated crustal thickness in the central GAB where oceanic crustal thickness is in the order of 6 to >6 km thick. Therefore, we suggest that an anomalously thin oceanic crust may not necessarily be an outcome of ultra slow seafloor-spreading model, and such models may not be fully predicting the petrological and tectonic processes that are occurring. Further research needs to be done to substantiate the relationship between oceanic crust thickness and the rate of seafloor spreading.

Brittle deformation represented as faulted oceanic crust has been interpreted in pre-early Eocene (chron 22) oceanic crust of the GAB. The brittle behaviour is confined to the slow-spreading oceanic crust, previously identified by Cande & Mutter (1982) and Tikku & Cande (1999). After that time, increased magma production, possibly related to a hotter asthenosphere, appears to have created the more typical, largely unstructured, oceanic basement.

**Magnetic anomaly 34**

Magnetic anomaly 34 has been interpreted as being present in the central GAB (Cande & Mutter, 1982; Tikku & Cande, 1999). However, this anomaly doesn't overlie oceanic crust but a basement ridge and 'transitional' crust within the COT. This may have implications for other rifted margins. Firstly, magnetic anomalies have been interpreted on other rifted margins (e.g. Iberia Margin) that are not as well covered by a comprehensive seismic grid as the Southern Margin of Australia (i.e. Survey 199). Seismic data allows a more comprehensive interpretation to be carried out. It follows that magnetic anomalies overlying transitional crust, previously thought of as resulting from of normal seafloor spreading, may in fact, be the result of another magmatic process predating normal seafloor spreading. Secondly, the deeper ocean areas of margins that are presently interpreted to be oceanic in nature may in fact be underlain by transitional continental crust. Thirdly, the COB may lie further seaward than is currently mapped.

**Basement ridge – COT**

The basement ridge in the GAB is large enough to be mapped as a separate

crustal province (Figure 15). It has thinned continental crust and continental blocks overlying and straddling it, but not underlying it. The basement ridge has been interpreted, in this study, as being largely igneous in nature. This differs from the interpretation of Stagg & Willcox (1992), who proposed that the feature was a metamorphic core complex – i.e. its origin was previously associated with detachment fault models, similar to those proposed by Lister et al. (1991).

The basement ridge partially coincides with the magnetic anomaly interpreted as 34y (i.e. 115–83 Ma) while unambiguous oceanic crust coincides with magnetic anomaly 33o (i.e. 83–75 Ma). This interpretation, together with evidence of downlapping sediments of interpreted Campanian age overlying the breakup unconformity, suggest that the emplacement of the basement ridge pre-dates breakup, here defined as the first appearance of seafloor-spreading oceanic crust (i.e. ~83 Ma). The assignment of an igneous origin for the basement ridge (Figure 27), as modelled by Sayers et al. (2001), is highly significant. It could, for example, represent a juvenile stage within the breakup process on the Southern Margin. A second implication is that angular unconformities seen in the sedimentary basins on the shallow margin, and usually interpreted to be related to final breakup may, in fact, be mis-identified with rift phases, particularly those related to deep thinning. Further work would, however, be required to ascertain the above more fully.

Refraction modelling of the basement ridge in this study has provided two estimates of velocity (i.e. 7.2 km/s and 7.4–7.55 km/s) for the deeper part of the ridge. Velocities in the shallower part of the ridge range from 5.2–6.2 km/s (Figure 19). A direct comparison with velocities of the peridotite ridges on the Iberia Margin is not possible due to the lack of velocity data there. We suggest, irrespective of the absence of velocities typical of peridotite, that velocities from the Southern Margin may also be representative of upper mantle suites (i.e. peridotite or equivalent) combined with altered upper mantle suites (see next section, ‘upper mantle composition’). An alternative model to the above would involve underplating beneath, and intrusion within the lower crust that would yield similar velocities. As the Southern Margin, like the Iberia Margin, is non-volcanic, underplating and intrusion within the lower crust is not expected. In contrast, a volcanic margin involving underplating would be associated with significantly large extrusive complexes similar to those found under the Wallaby Plateau (Sayers et al. 2002).

We propose that the basement ridge represents an intermediate stage between two end-members: (1) unroofed mantle, and (2) intrusions deriving from the mantle. The Iberia Margin would represent a type margin with a mantle significantly unroofed, with lower and upper continental crust outcropping as basement within the COT, as proposed by Krawczyk et al. (1996). We suggest that the Southern Margin basement ridge, at least within the study area, is intermediate between the two end-members, but closer to the end-member where intrusions occur related to partial melting accompanying the rising mantle.

### Upper mantle composition

Seismic reflection data, which have contributed to constraining crustal architecture of the COT from both the Iberia and Southern Margins, have been supplemented, in the GAB, with refraction-based modelled velocities. Velocities for the upper mantle, on the Iberia Margin, have been measured; 7.5 km/s modelled below thinned continental crust, and 7.55–7.6 km/s for the mantle underlying oceanic crust (Whitmarsh & Sawyer, 1996). On the Newfoundland Margin, conjugate margin to the Iberia Margin, the velocity modelled was 7.3 km/s. The above velocity estimates are significantly lower than global average velocities for upper mantle suites of 7.9–8.3 km/s (Christensen & Mooney, 1995). One explanation for the low velocities is that the upper mantle has been significantly altered prior and during breakup and contain recrystallised decompression melts. The only velocity estimates of altered mantle within the GAB study/project areas are those modelled across the basement ridge (i.e. 7.2 & 7.4–7.55 km/s; 7.4 km/s from Talwani et al. 1978). It is possible, therefore, that serpentinised peridotite and gabbro, as are found on the Iberia Margin, may represent the dominant composition of the altered mantle. Measured velocities more characteristic of global average mantle velocities are also found in the GAB and range from 8.0–8.5 km/s (König & Talwani, 1977; Talwani et al. 1978; see Appendix 3C).

The Iberia Margin has been extensively dredged and cored whereas no basement samples are available from the COT in the GAB. However, samples have been dredged from a somewhat similar setting to the COB in the Diamantina Zone, at the southwestern tip of Western Australia (Nicholls et al. 1981; Figure 5). Nicholls et al. (1981) identify two petrological assemblages that include Cr-spinel lherzolites and Al-spinel-olivine clinopyroxenites. They interpret the lherzolites as upper mantle residues emplaced within a shallow crust, and subsequently exposed by erosion. The pyroxenites are interpreted to be partly recrystallized cumulates from high-temperature basaltic magmas traversing a lherzolite mantle. The authors suggested that these rocks may have been emplaced in a similar way to the Iberian peridotites. These samples are important to the concept of an unroofed upper mantle together with intrusives that are injected during an earlier magmatic phase. For example, these melts may have been emplaced in the Santonian prior to seafloor spreading in the early Campanian.

More recent dredging in the Diamantina zone south of the Naturaliste Plateau recovered alkaline basalts from its inner part and highly altered peridotites from its outer part (Chatin et al. 1998). The alkalic nature of the basalts and the geochemical signature of the peridotites led Chatin et al. (1998) to conclude that the Diamantine Zone rocks may be the result of rapid mantle exhumation typical of continental rifts. Beslier et al. (2001) estimated that the emplacement of the peridotites occurred between 90 and 84 Ma, and this was just prior to the new breakup age of ~83 Ma (Sayers et al., 2001 and this report). Such a history of exhumation of sub-continental mantle is consistent with the model of Whitmarsh et al. (2001).

### Tectonic processes and rifting models

In the Southern Margin study area brittle deformation appears to be confined

to sediments, upper crust and upper mantle in contrast to ductile deformation in the lower crust and lithosphere mantle. North of the basement ridge, the gross geometry of the interpreted lower crust has a pinch-and-swell character, suggestive of extension involving a ductile rheology. A ductile rheology is also consistent with the interpretation of near complete rupture of lower crust above the basement ridge. In contrast, the uppermost mantle has responded to extension by brittle faulting resulting in large offsets of the Moho. In places, some of the upper mantle faults may have penetrated into the more ductile lower crust and influenced the geometry of the pinch and swell structures. These structures have, in turn, influenced the style and distribution of deposition and deformation of the Ceduna depocentre. Rifting has thus proceeded through depth-dependant extension and rheology-dependant strain (Figure 27a), covered more fully by Sayers et al. (2001). The reconstruction diagram proposed by Sayers et al. (2001) for the COT and general breakup model is reproduced in Figure 28.

Unroofing of mantle to the north of the COT appears to have had a number of effects (Figure 28a–b). Firstly, Sayers et al. (2001) and Sayers et al. (this report) conclude that the ascent and depressurisation of mantle under the extended and thinned continental crust resulted in melt formation and the subsequent intrusion of gabbroic dykes under the COT, as well as possible associated extrusive units (Figure 28b). A similar model has been proposed to explain the exposure of mantle rocks and associated partial melting products in the Diamantina Zone about 1000–1500 km to the west (Royer et al. 1999). Secondly, the geophysical character of the ?Proterozoic to Mesozoic pre- and syn-rift sediments and the lower crust has been altered by injection of mantle melts/intrusions. Thirdly, Sayers et al. (2001) and Sayers et al. (this report) have modelled highly magnetic serpentinised peridotite along the flattened planes of listric faults at the crust-mantle boundary (Figure 27b). This combination of processes and the associated production of magnetised rocks operating during the Cenomanian may have given rise to magnetic anomaly 34y within extended continental crust and pre-breakup sediments that, in its along-margin extent, is indistinguishable from a normal seafloor spreading magnetic anomaly. Fourthly, Sayers et al. (2001) and Sayers et al. (this report) interpret the mantle as being altered in the vicinity of the basement ridge as demonstrated by the upper mantle velocities (7.2–7.55 km/s). It is possible that serpentinised peridotite has been intruded along fault planes, possibly facilitated by water influx along fault planes.

Taken together, the evidence provides strong support for a four-layer lithosphere model of the type postulated to explain the extensional style and mantle exhumation processes of the Iberia non-volcanic rifted Margin (Brun & Beslier, 1996; Figure 26c). The evolution model proposed by Sayers et al. (2001) supports a four-layer lithosphere model that incorporates timing of extensional phases and emplacement of the basement ridge (Figure 28). The evidence from Survey 199 seismic data supports ductile thinning of the lower crust and faulting of the brittle upper mantle as in the model of Brun & Beslier (1996). Brun & Beslier (1996) suggest that this type of model, which gives rise to complex strain patterns, layer-parallel shearing of the ductile lower crust, boudinage of the brittle upper mantle, the formation of asymmetric fault

patterns, and diapiric upwelling of the deeper ductile mantle, is most likely to occur in an environment of pure-shear operating at a lithosphere scale.

Thus, the south Australian–Antarctic conjugate margins may appropriately be considered as a product of lithospheric-scale pure shear rather than of a composite model involving simple-shear extension of the upper crust on detachment faults above zones of distributed pure-shear (Etheridge et al. 1989; Lister et al. 1991). Our study has found no evidence of either lithosphere-penetrating detachments, or major upper crustal detachments beneath the COT. It could be reasonably argued that such detachments would be very difficult to image seismically in the complex COT zone. In Figure 28a we schematically illustrate a possible mid-crustal décollement that could be interpreted as a detachment in the sense of Lister et al. (1991), and in the easternmost part of the study area detachment-type faults may be present. Note that the detachment models previously proposed to explain the extensional development of the Southern Margin would produce brittle upper crustal faulting and deep, pure shear thinning of the lower crust and upper mantle. This is relatively similar, in broad terms, to the Brun & Beslier (1996) four-layer model, except for the lack of faulting in the brittle upper mantle.

# 9. ACKNOWLEDGMENTS

The Southern Margin Frontiers Project group, comprising Jennifer Totterdell, Jane Blevin and Barry Bradshaw had defined seismic sequences in the Bight Basin based on petroleum wells, and a study of regional seismic datasets. These group members transferred their knowledge and wrote the stratigraphy section contained in Section 5.1. We thank them for their contribution.

We extend our thanks to Mark Alcock who produced a complete listing of seismic parameters for most of the seismic surveys, included in Appendix 2. We also acknowledge the contribution of Barry Willcox who provided some of the text to 'Chapter 3 – Previous work'.

Extensive drafting and technical support was necessary to illustrate the data and technical ideas. We thank Lindell Emerton, Angie Jaensch, Rex Bates and Ross Hill from Geoscience Australia's drafting section for their professionalism and timeliness in regards to drafting of the figures and plates. We extend our thanks to Chris Lawson and Peter Butler from the technical support group who provided the digital data to produce some of the plates and figures. Lastly, we thank Gail Hill and Bruce Cotton for their contribution to some of the figures and plates in regards to the Law of the Sea boundaries.

No report is complete without a comprehensive review. In this regard, we are indebted to Howard Stagg, Jim Colwell and Phil Symonds (Law of the Sea Project) and Jennie Totterdell (Southern Australia Regional Project). Their comprehensive reviews were invaluable for enhancing the quality of this report, and we thank them for their contribution.

# 10. REFERENCES

Bein, J. & Taylor, M.L., 1981. The Eyre Sub-basin: recent exploration results. *APEA Journal*, 21, 91–98.

Beslier, M-O., Ask, M. & Boillot, G., 1993. Ocean–continent boundary in the Iberia Abyssal Plain from multichannel seismic data. *Tectonophysics*, 218, 383–393.

Beslier, M-O., Bitri, A. & Boillot, G., 1995. Structure de la transition continent-ocean d'une marge passive: sismique reflexion multitrace de la Plaine Abyssale Iberique (Portugal). *Comptes Rendues Academie Science Paris*, 320.

Beslier, M.-O., Le Bihan, T., Feraud, G. & Girardeau, J., 2001. Cretaceous ultra-slow spreading in the ocean-continent transition along the southwest Australian passive margin: constrains from $^{40}Ar/^{39}Ar$ dating. *Abstracts of the EUG XI meeting* (8-12 April 2001).

Blevin, J.E., Totterdell, J.M., Logan, G.A., Kennard, J.M., Struckmeyer, H.I.M. & Colwell, J.B. 2000. Hydrocarbon prospectivity of the Bight Basin – petroleum systems analysis in a frontier basin (extended abstract). In, Wood, G.R. (compiler), Second Sprigg Symposium, Frontier Basins, Frontier Ideas, Geological Society of Australia Inc., South Australian Division, GSA Abstracts No. 60, 24–29.

Boeuf, M.G. & Doust, H., 1975. Structure and development of the southern margin of Australia: Australian Petroleum Exploration Association Journal. 15, 33–43.

Boillot, G., Grimaud, S., Mauffret, A., Mougenot, D., Kornprobst, J., Mergoil-Daniel, J. & Torrent, G., 1980. Ocean–continent boundary off the Iberian margin: a serpentinite diapir west of the Galicia Bank. *Earth and Planetary Science Letters*, 48, 23–34.

Boillot, G., Winterer, E.L., Meyer, A.W. et al., 1987. *Proc. ODP, Sci. Results*, 103. College Station, TX (Ocean drilling Program).

Boillot, G., Beslier, M.-O., Krawczyk, C.M., Rappin, D. & Reston, T., 1997. The formation of passive margins: constraints from the crustal structure and segmentation of the deep Galicia margin (Spain). In: Scrutton, R. *et al*. (Eds), *Tectonics, Sedimentation and Palaeoceanography of the North Atlantic*. Geological Society Special Publication London.

Brown, B.J., 1999. Early Plate Tectonic Evolution of the Southern Ocean, Australia, Honours Thesis, University of Sydney (unpub).

Brun, J.P. & Beslier, M-O., 1996. Mantle exhumation at passive margins. *Earth and Planetary Science Letters*, 142, 161–173.

Buins, J., Longley, I.M., Fitzpatrick, J.P., King, S.J. & Sommerville, R.M., 2001. The Ceduna Sub-basin – An exploration update. PESA Eastern Australasian basins Symposium, Melbourne, Vic, 25–28 November 2001, 655–658.

Burns, B.J., 1981. Geochemical report Jerboa-1 well Eyre Basin, Western Australia. *Esso Australia Ltd report (unpub)*.

Cande, S.C. & Mutter, J.C., 1982. A revised identification of the oldest sea-floor spreading anomalies between Australia and Antarctica. *Earth and Planetary Science Letters*, 58, 151–160.

Chatin F., Robert U., Montigny R. & Whitechurch H., 1998. La Zone Diamantine (ocean Indien oriental), temoin de la separation entre l'Australie and l'Antarctique: arguments petrologique et geochimique. *C. R. Acad. Sci. Paris*, 326, 839-845.

Christensen, I.N. & Mooney, D.W., 1995. Seismic velocity structure and composition of the continental crust: a global view. *Journal of Geophysical Research*, 100 (B7), 9761–9788.

Cockshell, C.D., 1990. A seismic study of the Duntroon Basin*. South Australia Dept Mines & Energy Report Book* 90/28.

Collins, 1988. Seismic velocities in the crust and upper mantle of Australia. *Bureau of Mineral Resources, Geology and Geophysics*, Report 277.

Conolly, J.R. & von der Borch, C.C., 1967. Sedimentation and physiography of the sea-floor south of Australia. *Sedimentary Geology*, 1, 181–220.

Conolly, J.R., Flavelle, A. & Dietz, R.S., 1970. Continental margin of the Great Australian Bight. *Marine Geology*, 8, 31–58.

Davies, H.L., Clarke, J.D.A., Stagg, H.M.J., Shafik, S., McGowran, B., Alley, N.F. & Willcox, J.B., 1989. Maastrichtian and Younger Sediments from the Great Australian Bight. *Bureau of Mineral Resources, Geology and Geophysics, Report* 288.

Deighton, I., Falvey, D.A. & Taylor, D.J., 1976. Depositional environments and geotectonic framework — southern Australian continental margin. *APEA Journal*, 16, 25–36.

Department of Industry, Science and Resources, 1999. Release of offshore petroleum exploration areas Australia 1999, Commonwealth of Australia.

Edwards, D.S., Struckmeyer, H.I.M., Bradshaw, M.T. & Skinner, J.E., 1999. Geochemical characteristics of Australia's southern margin petroleum systems. *APPEA Journal,* 39, 297–321.

Eldholm, O., Tiede, J. & Taylor, E., 1989. Evolution of the Voring volcanic

margin. In Eldholm, O., Tiede, J., *et al*. (eds), *Proceedings of the Ocean Drilling Program, Scientific Results*, 104. College Station, TX (Ocean Drilling Program), 1033–1065.

Etheridge, M.A., Lister, G.S. & Symonds, P.A., 1989. Application of the detachment model to reconstruction of conjugate passive margins. In: Tankard A.J. & Balkwill H.R. (eds), *Extensional Tectonics and Stratigraphy of the North Atlantic Margins*, American Association of Petroleum Geologists Memoir 46, 23–40.

Exon, N.F., Cronan, D.S. & Colwell, J.B., 1990. New developments in manganese nodule prospects, with emphasis on the Australasian region. *Pacific Rim 90 Congress*, Australasian Institute of Mining & Metallurgy, 363–371.

Exon, N., Kennett, J., Malone, M. and the Leg 189 Shipboard Scientific Party. 1999. The opening of the Tasmanian Gateway Drove Global Cenozoic Paleoclimatic and Palaeoceanographic Changes: Results of Leg 189. Joides Journal, 26 (2), 11–18.

Falvey, D.A. & Mutter, C.J., 1981. Regional plate tectonics and evolution of Australia's passive continental margins. *BMR Journal of Australian Geology and Geophysics*, 4, 243–252.

Feary, D.A., 1993. Geological sampling in the Great Australian Bight: Scientific post-cruise report — R/V *Rig Seismic* Cruise 102. *AGSO Record* 1993/18.

Feary, D.A., Hine, A.C. & Malone, M.J., 1999. *Proc. ODP, Init. Repts*., 182 [CD-ROM] Available from: Ocean Drilling Program, Texas A&M University, College Station, TX 77845-9547, USA.

Fraser, A.R. & Tilbury L.A., 1979. Structure and stratigraphy of the Ceduna Terrace region, Great Australian Bight Basin. *APEA Journal*, 19, 53–65.

Froitzheim, N. & Manatschal, G., 1996. Kinematics of Jurassic rifting, mantle exhumation, and passive-margin formation in the Austroalpine and Penninic nappes (eastern Switzerland). *Geological Society of America Bulletin*, 108 (9), 1120–1133.

Fullerton, L.G., Sager, W.W. & Handschumacher, D.W. 1989. Late Jurassic-Early Cretaceous evolution of the eastern Indian Ocean adjacent to northwest Australia. *Journal of Geophysical Research*, 94, 2937–2953.

Hegarty, K.A, Weissel, J.K. & Mutter, J.C., 1988. Subsidence history of Australia's southern margin: constraints on basin models. *American Association of Petroleum Geologists Bulletin,* 72 (5), 615–633.

Horsefield, S.J., 1992. Crustal structure across the continent-ocean boundary *(Ph.D thesis)*. Cambridge University.

Jones, M.T., Tabor, A.R. & Weatherall, P., 1997. *Supporting volume to the GEBCO Digital Atlas.*

König, M. & Talwani, M., 1977. A geophysical study of the southern continental margin of Australia: Great Australian Bight and western sections*. Geological Society of America Bulletin*, 88, 1000–1014.

Krassay, A.A. & Totterdell, J.M., in press. Seismic stratigraphy of a large, Cretaceous shelf-margin delta complex, offshore southern Australia. *AAPG Bulletin*.

Krawczyk, C.M., Reston, T.J., Beslier, M-O. & Boillot, G., 1996. Evidence for detachment tectonics on the Iberia Abyssal Plain rifted margin. *In*: Whitmarsh, R.B., Sawyer, D.S., Klaus, A. and Masson, D.G. (Eds.), *Proceedings of the Ocean Drilling Program, Scientific Results*, Vol. 149: College Station, TX (Ocean Drilling Program), 603–615.

Lister, G.S., Etheridge, M.A. & Symonds, P.A., 1986. Detachment faulting and the evolution of passive continental margins. *Geology*, 14, 246–250.

Lister, G.S., Etheridge, M.A. & Symonds, P.A., 1991. Detachment models for the formation of passive continental margins. *Tectonics,* 10 (5), 1038–1064.

Logan, G., 1999. Palaeo-oil zone in Jerboa-1. *PESA News*, April/May 1999, 55.

Longley, I., 2003. Great Australian Bight – Recent chronology of a gnarly area. *PESA News February/March 2003*, 24–26.

Macdonald, K.C., Fox, P.J., Alexander, R.T., Pockalny, R. & Gente, P., 1996. Volcanic growth faults and the origin of Pacific abyssal hills. *Nature*, 380, 125–129.

Magoon, L.B. & Dow, W.G., 1991. The petroleum system — from source to trap. *AAPG Bulletin*, 75 (3), 627.

McKirdy, D.M., 1984. Coastal bitumen and potential source rocks, Duntroon Basin, South Australia. Report 84 for Getty Oil Development Co. Ltd. South Australia Dept Mines & Energy Open File Envelope.

Messent, B.E.J., 1998. Great Australian Bight: Well Audit. *Australian Geological Survey Organisation, Record 1998/37*.

Middleton, M.F., 1991. Tectonic history of the southern continental margin of Western Australia. *Geological Survey of Western Australia Record 1990/8.*

Müeller, D.R., Mihut, D. & Baldwin, S. 1998. A new kinematic model for the formation and evolution of the west and northwest Australian margin, In: Purcell, P.G. & Purcell, R.R. (eds), *The Sedimentary Basins of Western*

*Australia* 2, Proceedings of Petroleum Exploration Society of Australia Symposium, Perth, 1998, 55–71.

Murillas, J., Mougenot, D., Boillot, G., Comas, M.C., Banda, E., Mauffret, A., 1990. Structure and evolution of the Galicia Interior basin (Atlantic western Iberian continental margin). *Tectonophysics*, 184: 297–319.

Mutter, J.C., Hegarty, K.A., Cande, S.C. & Weissel, J.K., 1985. Break-up between Australia and Antarctica: a brief review in the light of new data. *Tectonophysics,* 114, 255–279.

Nicholls, I.A., Ferguson, J., Jones, H., Marks, G.P. & Mutter, J.C., 1981. Ultramafic blocks from the ocean floor southwest of Australia. *Earth and Planetary Science Letters*, 56, 362–374.

Norvick, M. & Smith, M. 2001. Mapping the plate tectonic reconstruction of southern and southeastern Australia and implications for petroleum systems. *APPEA Journal*, 41, 15–35.

Pérez-Gussinyé, M., Reston, T.J. & Phipps Morgan, J., 2001. Serpentinization and magmatism during extension at non-volcanic margins: the effect of initial lithospheric structure. *In*: Wilson, R.C.L., Whitmarsh, R.B., Taylor, B. & Froitzheim, N. 2001. *Non-Volcanic Rifting of Continental Margins: A Comparison of Evidence from Land and Sea*. Geological Society, London. Special Publications, 187, 551–576.

Petkovic, P. & Buchanan, C., 2002. *Australian Bathymetry and Topography Grid (January 2002)*, Geoscience Australia, Canberra (CD ROM).

Petkovic, P., Brett, J., Morse, M.P., Hatch, L., Webster, M.A. & Roche, P. 1999. Gravity, Magnetic and Bathymetry Grids from Levelled Data for Southwest Australia — Great Australian Bight. *Australian Geological Survey Organisation, Record 1999/48*.

Reid, I., 1994. Crustal structure of a nonvolcanic rifted margin east of Newfoundland. *Journal of Geophysical Res*earch, 99, 15161–15180.

Rollet, N., Fellows, M.E., Struckmeyer, H.I.M. & Bradshaw, B.E., 2001. Seabed character mapping in the Great Australian Bight, *Geoscience Australia Record 2001/42.*

Royer, J-Y, Beslier, M-O, Hill, P.J. & MARGAU Scientific Party, 1999. Southwest Australian margin: evidence for mantle exhumation along a wide ocean–continent transition zone. *Abstract Volume, American Geophysical Union,* 1999 *Spring Meeting*, S321.

Ruble, T.E, Logan, G.A., Blevin, J.E., Struckmeyer, H.I.M., Liu, k., Ahmed, M., eadington, P.J. & Quezada, R.A., 2001. Geochemistry and charge history of a palaeo-oil column: Jerboa-1, Eyre Sub-basin, Great Australian Bight. PESA Eastern Australasian basins Symposium, Melbourne, Vic, 25–28

November 2001, 521–529.

Sandwell, D.T. & Smith, W.H.F., 1995. Marine gravity field from declassified Geosat and ERS-1 altimetry. *EOS Transcripts, Abstract Volume*, *American Geophysical Union*, Fall 1995, AGU Meeting Supplement, 156.

Sandwell, D.T. & Smith, W.H.F., 1997. Global seafloor topography from satellite altimetry and ship depth soundings. *Science*, 277, 1956–1962.

Sayers, J., Symonds, P., Direen, N.G. & Bernardel, G. 2001. Nature of the continent–ocean transition on the non-volcanic rifted margin of the central Great Australian Bight. *In*: Wilson, R.C.L., Whitmarsh, R.B., Taylor, B. & Froitzheim, N. 2001. *Non-Volcanic Rifting of Continental Margins: A Comparison of Evidence from Land and Sea*. Geological Society, London. Special Publications, 187, 51–77.

Sayers, J., Borissova, I., Ramsay, D. & Symonds, P.A., 2002. Geological Framework of the Wallaby Plateau and Adjacent Ocean Basins. *Geoscience Australia Record 2002/21*.

Sibuet, J-C., Louvel, V., Whitmarsh, R.B., White, R.S., Horsefield, S.J., Sichler, B., Leon, P. & Recq, M., 1995. Constraints on rifting processes from refraction and deep-tow magnetic data: the example of the Galicia continental margin (West Iberia). In: Banda, E., Torne, M. & Talwani, M. (eds), *Rifted Ocean–Continent Boundaries*. Amsterdam (Kluwer), 197–218.

Smith, A.G. & Hallam, A., 1970. The fit of the southern continents. *Nature*, 225, 139–144.

Sproll, W.P. & Dietz, R.S., 1969. Morphological continental drift fit of Australia and Antarctica. *Nature*, 222, 345–348.

Stagg, H.M.J. & Willcox, J.B., 1992. A case for Australia–Antarctica separation in the Neocomian (ca. 125 Ma). *Tectonophysics*, 210, 21–32.

Stagg, H.M.J., Willcox, J.B. & Needham, D.J.L., 1989. Werner deconvolution of magnetic data: theoretical models and application to the Great Australian Bight*. Australian Journal of Earth Sciences*, 36, 109–122.

Stagg, H.M.J., Willcox, J.B. & Needham, D.J.L., 1992. The Polda Basin — a seismic interpretation of a Proterozoic-Mesozoic rift in the Great Australian Bight*. BMR Journal of Australian Geology and Geophysics*, 13, 1–13.

Stagg, H.M.J., Willcox, J.B., Needham, D.J.L., O'Brien, G.W., Cockshell, C.D., Hill, A.J., Thomas, B. & Hough, L.P., 1990. Basins of the Great Australian Bight region: geology and petroleum potential. *Bureau of Mineral Resources, Continental Margins Program* Folio 5, 1–143.

Struckmeyer, H.I.M., Totterdell, J.M., Blevin, J.E., Logan, G.A., Boreham, C.J., Deighton, I., Krassay, A.A. & Bradshaw, M.T. 2001. Character,

maturity and distribution of potential Cretaceous oil source rocks in the Ceduna Sub-basin, Bight Basin, Great Australian Bight. PESA Eastern Australasian basins Symposium, Melbourne, Vic, 25–28 November 2001, 543–552.

Symonds, P.A. & Willcox, B.J., 1989. Australia's petroleum potential beyond an Exclusive Economic Zone. *BMR Journal of Australian Geology and Geophysics*, 11, 11–36.

Symonds, P.A., Murphy, B., Ramsay, D., Lockwood, K. & Borissova, I., 1998a. The outer limits of Australia's resource jurisdiction off Western Australia. In: Purcell, P.G. & Purcell, R.R. (eds), *The Sedimentary Basins of Western Australia* 2, Proceedings of Petroleum Exploration Society of Australia Symposium, Perth, 1998, 3–19.

Symonds, P.A., Planke, S., Frey, O. & Skogseid, J. 1998b. Volcanic evolution of the western Australian continental margin and its implications for basin development. In: Purcell, P.G. & Purcell, R.R. (eds), *The Sedimentary Basins of Western Australia* 2, Proceedings of Petroleum Exploration Society of Australia Symposium, Perth, 1998, 33–54.

Talwani, M., Mutter, M., Houtz, R. & König M., 1978. The crustal structure and evolution of the area underlying the magnetic quiet zone on the margin south of Australia. In: Watkins, J., Montadert, L. & Dickenson, P. (eds), *Geological and Geophysical Investigations of Continental Margins. American Association of Petroleum Geologists Memoir* 29, 151–175.

Tikku, A.A. & Cande, S.C., 1999. The oldest magnetic anomalies in the Australian–Antarctic Basin: are they isochrons? *Journal of Geophysical Research*, 104 (B1), 661–677.

Totterdell, J.M., Blevin, J.E., Struckmeyer, H.I.M., Bradshaw, B.E., Colwell, J.B. & Kennard, J.M., 2000. A new sequence framework for the Great Australian Bight: starting with a clean slate. *APPEA Journal*, 40 (1), 95–117.

Trudgill, B.D., Rowan, M.G., Fiduk, J.C., Weimer, P., Gale, P.E., Korn, B.E., Phair, R.L., Gafford, W.T., Roberts, G.R. & Dobbs, S.W., 1999. The Perdido Fold Belt, Northwestern Deep Gulf of Mexico, Part 1: structural geometry, evolution and regional implications. *AAPG Bulletin*, 83 (1), 88–113.

Veevers, J.J., 1982. Australian–Antarctic depression from the mid-ocean ridge to adjacent continents. *Nature*, 295, 315–317.

Veevers, J.J., 1986. Breakup of Australia and Antarctica estimated as mid-Cretaceous (95 +/- 5 Ma) from magnetic and seismic data at the continental margin. *Earth and Planetary Science Letters*, 77, 91–99.

Veevers, J.J. & Eittreim, S.L., 1988. Reconstruction of Antarctica and

Australia at break-up (95 +/- 5 Ma) and before rifting (160 Ma). *Australian Journal of Earth Sciences*, 35, 355–362.

Veevers, J.J., Stagg, H.M.J., Willcox, J.B. & Davies, H.L., 1990. Pattern of slow seafloor spreading (<4 mm/year) from break-up (96 Ma) to A20 (44.5 Ma) off the southern margin of Australia. *BMR Journal of Australian Geology & Geophysics*, 11, 499–507.

Veevers, J.J., Powell, C.M. & Roots, S.R. 1991. Review of seafloor spreading around Australia. I. Synthesis of the patterns of spreading, *Australian Journal of Earth Sciences*, 38, 373–389.

Weissel, J.K. & Hayes, D.E., 1972. Magnetic anomalies in the southeast Indian Ocean. In Hayes, D.E. (ed.), Antarctic Oceanology II: Australian–New Zealand Sector. *Antarctica Research Series*, 19, 234–249.

Wernicke, B., 1985. Uniform-sense normal simple shear of the continental lithosphere. *Canadian Journal of Earth Sciences*, 22, 108–125.

Wernicke, B. & Burchfiel, B.C., 1982. Modes of extensional tectonics. *Journal of Structural Geology,* 4, 105–115.

White, R.S., McKenzie, D. & O'Nions, R.K., 1992. Oceanic crustal thickness from seismic measurements and rare earth element inversions. *Journal of Geophysical Res*earch, 97, 19683–19715.

Whitmarsh, R.B., Miles, P.R. & Mauffret, A., 1990. The ocean-continent boundary off the western continental margin of Iberia. Crustal structure at 40º 30'N. *Geophysical Journal International*, 103: 509–531.

Whitmarsh, R.B. & Miles, P.R., 1995. Models of the development of the West Iberia rifted continental margin at 40d 30' deduced from surface and deep-tow magnetic anomalies. *Journal of Geophysical Research*, 100 (B3), 3789–3806.

Whitmarsh, R.B. & Sawyer, D.S., 1996. The ocean/continent transition beneath the Iberia Abyssal Plain and continental-rifting to seafloor-spreading processes, *Proceedings of the Ocean Drilling Program, Scientific Results*, 149: College Station, TX (Ocean Drilling Program).

Whitmarsh, R.B., Pinheiro, L.M., Miles, P.R., Recq, M. &, Sibuet, J.C., 1993. Thin crust at the western Iberia ocean–continent transition and ophiolites. *Tectonics*, 12, 1230–1239.

Whitmarsh, R.B., Sawyer, D.S., Klaus, A. & Masson, D.G. (eds.), 1996. *Proc. ODP, Sci. Results*, 149: College Station, TX (Ocean Drilling Program).

Whitmarsh, R.B., Beslier, M-O. & Wallace, P.J., 1998. *Proc. ODP, Init. Repts*, 173: College Station, TX (Ocean Drilling Program).

Whitmarsh, R.B., Manatschal, G. & Minshull, T.A., 2001. Evolution of magma-poor continental margins from rifting to seafloor spreading. *Nature*, 413, 150–154.

Whyte, R.K., 1978. Shell's Offshore Venture, in South Australia. *APEA Journal*, 18, 44–51.

Willcox, J.B., 1978. The Great Australian Bight — A Regional Interpretation of Gravity, Magnetic, and Seismic Data from the Continental Margin Survey. *Bureau of Mineral Resources Australia, Report 201, 1–111.*

Willcox, J.B., 1990. Gravity trends as an expression of lithospheric extension on the southern margin of Australia. *Australian Journal of Earth Sciences*, 37, 85–91.

Willcox, J.B. & Stagg, H.M.J., 1990. Australia's southern margin: a product of oblique extension. *Tectonophysics*, 173, 269–281.

Willcox, J.B., Stagg, H.M.J., Davies, H.L. *et al.*, 1988. Rig Seismic research cruises 10 & 11: Geology of the Central Great Australian Bight Region. *Bureau of Mineral Resources, Report 286*, 1–140.

Williamson, P.E., Collins, C.D. & Falvey, D.A., 1989. Crustal structure and formation of a magnetic quiet zone in the Australian southern margin. *Marine and Petroleum Geology*, 6, 221–231.

Wilson, R.C.L., Whitmarsh, R.B., Taylor, B. & Froitzheim, N. 2001. *Non-Volcanic Rifting of Continental Margins: A Comparison of Evidence from Land and Sea*. Geological Society, London. Special Publications, 187, 585p.

# 11. APPENDICES

## Appendix 1: 1982 United Nations Convention on the Law of the Sea (UNCLOS)

### Article 76: Definition of the continental shelf

1. The continental shelf of a coastal State comprises the seabed and subsoil of the submarine areas that extend beyond its territorial sea throughout the natural prolongation of its land territory to the outer edge of the continental margin, or to a distance of 200 nautical miles from the baselines from which the breadth of the territorial sea is measured where the outer edge of the continental margin does not extend up to that distance.

2. The continental shelf of a coastal State shall not extend beyond the limits provided for in paragraphs 4 to 6.

3. The continental margin comprises the submerged prolongation of the land mass of the coastal State, and consists of the seabed and subsoil of the shelf, the slope and the rise. It does not include the deep ocean floor with its oceanic ridges or the subsoil thereof.

4. (a) For the purposes of this Convention, the coastal State shall establish the outer edge of the continental margin wherever the margin extends beyond 200 nautical miles from the baselines from which the breadth of the territorial sea is measured, by either:

   (i) a line delineated in accordance with paragraph 7 by reference to the outermost fixed points at each of which the thickness of sedimentary rocks is at least 1 per cent of the shortest distance from such point to the foot of the continental slope; or

   (ii) a line delineated in accordance with paragraph 7 by reference to fixed points not more than 60 nautical miles from the foot of the continental slope.

   (b) In the absence of evidence to the contrary, the foot of the continental slope shall be determined as the point of maximum change in the gradient at its base.

5. The fixed points comprising the line of the outer limits of the continental shelf on the seabed, drawn in accordance with paragraph 4 (a) (I) and (ii), either shall not exceed 350 nautical miles from the baselines from which the breadth of the territorial sea is measured or shall not exceed 100 nautical miles from the 2,500 metre isobath, which is a line connecting the depths of 2,500 metres.

6. Notwithstanding the provisions of paragraph 5, on submarine ridges, the outer limit of the continental shelf shall not exceed 350 nautical miles from the baselines from which the breadth of the territorial sea is measured. This paragraph does not apply to submarine elevations that are natural components of the continental margin, such as its plateaux, rises, caps, banks and spurs.

7. The coastal State shall delineate the outer limits of its continental shelf, where that shelf extends beyond 200 nautical miles from the baselines from which the breadth of the territorial sea is measured, by straight lines not exceeding 60 nautical miles in length, connecting fixed points, defined by coordinates of latitude and longitude.

8. Information on the limits of the continental shelf beyond 200 nautical miles from the baselines from which the breadth of the territorial sea is measured shall be submitted by the coastal State to the Commission on the Limits of the Continental Shelf set up under Annex II on the basis of equitable geographical representation. The Commission shall make recommendations to coastal States on matters related to the establishment of the outer limits of their continental shelf. the limits of the shelf established by a coastal State on the basis of these recommendations shall be final and binding.

9. The coastal State shall deposit with the Secretary-General of the United Nations charts and relevant information, including geodetic data, permanently describing the outer limits of its continental shelf. The Secretary-General shall give due publicity thereto.

10. The provisions of this article are without prejudice to the question of delimitation of the continental shelf between States with opposite or adjacent coasts.

# Appendix 2: Details of Seismic Surveys

| | |
|---|---|
| **Survey** | 199 |
| **Contractor** | AGSO |
| **Vessel** | Rig Seismic |
| **Year** | 1997 |
| **Streamer length (m)** | 4000m |
| **Seismic channels** | 320 |
| **Group length/interval (m)** | 12.5/12.5 |
| **Shot interval (m)** | 50 |
| **Cable depth (m)** | 10m |
| **Source type/power or volume** | 20 Sleeve guns/49.2 litres |
| **Nominal vessel speed (kn)** | 5 |
| **Primary navigation** | differential GPS |
| **Secondary navigation** | differential GPS |
| **Tertiary navigation** | Dead Reckoning |
| **Primary echo-sounder** | 12 KHz |
| **Secondary echo-sounder** | 3.5 KHz |
| **Magnetic data** | yes |
| **Gravity data** | yes |

| | |
|---|---|
| **Survey** | 169 |
| **Contractor** | AGSO |
| **Vessel** | Rig Seismic |
| **Year** | 1996 |
| **Streamer length (m)** | 1000m |
| **Seismic channels** | 80 |
| **Group length/interval (m)** | 12.5/12.5 |
| **Shot interval (m)** | 100 |
| **Cable depth (m)** | 3m |
| **Source type/power or volume** | 3 and 6 GI guns in GI mode/7.4 litres and 14.8 litres |
| **Nominal vessel speed (kn)** | 5 |
| **Primary navigation** | differential GPS |
| **Secondary navigation** | differential GPS |
| **Tertiary navigation** | Dead Reckoning |
| **Primary echo-sounder** | 12 KHz |
| **Secondary echo-sounder** | 3.5 KHz |
| **Magnetic data** | yes |
| **Gravity data** | yes |

| | |
|---|---|
| **Survey** | 65 |
| **Contractor** | AGSO |
| **Vessel** | Rig Seismic |
| **Year** | 1987 |
| **Streamer length (m)** | 2400 and 600 |
| **Seismic channels** | 48 and 12 |
| **Sample rate/rec. length (ms)** | 2/6000 |
| **Group length/interval (m)** | 50/50 |

| | |
|---|---|
| **Shot interval (m)** | 50 and 25 |
| **Cable depth (m)** | ? |
| **Source type/power or volume** | 10 GSI waterguns/26.2 litres |
| **Nominal vessel speed (kn)** | 5 |
| **Primary navigation** | Transit and Magnavox sonar doppler |
| **Secondary navigation** | GPS |
| **Primary echo-sounder** | 12 KHz |
| **Secondary echo-sounder** | 3.5 KHz |
| **Magnetic data** | yes |
| **Gravity data** | yes |

| | |
|---|---|
| **Survey** | Roving reconnaissance seismic (N) |
| **Contractor** | Shell Internationale Petroleum Maatschappij N.V. |
| **Vessel** | Petrel |
| **Year** | 1971 |
| **Streamer length (m)** | 2400 |
| **Seismic channels** | 24 |
| **Sample rate/record length (ms)** | 4/6000 |
| **Group length/interval (m)** | 50/100 |
| **Shot interval (m)** | 50 |
| **Cable depth (m)** | 15 |
| **Source type/power or volume** | airgun array/6.4 litres |
| **Nominal vessel speed (kn)** | 6 |
| **Primary navigation** | Transit Satnav + Marquardt sonar doppler |
| **Primary echo-sounder** | Not known |
| **Magnetic data** | yes; analogue only |
| **Gravity data** | yes; analogue only |

| | |
|---|---|
| **Survey** | JA90 |
| **Contractor** | for Japanese National Oil Company |
| **Year** | 1990 |
| **Streamer length (m)** | 3000 |
| **Seismic channels** | 240 |
| **Sample rate/record length (ms)** | 2/6000 |
| **Group length/interval (m)** | 25/25 |
| **Shot interval (m)** | 25 |
| **Cable depth (m)** | 12.5 |
| **Source type/power or volume** | 64 x sleeve airguns/35.7 litres |
| **Nominal vessel speed (kn)** | 5 |

| | |
|---|---|
| **Survey** | DWGAB |
| **Contractor** | Seismic Australia |
| **Vessel** | M/V Sea Challenger |
| **Year** | 1998 |
| **Streamer length (m)** | 3570 |
| **Seismic channels** | 120 |
| **Group length/interval (m)** | 30/30 |
| **Shot interval (m)** | 30 |

| | |
|---|---|
| **Cable depth (m)** | 8 |
| **Sample rate/record length (ms)** | 2/10000 |
| **Source type/power or volume** | Air gun array, 1310 cubic inch |

| | |
|---|---|
| **Survey** | HRGAB |
| **Contractor** | Seismic Australia |
| **Vessel** | M/V Sea Challenger |
| **Year** | 1998 |
| **Streamer length (m)** | 1785 |
| **Seismic channels** | 120 |
| **Group length/interval (m)** | 15/15 |
| **Shot interval (m)** | 15 |
| **Cable depth (m)** | 7 |
| **Sample rate/record length (ms)** | 2/5000 |
| **Source type/power or volume** | Air gun array, 470 cubic inch |

# Appendix 3A: Modelling Sonobuoy Data

## Introduction

Refraction modelling was carried out on sonobuoy records acquired during the 1997 Survey 199 by the *Rig Seismic*. There were a total of 17 sonobuoys deployed during the survey, 15 of which were interpreted, and subsequently modelled. The information gained in the modelling was used to either complement or reinforce the geological interpretation that had been done on the reflection seismic sections. It is most useful in verifying, if possible, the velocity of the layers down to the bottom-most horizon, thus aiding geological interpretation, and also providing density control for future gravity or rheological modelling.

At each sonobuoy location, a record was acquired in one direction only. The sonobuoy records have a maximum offset of approximately 35 km (see the table in this section for details). The nominal shotpoint (SP) interval for the survey was 50 metres.

## Procedure

### *Sonobuoy data*

The sonobuoy records were initially interpreted with all significant events being marked and individually digitised. The events chosen were the direct arrival, the pre-critical water bottom reflection, other reflections, all first-break refraction energy, and other deeper events. The data were then exported into an ASCII file, reformatted, and finally input into MacRay[3].

In most instances, the records were artificially stretched or compressed due to sonobuoy drift. This was readily noticeable when modelling the direct arrival, which in the normal case is expected to have a velocity equal to the speed of sound in water (~1500 m/s). However, the apparent direct arrival velocity (adav) varied between 1390 and 1660 m/s over the survey. To correct for this, the direct arrival was initially modelled on each record. If adav differed from 1500 m/s, the shotpoint interval was adjusted according to the formula:

Scaled SP interval = 1500/adav * nominal SP interval

The above relationship assumes a constant speed of drift in the direction of shooting of the seismic survey. In our procedure, irregular and lateral drift cannot be corrected nor detected respectively. However, there was little evidence of irregular drift in this study while the effect of lateral drift is comparatively small generally.

The data were then formatted a second time using the scaled SP interval rather than the nominal SP interval to determine along-line distance; values can be seen in the table following. This data file was then re-imported into MacRay and was ready for final modelling.

[3] USGS 2D raypath modelling software package (for Macintosh operating system)

### *Model data*

Reflection seismic data for the relevant portion of the seismic line were initially interpreted and digitised on-screen using an interpretation package. The seismic section was plotted and each horizon assigned a name label. Each layer was initially given an approximate interval velocity, which was determined by averaging the interval velocities of the layer from time-velocity information on accompanying reflection seismic sections. Using the Petroseis[4] package, the horizons were then manually digitised in two-way time and converted to depth using the layer velocities. The depths to each horizon were output to an ASCII file, which was reformatted and finally imported into MacRay for modelling.

### Modelling techniques

In order to initially verify the data, the direct arrival was modelled and pre-critical reflection raypaths off the water bottom were matched with the hyperbolic first breaks. The shallow horizons posed little problem in providing a good match with the observed events on the sonobuoy records.

The modelling procedure involved modifying and fine-tuning each interface starting from the top downward. When testing refraction events, the first-break refraction arrival was first interpreted as a number of discrete straight-line segments with different slopes. Each refractor interface in turn had the velocity altered in order to best match the slope of the segment. The interface was subsequently moved up or down to provide the optimum match with the observed event. When a best fit was made to the first segment, the next deeper horizon was modified for velocity and depth to match the next segment and so on, until all segments were modelled by refracting horizons.

Generally, a layer was given a velocity range of 0.2 km/s, which increased with depth. It is expected that this would approximately represent the physical nature of a given thick rock layer which becomes more compacted with depth.

The deeper horizons, in particular, give rise to events on the records that cannot be modelled with the refraction technique, as valid raypaths cannot be returned within the maximum offset. In some instances, reflection and pre-critical reflection raypaths were used during the study to successfully model deeper horizons including the Moho.

As a general rule, the original input model was modified as little as possible while providing the best fit. This ensured minimum departure from the original depth-converted model.

### Discussion of errors

The final velocity and depth model is subject to some errors. They are difficult to quantify and are briefly outlined below.

- As mentioned above, sonobuoy drift will contribute an error into calculations.

[4] Petroseis software, Petrosys Pty Ltd.

- The assumption is made in the depth conversion that: (i) there are no lateral velocity variations in the layers; and (ii) the true interval velocity is an averaged value determined from the stacking velocities on reflection seismic sections. This is obviously not the physical reality within the earth, but it is the best that can be done at the present time. It is difficult to quantify the error in depth and velocity, as a different velocity field will influence the raypath geometry.
- The modelling is not as constrained as it could be because the refraction records are acquired in one direction only. The main advantage of reciprocal shooting is that, as well as providing double the amount of data to be matched, the technique allows a way of distinguishing the cause of a change of refraction slope between dip effects and the velocities. In our case, however, provided that the depth conversion is reasonably accurate, the starting layered model should reflect the true dip. It is difficult to say just how much error is involved. What can be said with certainty is that the depth conversion technique will be improved in the future by using modern software that is attuned to the problem of true depth conversion.
- In conjunction with the point above, there will be some thickness/velocity 'invariance'. Individual layer thicknesses and velocities within a multi-layered system can be modified in combination to give similar modelled results. The error in layer velocity is difficult to quantify, but it is estimated to be in the order of $1\sigma \approx \pm 100$ m/s.

**Interpreted Results**

Appendix 3B tabulates the derived depth–velocity information for each horizon/layer for all 15 modelled sonobuoys from Survey 199. Appendix 3C shows depth–velocity information obtained from data acquired during *Eltanin* Cruise 55 and *Vema* Cruise 33. An interpretation of the sonobuoy records can be found in Chapter 6.

| Sono. No. | Seismic Line | Latitude | Longitude | WD (m) | Launch SP | End SP | SP Origin model | Sonobuoy Depth (m) | Offset range (km) | Adav (m/s) | Scaled SP int (m) |
|---|---|---|---|---|---|---|---|---|---|---|---|
| 1 | 199/01 | 37 10 05.51S | 127 10 52.88E | 5559 | 2875 | 3399 | 2870 | 122 | 0.25 - 27 | 1500 | 50.0 |
| 2 | 199/01 | 36 08 43.32S | 127 24 05.77E | 5521 | 5179 | 5858 | 5170 | 122 | 0.45 - 35 | 1660 | 45.2 |
| 5 | 199/02 | 36 37 24.49S | 128 04 50.90E | 5536 | 4537 | 5085 | 4530 | 122 | 0.35 - 28 | 1460 | 51.4 |
| 6 | 199/03 | 36 14 29.21S | 128 50 17.61E | 5542 | 3439 | 4021 | 3430 | 122 | 0.45 - 30 | 1610 | 46.6 |
| 9 | 199/04 | 35 19 10.62S | 129 43 13.39E | 4830 | 2075 | 2604 | 2070 | 122 | 0.25 - 27 | 1510 | 49.7 |
| 10 | 199/04 | 36 09 28.88S | 129 28 36.49E | 5537 | 3987 | 4533 | 3980 | 122 | 0.35 - 28 | 1520 | 49.3 |
| 11 | 199/05 | 36 26 39.16S | 130 00 32.13E | 5548 | 3000 | 3570 | 2990 | 122 | 0.50 - 29 | 1510 | 49.7 |
| 12 | 199/05 | 35 33 34.70S | 130 11 11.83E | 5172 | 4989 | 5580 | 4980 | 305 | 0.45 - 30 | 1550 | 48.4 |
| 13 | 199/06 | 36 10 45.87S | 130 37 04.06E | 5535 | 2301 | 2836 | 2301 | 122 | 0.00 - 27 | 1500 | 50.0 |
| 15 | 199/07 | 36 51 31.41S | 131 02 25.89E | 5559 | 1969 | 2465 | 1960 | 305 | 0.45 - 26 | 1550 | 48.4 |
| 16 | 199/08 | 34 55 12.43S | 131 32 35.25E | 1506 | 3312 | 4005 | 3310 | 122 | 0.10 - 35 | 1550 | 48.4 |
| 17 | 199/08 | 34 14 44.87S | 131 12 05.88E | 1258 | 4934 | 5718 | 4930 | 305 | 0.20 - 40 | 1560 | 48.1 |
| 18 | 199/08 | 33 10 41.77S | 130 39 57.28E | 111 | 7502 | 8640 | 7500 | 18 | 0.10 - 57 | 1390 | 54.0 |
| 19 | 199/09 | 34 39 43.94S | 128 05 26.31E | 4304 | 5395 | 6043 | 5390 | 305 | 0.25 - 33 | 1500 | 50.0 |
| 20 | 199/10 | 37 11 56.02S | 131 39 24.35E | 5562 | 2812 | 3364 | 2810 | 305 | 0.10 - 28 | 1470 | 51.0 |
| 22 | 199/10 | 36 04 52.90S | 131 55 27.23E | 4939 | 5338 | 5955 | 5330 | 122 | 0.40 - 32 | 1640 | 45.7 |
| 26 | 199/11 | 36 22 21.85S | 132 17 19.83E | 5550 | 2586 | 3224 | 2580 | 122 | 0.30 - 33 | 1530 | 49.0 |

**Notes:**

1. The nominal shotpoint interval for the survey was 50 m.
2. Shading identifies the sonobuoys that were not modelled.
3. The latitude/longitude pair is the location of the launch SP.
4. adav = apparent direct arrival velocity. The missing sonobuoy numbers were assigned to devices that either sank immediately on launching, or stopped communicating before any useful data were received from them.
5. Column ‘Scaled SP interval ‘ shows the variation of the SP interval caused by sonobuoy drift.

## Appendix 3B: Refraction Velocities from Survey 199

Note 1: middle columns 'Depth top' to 'twt base' summarise the 1-D model of refraction-based velocities and depths at the sonobuoy released location, while end columns 'Depth top' to 'twt base' represent the 1-D model averaged across the shotpoint range of the original 2-D model produced in the MacRay software.
Note 2: The twt was calculated from the depths and velocities obtained from the model; twt facilitates the matching of velocities to the seismic section.
Note 3: abbreviations are as follows, COB – continent-ocean boundary, MQZ – magnetic quiet zone.

| Sonabuoy No | Survey no | Geographical location | Layer name or no | Depth top | twt top | Velocity top | Thickness | Velocity base | Depth base | twt base | Basis for modelled thickness and velocity | Depth top | twt top | Depth base | twt base |
|---|---|---|---|---|---|---|---|---|---|---|---|---|---|---|---|
| 1 | 199 | abyssal plain | water | 0 | 0 | 1.49 | 5.57 | 1.51 | 5.57 | 7.43 | reflection seismic data | 0 | 0 | 5.57 | 7.42 |
| 1 | 199 | abyssal plain | post-Miocene | 5.57 | 7.43 | 1.89 | 0.21 | 1.91 | 5.78 | 7.65 | reflection seismic data | 5.57 | 7.42 | 5.78 | 7.65 |
| 1 | 199 | abyssal plain | Dugong | | | | | | | | interpretation uncertain | | | | |
| 1 | 199 | abyssal plain | Wobbegong | | | | | | | | interpretation uncertain | | | | |
| 1 | 199 | abyssal plain | volcanic | 5.78 | 7.65 | 2.09 | 0.51 | 2.11 | 6.29 | 8.13 | reflection seismic data | 5.78 | 7.65 | 6.2 | 8.05 |
| 1 | 199 | abyssal plain | Hammerhead | | | | | | | | layer absent | | | | |
| 1 | 199 | abyssal plain | Tiger | | | | | | | | layer absent | | | | |
| 1 | 199 | abyssal plain | White pointer | | | | | | | | layer absent | | | | |
| 1 | 199 | abyssal plain | Blue whale | | | | | | | | layer absent | | | | |
| 1 | 199 | abyssal plain | Bronze whaler | | | | | | | | layer absent | | | | |
| 1 | 199 | abyssal plain | Southern right | | | | | | | | layer absent | | | | |
| 1 | 199 | abyssal plain | Minke | | | | | | | | layer absent | | | | |
| 1 | 199 | abyssal plain | Sea Lion | | | | | | | | layer absent | | | | |
| 1 | 199 | abyssal plain | layer 1 (base) | 6.29 | 8.13 | 2.29 | 0.05 | 2.31 | 6.34 | 8.18 | reflection seismic data | 6.2 | 8.05 | 6.29 | 8.12 |
| 1 | 199 | abyssal plain | layer 2 | 6.34 | 8.18 | 4.1 | 0.95 | 4.3 | 7.29 | 8.63 | primary refraction | 6.29 | 8.12 | 7.34 | 8.62 |
| 1 | 199 | abyssal plain | layer 3 | 7.29 | 8.63 | 5.7 | 1.74 | 6.1 | 9.03 | 9.22 | primary refraction | 7.34 | 8.62 | 9.1 | 9.22 |
| 1 | 199 | abyssal plain | layer 4 | 9.03 | 9.22 | 6.8 | 5.78 | 7 | 14.81 | 10.9 | primary refraction | 9.1 | 9.22 | 14.71 | 10.85 |
| 2 | 199 | COB | water | 0 | 0 | 1.49 | 5.53 | 1.51 | 5.53 | 7.37 | reflection seismic data | 0 | 0 | 5.5 | 7.34 |
| 2 | 199 | COB | post-Miocene | | | | | | | | layer absent | | | | |
| 2 | 199 | COB | Dugong | 5.53 | 7.37 | 1.69 | 0.29 | 1.71 | 5.82 | 7.71 | reflection seismic data | 5.5 | 7.34 | 5.6 | 7.45 |
| 2 | 199 | COB | Wobbegong | 5.82 | 7.71 | 1.89 | 0.31 | 1.91 | 6.13 | 8.04 | reflection seismic data | 5.6 | 7.45 | 5.92 | 7.79 |

| | | | | | | | | | | | | | | | |
|---|---|---|---|---|---|---|---|---|---|---|---|---|---|---|---|
| 2 | 199 | COB | volcanic | | | | | | | | interpretation uncertain | | | | |
| 2 | 199 | COB | Hammerhead | | | | | | | | interpretation uncertain | | | | |
| 2 | 199 | COB | Tiger | 6.13 | 8.04 | 2.19 | 0.03 | 2.21 | 6.16 | 8.06 | reflection seismic data | 5.92 | 7.79 | 6.18 | 8.02 |
| 2 | 199 | COB | White pointer | | | | | | | | interpretation uncertain | | | | |
| 2 | 199 | COB | Blue whale | | | | | | | | probably absent | | | | |
| 2 | 199 | COB | Bronze whaler | | | | | | | | layer absent | | | | |
| 2 | 199 | COB | Southern right | | | | | | | | layer absent | | | | |
| 2 | 199 | COB | Minke | | | | | | | | layer absent | | | | |
| 2 | 199 | COB | Sea Lion | | | | | | | | layer absent | | | | |
| 2 | 199 | COB | layer 1 (base) | 6.16 | 8.06 | 3.9 | 0.05 | 4.1 | 6.21 | 8.09 | reflection seismic data | 6.18 | 8.02 | 6.95 | 8.41 |
| 2 | 199 | COB | layer 2 | 6.21 | 8.09 | 4.4 | 1.92 | 4.6 | 8.12 | 8.94 | primary refraction | 6.95 | 8.41 | 11.37 | 10.37 |
| 2 | 199 | COB | layer 3 | 8.12 | 8.94 | 5.5 | 3.19 | 5.7 | 11.32 | 10.08 | primary refraction | 11.37 | 10.37 | 13.2 | 11.03 |
| 2 | 199 | COB | layer 4 | 11.32 | 10.08 | 5.9 | 4.38 | 6.4 | 15.69 | 11.51 | primary refraction | 13.2 | 11.03 | 15.9 | 11.91 |
| 2 | 199 | COB | | | | | | | | | thickness uncertain | | | | |
| 2 | 199 | COB | upper mantle | 15.69 | 11.51 | 7.9 | n/a | 7.9 | n/a | n/a | possible near Moho | 15.69 | 11.91 | n/a | n/a |
| 5 | 199 | abyssal plain | water | 0 | 0 | 1.49 | 5.55 | 1.51 | 5.55 | 7.4 | reflection seismic data | 0 | 0 | 5.55 | 7.4 |
| 5 | 199 | abyssal plain | post-Miocene | 5.55 | 7.4 | 1.69 | 0.12 | 1.71 | 5.68 | 7.55 | reflection seismic data | 5.55 | 7.4 | 5.67 | 7.54 |
| 5 | 199 | abyssal plain | Dugong | 5.68 | 7.55 | 1.99 | 0.4 | 2.01 | 6.08 | 7.95 | reflection seismic data | 5.67 | 7.54 | 6.1 | 7.98 |
| 5 | 199 | abyssal plain | Wobbegong | | | | | | | | interpretation uncertain | | | | |
| 5 | 199 | abyssal plain | volcanic | 6.08 | 7.95 | 2.29 | 0.58 | 2.31 | 6.65 | 8.45 | reflection seismic data | 6.1 | 7.98 | 6.41 | 8.24 |
| 5 | 199 | abyssal plain | Hammerhead | | | | | | | | interpretation uncertain | | | | |
| 5 | 199 | abyssal plain | Tiger | | | | | | | | layer absent | | | | |
| 5 | 199 | abyssal plain | White pointer | | | | | | | | layer absent | | | | |
| 5 | 199 | abyssal plain | Blue whale | | | | | | | | layer absent | | | | |
| 5 | 199 | abyssal plain | Bronze whaler | | | | | | | | layer absent | | | | |
| 5 | 199 | abyssal plain | Southern right | | | | | | | | layer absent | | | | |
| 5 | 199 | abyssal plain | Minke | | | | | | | | layer absent | | | | |
| 5 | 199 | abyssal plain | Sea Lion | | | | | | | | layer absent | | | | |
| 5 | 199 | abyssal plain | layer 1 (base) | 6.65 | 8.45 | 2.49 | 0.14 | 2.51 | 6.79 | 8.56 | reflection seismic data | 6.41 | 8.24 | 6.6 | 8.39 |
| 5 | 199 | abyssal plain | layer 2 | 6.79 | 8.56 | 3.8 | 0.85 | 4 | 7.64 | 9 | reflection seismic data | 6.6 | 8.39 | 7.64 | 8.93 |
| 5 | 199 | abyssal plain | layer 3 | 7.64 | 9 | 5.3 | 1.53 | 5.5 | 9.17 | 9.56 | primary refraction | 7.64 | 8.93 | 9.17 | 9.49 |
| 5 | 199 | abyssal plain | layer 4 | 9.17 | 9.56 | 6.3 | 4.94 | 6.5 | 14.11 | 11.11 | primary refraction | 9.17 | 9.49 | 14.29 | 11.09 |
| 5 | 199 | abyssal plain | | | | | | | | | thickness uncertain | | | | |
| 5 | 199 | abyssal plain | upper mantle | 14.11 | 11.11 | 7.9 | n/a | 7.9 | n/a | n/a | possible near Moho | 14.11 | 11.09 | n/a | n/a |
| 6 | 199 | near-COB | water | 0 | 0 | 1.49 | 5.55 | 1.51 | 5.55 | 7.4 | reflection seismic data | 0 | 0 | 5.54 | 7.39 |

| | | | | | | | | | | | | | | | |
|---|---|---|---|---|---|---|---|---|---|---|---|---|---|---|---|
| 6 | 199 | near-COB | post-Miocene | 5.55 | 7.4 | 1.69 | 0.15 | 1.71 | 5.7 | 7.57 | reflection seismic data | 5.54 | 7.39 | 5.7 | 7.58 |
| 6 | 199 | near-COB | Dugong | 5.7 | 7.57 | 1.89 | 0.28 | 1.91 | 5.98 | 7.87 | reflection seismic data | 5.7 | 7.58 | 5.99 | 7.88 |
| 6 | 199 | near-COB | Wobbegong | 5.98 | 7.87 | 1.99 | 0.02 | 2.01 | 6 | 7.89 | reflection seismic data | 5.99 | 7.88 | 6.29 | 8.18 |
| 6 | 199 | near-COB | volcanic | | | | | | | | interpretation uncertain | | | | |
| 6 | 199 | near-COB | Hammerhead | 6 | 7.89 | 2.29 | 0.02 | 2.31 | 6.02 | 7.91 | reflection seismic data | 6.29 | 8.18 | 6.56 | 8.42 |
| 6 | 199 | near-COB | Tiger | 6.02 | 7.91 | 2.89 | 0.11 | 2.91 | 6.13 | 7.99 | reflection seismic data | 6.56 | 8.42 | 6.76 | 8.55 |
| 6 | 199 | near-COB | White pointer | | | | | | | | interpretation uncertain | | | | |
| 6 | 199 | near-COB | Blue whale | | | | | | | | interpretation uncertain | | | | |
| 6 | 199 | near-COB | Bronze whaler | | | | | | | | interpretation uncertain | | | | |
| 6 | 199 | near-COB | Southern right | | | | | | | | layer probably absent | | | | |
| 6 | 199 | near-COB | Minke | | | | | | | | layer probably absent | | | | |
| 6 | 199 | near-COB | Sea Lion | | | | | | | | layer probably absent | | | | |
| 6 | 199 | near-COB | layer 1 | 6.13 | 7.99 | 3.4 | 0.05 | 3.6 | 6.18 | 8.01 | reflection seismic data | 6.76 | 8.55 | 7.34 | 8.88 |
| 6 | 199 | near-COB | layer 2 | 6.18 | 8.01 | 3.7 | 1.32 | 4.3 | 7.5 | 8.67 | refraction/reflection | 7.34 | 8.88 | 9.1 | 9.77 |
| 6 | 199 | near-COB | lower crust ? | 7.5 | 8.67 | 6.2 | 1.81 | 6.4 | 9.31 | 9.25 | primary refraction | 9.1 | 9.77 | 10.69 | 10.27 |
| 9 | 199 | MQZ | water | 0 | 0 | 1.49 | 4.85 | 1.51 | 4.85 | 6.46 | reflection seismic data | 0 | 0 | 5.03 | 6.7 |
| 9 | 199 | MQZ | post-Miocene | | | | | | | | layer absent | | | | |
| 9 | 199 | MQZ | Dugong | | | | | | | | layer absent | | | | |
| 9 | 199 | MQZ | Wobbegong | 4.85 | 6.46 | 1.74 | 0.2 | 1.76 | 5.05 | 6.69 | reflection seismic data | 5.03 | 6.7 | 5.28 | 7 |
| 9 | 199 | MQZ | volcanic | | | | | | | | layer absent | | | | |
| 9 | 199 | MQZ | Hammerhead | 5.05 | 6.69 | 1.89 | 0.36 | 1.91 | 5.41 | 7.08 | reflection seismic data | 5.28 | 7 | 5.48 | 7.2 |
| 9 | 199 | MQZ | Tiger | | | | | | | | interpretation uncertain | | | | |
| 9 | 199 | MQZ | White pointer | | | | | | | | interpretation uncertain | | | | |
| 9 | 199 | MQZ | Blue whale | | | | | | | | interpretation uncertain | | | | |
| 9 | 199 | MQZ | Bronze whaler | | | | | | | | interpretation uncertain | | | | |
| 9 | 199 | MQZ | Southern right | | | | | | | | interpretation uncertain | | | | |
| 9 | 199 | MQZ | Minke | | | | | | | | interpretation uncertain | | | | |
| 9 | 199 | MQZ | Sea Lion | | | | | | | | interpretation uncertain | | | | |
| 9 | 199 | MQZ | layer 1 | 5.41 | 7.08 | 2.79 | 1.53 | 2.81 | 6.94 | 8.17 | reflection seismic data | 5.48 | 7.2 | 6.94 | 8.25 |
| 9 | 199 | MQZ | layer 2 | 6.94 | 8.17 | 4 | 0.83 | 4.2 | 7.78 | 8.58 | primary refraction | 6.94 | 8.25 | 7.78 | 8.65 |
| 9 | 199 | MQZ | layer 3 | 7.78 | 8.58 | 4.6 | 2.22 | 4.8 | 10 | 9.52 | primary refraction | 7.78 | 8.65 | 10 | 9.6 |
| 9 | 199 | MQZ | upper crust ? | 10 | 9.52 | 6.3 | 0.83 | 6.5 | 10.83 | 9.78 | primary refraction | 10 | 9.6 | 10.92 | 9.89 |
| 9 | 199 | MQZ | lower crust ? | 10.83 | 9.78 | 6.6 | 6.67 | 6.8 | 17.5 | 11.77 | pre-critical/reflection | 10.92 | 9.89 | 15.11 | 11.14 |
| 9 | 199 | MQZ | upper mantle | 17.5 | 11.77 | | n/a | ? | n/a | n/a | pre-critical/reflection | 22.68 | 11.14 | ? | ? |
| 10 | 199 | COB | water | 0 | 0 | 1.49 | 5.55 | 1.51 | 5.55 | 7.39 | reflection seismic data | 0 | 0 | 5.55 | 7.41 |

| | | | | | | | | | | | | | | | |
|---|---|---|---|---|---|---|---|---|---|---|---|---|---|---|---|
| 10 | 199 | COB | post-Miocene | 5.55 | 7.39 | 1.69 | 0.17 | 1.71 | 5.72 | 7.6 | reflection seismic data | 5.55 | 7.41 | 5.74 | 7.62 |
| 10 | 199 | COB | Dugong | 5.72 | 7.6 | 2.09 | 0.23 | 2.11 | 5.95 | 7.82 | reflection seismic data | 5.74 | 7.62 | 6.17 | 8.03 |
| 10 | 199 | COB | Wobbegong | 5.95 | 7.82 | 2.29 | 0.46 | 2.31 | 6.41 | 8.22 | reflection seismic data | 6.17 | 8.03 | 6.59 | 8.4 |
| 10 | 199 | COB | volcanic | | | | | | | | interpretation uncertain | | | | |
| 10 | 199 | COB | Hammerhead | 6.41 | 8.22 | 2.39 | 0.37 | 2.41 | 6.77 | 8.52 | reflection seismic data | 6.59 | 8.4 | 6.82 | 8.59 |
| 10 | 199 | COB | Tiger | 6.77 | 8.52 | 2.49 | 0.24 | 2.51 | 7.01 | 8.71 | reflection seismic data | 6.82 | 8.59 | 7.02 | 8.75 |
| 10 | 199 | COB | White pointer | | | | | | | | interpretation uncertain | | | | |
| 10 | 199 | COB | Blue whale | | | | | | | | interpretation uncertain | | | | |
| 10 | 199 | COB | Bronze whaler | | | | | | | | interpretation uncertain | | | | |
| 10 | 199 | COB | Southern right | | | | | | | | interpretation uncertain | | | | |
| 10 | 199 | COB | Minke | | | | | | | | interpretation uncertain | | | | |
| 10 | 199 | COB | Sea Lion | | | | | | | | interpretation uncertain | | | | |
| 10 | 199 | COB | layer 1 | 7.01 | 8.71 | 3.5 | 1.81 | 3.7 | 8.82 | 9.71 | refraction modelling | 7.02 | 8.75 | 7.87 | 9.22 |
| 10 | 199 | COB | layer 2 | 8.82 | 9.71 | 4.3 | 1.04 | 4.5 | 9.86 | 10.19 | refraction modelling | 7.87 | 9.22 | 9.42 | 9.92 |
| 10 | 199 | COB | lower crust ? | 9.86 | 10.19 | 6.5 | 1.25 | 6.8 | 11.11 | 10.56 | primary refraction | 9.42 | 9.92 | 11.11 | 10.43 |
| 11 | 199 | COB | water | 0 | 0 | 1.49 | 5.56 | 1.51 | 5.56 | 7.41 | reflection seismic data | 0 | 0 | 5.56 | 7.41 |
| 11 | 199 | COB | post-Miocene | 5.56 | 7.41 | 1.92 | 0.2 | 1.94 | 5.76 | 7.62 | reflection seismic data | 5.56 | 7.41 | 5.77 | 7.63 |
| 11 | 199 | COB | Dugong | 5.76 | 7.62 | 1.99 | 0.38 | 2.01 | 6.14 | 8 | reflection seismic data | 5.77 | 7.63 | 6.14 | 8 |
| 11 | 199 | COB | Wobbegong | 6.14 | 8 | 2.09 | 0.03 | 2.11 | 6.16 | 8.02 | reflection seismic data | 6.14 | 8 | 6.58 | 8.42 |
| 11 | 199 | COB | volcanic | | | | | | | | interpretation uncertain | | | | |
| 11 | 199 | COB | Hammerhead | 6.16 | 8.02 | 2.19 | 0.02 | 2.21 | 6.19 | 8.04 | reflection seismic data | 6.58 | 8.42 | 6.72 | 8.55 |
| 11 | 199 | COB | Tiger | 6.19 | 8.04 | 2.49 | 0.01 | 2.51 | 6.2 | 8.05 | reflection seismic data | 6.72 | 8.55 | 6.92 | 8.71 |
| 11 | 199 | COB | White pointer | | | | | | | | interpretation uncertain | | | | |
| 11 | 199 | COB | Blue whale | | | | | | | | interpretation uncertain | | | | |
| 11 | 199 | COB | Bronze whaler | | | | | | | | interpretation uncertain | | | | |
| 11 | 199 | COB | Southern right | | | | | | | | interpretation uncertain | | | | |
| 11 | 199 | COB | Minke | | | | | | | | layer probably absent | | | | |
| 11 | 199 | COB | Sea Lion | | | | | | | | layer probably absent | | | | |
| 11 | 199 | COB | layer 1 | 6.2 | 8.05 | 3.4 | 0.08 | 3.6 | 6.27 | 8.1 | reflection seismic data | 6.92 | 8.71 | 7.45 | 9.01 |
| 11 | 199 | COB | layer 2 | 6.27 | 8.1 | 3.8 | 2.34 | 4 | 8.61 | 9.29 | pre-critical/reflection | 7.45 | 9.01 | 8.91 | 9.76 |
| 11 | 199 | COB | upper crust ? | 8.61 | 9.29 | 6.1 | 2.22 | 6.3 | 10.83 | 10.01 | pre-critical/reflection | 8.91 | 9.76 | 10.76 | 10.36 |
| 11 | 199 | COB | lower crust ? | 10.83 | 10.01 | 6.5 | 2.85 | 6.7 | 13.68 | 10.87 | pre-critical/reflection | 10.76 | 10.36 | 13.01 | 11.04 |
| 12 | 199 | MQZ | water | 0 | 0 | 1.49 | 5.14 | 1.51 | 5.14 | 6.85 | reflection seismic data | 0 | 0 | 4.89 | 6.52 |

| | | | | | | | | | | | | | | | |
|---|---|---|---|---|---|---|---|---|---|---|---|---|---|---|---|
| 12 | 199 | MQZ | post-Miocene | | | | | | | | layer absent | | | | |
| 12 | 199 | MQZ | Dugong | | | | | | | | layer absent | | | | |
| 12 | 199 | MQZ | Wobbegong | 5.14 | 6.85 | 1.79 | 0.33 | 1.81 | 5.46 | 7.21 | reflection seismic data | 4.89 | 6.52 | 5.11 | 6.77 |
| 12 | 199 | MQZ | volcanic | | | | | | | | layer absent | | | | |
| 12 | 199 | MQZ | Hammerhead | 5.46 | 7.21 | 1.89 | 0.33 | 1.91 | 5.8 | 7.56 | reflection seismic data | 5.11 | 6.77 | 5.42 | 7.09 |
| 12 | 199 | MQZ | Tiger | 5.8 | 7.56 | 2.29 | 0.52 | 2.31 | 6.32 | 8.02 | reflection seismic data | 5.42 | 7.09 | 5.67 | 7.31 |
| 12 | 199 | MQZ | White pointer | | | | | | | | interpretation uncertain | | | | |
| 12 | 199 | MQZ | Blue whale | | | | | | | | interpretation uncertain | | | | |
| 12 | 199 | MQZ | Bronze whaler | | | | | | | | interpretation uncertain | | | | |
| 12 | 199 | MQZ | Southern right | | | | | | | | interpretation uncertain | | | | |
| 12 | 199 | MQZ | Minke | | | | | | | | interpretation uncertain | | | | |
| 12 | 199 | MQZ | Sea Lion | | | | | | | | interpretation uncertain | | | | |
| 12 | 199 | MQZ | layer 2 | 6.32 | 8.02 | 3.29 | 1.04 | 3.31 | 7.36 | 8.65 | reflection seismic data | 5.67 | 7.31 | 6.94 | 8.08 |
| 12 | 199 | MQZ | layer 3 | 7.36 | 8.65 | 3.5 | 0.83 | 3.7 | 8.19 | 9.11 | pre-critical reflection | 6.94 | 8.08 | 7.67 | 8.48 |
| 12 | 199 | MQZ | layer 4 | 8.19 | 9.11 | 4.3 | 2.45 | 4.5 | 10.64 | 10.22 | primary refraction | 7.67 | 8.48 | 10.12 | 9.6 |
| 12 | 199 | MQZ | upper crust ? | 10.64 | 10.22 | 5.8 | 1.64 | 6 | 12.28 | 10.78 | primary refraction | 10.12 | 9.6 | 11.84 | 10.18 |
| 12 | 199 | MQZ | lower crust ? | 12.28 | 10.78 | 6.5 | 1.64 | 6.7 | 13.92 | 11.28 | primary refraction | 11.84 | 10.18 | 15.61 | 11.32 |
| 13 | 199 | near-COB | water | 0 | 0 | 1.49 | 5.55 | 1.51 | 5.55 | 7.4 | reflection seismic data | 0 | 0 | 5.56 | 7.41 |
| 13 | 199 | near-COB | post-Miocene | 5.55 | 7.4 | 1.849 | 0.24 | 1.851 | 5.79 | 7.66 | reflection seismic data | 5.56 | 7.41 | 5.81 | 7.68 |
| 13 | 199 | near-COB | Dugong | 5.79 | 7.66 | 2.09 | 0.17 | 2.11 | 5.95 | 7.82 | reflection seismic data | 5.81 | 7.68 | 6.13 | 7.98 |
| 13 | 199 | near-COB | Wobbegong | 5.95 | 7.82 | 2.24 | 0.59 | 2.26 | 6.55 | 8.34 | reflection seismic data | 6.13 | 7.98 | 6.76 | 8.55 |
| 13 | 199 | near-COB | volcanic | | | | | | | | layer absent | | | | |
| 13 | 199 | near-COB | Hammerhead | 6.55 | 8.34 | 2.34 | 0.16 | 2.36 | 6.7 | 8.48 | reflection seismic data | 6.76 | 8.55 | 6.94 | 8.7 |
| 13 | 199 | near-COB | Tiger | | | | | | | | interpretation uncertain | | | | |
| 13 | 199 | near-COB | White pointer | | | | | | | | interpretation uncertain | | | | |
| 13 | 199 | near-COB | Blue whale | | | | | | | | interpretation uncertain | | | | |
| 13 | 199 | near-COB | Bronze whaler | | | | | | | | interpretation uncertain | | | | |
| 13 | 199 | near-COB | Southern right | | | | | | | | interpretation uncertain | | | | |
| 13 | 199 | near-COB | Minke | | | | | | | | layer probably absent | | | | |
| 13 | 199 | near-COB | Sea Lion | | | | | | | | layer probably absent | | | | |
| 13 | 199 | near-COB | layer 1 | 6.7 | 8.48 | 3.2 | 0.82 | 3.4 | 7.52 | 8.97 | reflections/pre-critical | 6.94 | 8.7 | 7.88 | 9.27 |
| 13 | 199 | near-COB | layer 2 | 7.52 | 8.97 | 4.3 | 0.7 | 4.5 | 8.22 | 9.29 | reflections/pre-critical | 7.88 | 9.27 | 8.67 | 9.63 |
| 13 | 199 | near-COB | layer 3 | 8.22 | 9.29 | 5 | 0.93 | 5.5 | 9.14 | 9.64 | primary refraction | 8.67 | 9.63 | 9.65 | 10 |
| 13 | 199 | near-COB | upper crust ? | 9.14 | 9.64 | 5.8 | 0.75 | 6.4 | 9.9 | 9.89 | primary refraction | 9.65 | 10 | 10.33 | 10.23 |
| 13 | 199 | near-COB | lower crust ? | 9.9 | 9.89 | 6.7 | 1.56 | 7.3 | 11.46 | 10.33 | primary refraction | 10.33 | 10.23 | 11.54 | 10.57 |

| | | | | | | | | | | | | | | | |
|---|---|---|---|---|---|---|---|---|---|---|---|---|---|---|---|
| 13 | 199 | near-COB | upper mantle ? | 11.46 | 10.33 | 7.4 | 1.91 | 7.55 | 13.37 | 10.85 | primary refraction | 11.54 | 10.57 | 13.51 | 11.1 |
| 15 | 199 | abyssal plain | water | 0 | 0 | 1.49 | 5.57 | 1.51 | 5.57 | 7.43 | reflection seismic data | 0 | 0 | 5.57 | 7.43 |
| 15 | 199 | abyssal plain | post-Miocene | 5.57 | 7.43 | 1.89 | 0.28 | 1.91 | 5.85 | 7.72 | reflection seismic data | 5.57 | 7.43 | 5.82 | 7.69 |
| 15 | 199 | abyssal plain | Dugong | 5.85 | 7.72 | 2.09 | 0.44 | 2.11 | 6.29 | 8.14 | reflection seismic data | 5.82 | 7.69 | 6.23 | 8.08 |
| 15 | 199 | abyssal plain | Wobbegong | | | | | | | | interpretation uncertain | | | | |
| 15 | 199 | abyssal plain | volcanic | 6.29 | 8.14 | 2.29 | 0.36 | 2.31 | 6.66 | 8.46 | reflection seismic data | 6.23 | 8.08 | 6.51 | 8.32 |
| 15 | 199 | abyssal plain | Hammerhead | | | | | | | | layer absent | | | | |
| 15 | 199 | abyssal plain | Tiger | | | | | | | | layer absent | | | | |
| 15 | 199 | abyssal plain | White pointer | | | | | | | | layer absent | | | | |
| 15 | 199 | abyssal plain | Blue whale | | | | | | | | layer absent | | | | |
| 15 | 199 | abyssal plain | Bronze whaler | | | | | | | | layer absent | | | | |
| 15 | 199 | abyssal plain | Southern right | | | | | | | | layer absent | | | | |
| 15 | 199 | abyssal plain | Minke | | | | | | | | layer absent | | | | |
| 15 | 199 | abyssal plain | Sea Lion | | | | | | | | layer absent | | | | |
| 15 | 199 | abyssal plain | layer 1 (base) | 6.66 | 8.46 | 2.49 | 0.12 | 2.51 | 6.77 | 8.55 | reflection seismic data | 6.51 | 8.32 | 6.65 | 8.44 |
| 15 | 199 | abyssal plain | layer 2 | 6.77 | 8.55 | 4.4 | 0.59 | 4.6 | 7.36 | 8.81 | primary refractions | 6.65 | 8.44 | 7.5 | 8.81 |
| 15 | 199 | abyssal plain | layer 3 | 7.36 | 8.81 | 5 | 2.22 | 5.2 | 9.58 | 9.69 | primary refractions | 7.5 | 8.81 | 9.86 | 9.74 |
| 16 | 199 | Ceduna Terrace | water | 0 | 0 | 1.49 | 1.46 | 1.51 | 1.53 | 2.04 | reflection seismic data | 0 | 0 | 1.47 | 1.96 |
| 16 | 199 | Ceduna Terrace | post-Miocene | 1.53 | 1.94 | 1.69 | 0.3 | 1.71 | 1.75 | 2.29 | reflection seismic data | 1.47 | 1.96 | 1.72 | 2.26 |
| 16 | 199 | Ceduna Terrace | Dugong | | | | | | | | interpretation uncertain | | | | |
| 16 | 199 | Ceduna Terrace | Wobbegong | 1.75 | 2.29 | 1.89 | 0.13 | 1.91 | 1.89 | 2.43 | reflection seismic data | 1.72 | 2.26 | 1.86 | 2.4 |
| 16 | 199 | Ceduna Terrace | volcanic | | | | | | | | layer absent | | | | |
| 16 | 199 | Ceduna Terrace | Hammerhead | 1.89 | 2.43 | 2.09 | 1.12 | 2.11 | 3.01 | 3.5 | reflection seismic data | 1.86 | 2.4 | 3.01 | 3.5 |
| 16 | 199 | Ceduna Terrace | Tiger | 3.01 | 3.5 | 3.4 | 0.81 | 3.6 | 3.82 | 3.96 | primary refractions | 3.01 | 3.5 | 3.79 | 3.94 |
| 16 | 199 | Ceduna Terrace | White pointer | | | | | | | | interpretation uncertain | | | | |
| 16 | 199 | Ceduna Terrace | Blue whale | | | | | | | | interpretation uncertain | | | | |
| 16 | 199 | Ceduna Terrace | Bronze whaler | | | | | | | | interpretation uncertain | | | | |
| 16 | 199 | Ceduna Terrace | Southern right | | | | | | | | interpretation uncertain | | | | |
| 16 | 199 | Ceduna Terrace | Minke | | | | | | | | interpretation uncertain | | | | |
| 16 | 199 | Ceduna Terrace | Sea Lion | | | | | | | | interpretation uncertain | | | | |
| 16 | 199 | Ceduna Terrace | layer 1 | 3.82 | 3.96 | 3.8 | 1.32 | 4 | 5.14 | 4.64 | primary refractions | 3.79 | 3.94 | 5.19 | 4.66 |
| 16 | 199 | Ceduna Terrace | layer 2 | 5.14 | 4.64 | 4.15 | 1.83 | 4.35 | 6.97 | 5.5 | primary refractions | 5.19 | 4.66 | 6.86 | 5.45 |
| 19 | 199 | MQZ | water | 0 | 0 | 1.49 | 4.32 | 1.51 | 4.32 | 5.76 | reflection seismic data | 0 | 0 | 4.4 | 5.87 |
| 19 | 199 | MQZ | post-Miocene | 4.32 | 5.76 | 1.54 | 0.16 | 1.56 | 4.48 | 5.97 | reflection seismic data | 4.4 | 5.87 | 4.55 | 6.06 |
| 19 | 199 | MQZ | Dugong | | | | | | | | layer absent | | | | |

| | | | | | | | | | | | | | | | |
|---|---|---|---|---|---|---|---|---|---|---|---|---|---|---|---|
| 19 | 199 | MQZ | Wobbegong | 4.48 | 5.97 | 1.59 | 0.11 | 1.61 | 4.59 | 6.1 | reflection seismic data | 4.55 | 6.06 | 4.66 | 6.2 |
| 19 | 199 | MQZ | volcanic | | | | | | | | layer absent | | | | |
| 19 | 199 | MQZ | Hammerhead | 4.59 | 6.1 | 1.69 | 0.15 | 1.71 | 4.73 | 6.27 | reflection seismic data | 4.66 | 6.2 | 4.86 | 6.43 |
| 19 | 199 | MQZ | Tiger | 4.73 | 6.27 | 1.79 | 0.44 | 1.81 | 5.17 | 6.76 | reflection seismic data | 4.86 | 6.43 | 5.21 | 6.83 |
| 19 | 199 | MQZ | White pointer | 5.17 | 6.76 | 2.29 | 0.59 | 2.31 | 5.76 | 7.27 | reflection seismic data | 5.21 | 6.83 | 5.9 | 7.42 |
| 19 | 199 | MQZ | Blue whale | 5.76 | 7.27 | 2.59 | 0.28 | 2.61 | 6.04 | 7.49 | reflection seismic data | 5.9 | 7.42 | 6.16 | 7.62 |
| 19 | 199 | MQZ | arbitrary | 6.04 | 7.49 | 3.1 | 0.52 | 3.3 | 6.56 | 7.81 | reflection seismic data | 6.16 | 7.62 | 6.65 | 7.93 |
| 19 | 199 | MQZ | Bronze whaler | 6.56 | 7.81 | 4.15 | 1.22 | 4.35 | 7.78 | 8.39 | primary refraction | 6.65 | 7.93 | 7.82 | 8.48 |
| 19 | 199 | MQZ | Southern right | 7.78 | 8.39 | 5 | 1.57 | 5.2 | 9.35 | 9 | primary refraction | 7.82 | 8.48 | 9.44 | 9.12 |
| 19 | 199 | MQZ | Minke | 9.35 | 9 | 5.6 | 1.86 | 5.8 | 11.2 | 9.65 | primary refraction | 9.44 | 9.12 | 11.22 | 9.74 |
| 19 | 199 | MQZ | Sea Lion | | | | | | | | interpretation uncertain | | | | |
| 19 | 199 | MQZ | upper crust ? | 11.2 | 9.65 | 5.9 | 1.94 | 6.1 | 13.15 | 10.3 | primary refraction | 11.22 | 9.74 | 12.89 | 10.3 |
| 20 | 199 | abyssal plain | water | 0 | 0 | 1.49 | 5.57 | 1.51 | 5.57 | 7.43 | reflection seismic data | 0 | 0 | 5.57 | 7.43 |
| 20 | 199 | abyssal plain | post-Miocene | 5.57 | 7.43 | 1.86 | 0.31 | 1.88 | 5.88 | 7.76 | reflection seismic data | 5.57 | 7.43 | 5.85 | 7.73 |
| 20 | 199 | abyssal plain | Dugong | 5.88 | 7.76 | 2.09 | 0.6 | 2.11 | 6.48 | 8.33 | reflection seismic data | 5.85 | 7.73 | 6.29 | 8.15 |
| 20 | 199 | abyssal plain | Wobbegong | 6.48 | 8.33 | 2.49 | 0.17 | 2.51 | 6.65 | 8.46 | reflection seismic data | 6.29 | 8.15 | 6.45 | 8.27 |
| 20 | 199 | abyssal plain | volcanic(base) | 6.65 | 8.46 | 2.59 | 0.23 | 2.61 | 6.88 | 8.64 | reflection seismic data | 6.45 | 8.27 | 6.76 | 8.52 |
| 20 | 199 | abyssal plain | Potoroo | | | | | | | | layer absent | | | | |
| 20 | 199 | abyssal plain | Wigunda | | | | | | | | layer absent | | | | |
| 20 | 199 | abyssal plain | Platypus | | | | | | | | layer absent | | | | |
| 20 | 199 | abyssal plain | Ceduna | | | | | | | | layer absent | | | | |
| 20 | 199 | abyssal plain | Numbat | | | | | | | | layer absent | | | | |
| 20 | 199 | abyssal plain | Borda | | | | | | | | layer absent | | | | |
| 20 | 199 | abyssal plain | Neptune | | | | | | | | layer absent | | | | |
| 20 | 199 | abyssal plain | Echidna | | | | | | | | layer absent | | | | |
| 20 | 199 | abyssal plain | Loongana | | | | | | | | layer absent | | | | |
| 20 | 199 | abyssal plain | layer 1 | 6.88 | 8.64 | 2.9 | 0.28 | 3.1 | 7.15 | 8.82 | reflection seismic data | 6.76 | 8.52 | 7.04 | 8.7 |
| 20 | 199 | abyssal plain | layer 2 | 7.15 | 8.82 | 3.4 | 0.33 | 3.6 | 7.48 | 9.01 | reflection seismic data | 7.04 | 8.7 | 7.63 | 9.04 |
| 20 | 199 | abyssal plain | layer 3 | 7.48 | 9.01 | 3.8 | 0.23 | 4 | 7.71 | 9.13 | reflection seismic data | 7.63 | 9.04 | 7.93 | 9.19 |
| 20 | 199 | abyssal plain | layer 4 | 7.71 | 9.13 | 5.5 | 0.62 | 5.7 | 8.33 | 9.35 | primary refraction | 7.93 | 9.19 | 8.42 | 9.36 |
| 20 | 199 | abyssal plain | layer 5 | 8.33 | 9.35 | 6.2 | 1.88 | 6.4 | 10.21 | 9.95 | primary refraction | 8.42 | 9.36 | 10.17 | 9.92 |
| 20 | 199 | abyssal plain | layer 6 | 10.21 | 9.95 | 7.2 | 3.46 | 7.4 | 13.66 | 10.89 | primary refraction | 10.17 | 9.92 | 13.97 | 10.96 |
| 22 | 199 | MQZ | water | 0 | 0 | 1.49 | 4.96 | 1.51 | 4.96 | 6.62 | reflection seismic data | 0 | 0 | 4.58 | 6.11 |
| 22 | 199 | MQZ | post-Miocene | | | | | | | | layer absent | | | | |
| 22 | 199 | MQZ | Dugong | | | | | | | | layer absent | | | | |

| | | | | | | | | | | | | | | | |
|---|---|---|---|---|---|---|---|---|---|---|---|---|---|---|---|
| 22 | 199 | MQZ | Wobbegong | 4.96 | 6.62 | 1.79 | 0.66 | 1.81 | 5.62 | 7.35 | reflection seismic data | 4.58 | 6.11 | 4.83 | 6.38 |
| 22 | 199 | MQZ | volcanic | | | | | | | | layer absent | | | | |
| 22 | 199 | MQZ | Hammerhead | 5.62 | 7.35 | 1.99 | 0.14 | 2.01 | 5.75 | 7.48 | reflection seismic data | 4.83 | 6.38 | 4.97 | 6.52 |
| 22 | 199 | MQZ | Tiger | 5.75 | 7.48 | 2.09 | 0.18 | 2.11 | 5.94 | 7.66 | reflection seismic data | 4.97 | 6.52 | 5.2 | 6.74 |
| 22 | 199 | MQZ | White pointer | | | | | | | | interpretation uncertain | | | | |
| 22 | 199 | MQZ | Blue whale | | | | | | | | interpretation uncertain | | | | |
| 22 | 199 | MQZ | Bronze whaler | | | | | | | | interpretation uncertain | | | | |
| 22 | 199 | MQZ | Southern right | | | | | | | | interpretation uncertain | | | | |
| 22 | 199 | MQZ | Minke | | | | | | | | interpretation uncertain | | | | |
| 22 | 199 | MQZ | Sea Lion | | | | | | | | interpretation uncertain | | | | |
| 22 | 199 | MQZ | layer 1 | 5.94 | 7.66 | 2.69 | 0.73 | 2.71 | 6.67 | 8.2 | primary refraction | 5.2 | 6.74 | 7.03 | 8.1 |
| 22 | 199 | MQZ | layer 2 | 6.67 | 8.2 | 3.9 | 1.67 | 4.1 | 8.33 | 9.03 | primary refraction | 7.03 | 8.1 | 9.16 | 9.17 |
| 22 | 199 | MQZ | layer 3 | 8.33 | 9.03 | 5.1 | 0.97 | 5.3 | 9.31 | 9.4 | primary refraction | 9.16 | 9.17 | 11.22 | 9.96 |
| 22 | 199 | MQZ | upper crust ? | 9.31 | 9.4 | 6.1 | 1.11 | 6.3 | 10.42 | 9.76 | primary refraction | 11.22 | 9.96 | 12.32 | 10.31 |
| 22 | 199 | MQZ | upper mantle ? | 10.42 | 9.76 | 7.1 | 5.42 | 7.3 | 15.83 | 11.27 | primary refraction | 12.32 | 10.31 | 16.15 | 11.38 |
| 26 | 199 | MQZ | water | 0 | 0 | 1.49 | 5.57 | 1.51 | 5.57 | 7.42 | reflection seismic data | 0 | 0 | 5.55 | 7.4 |
| 26 | 199 | MQZ | post-Miocene | 5.57 | 7.42 | 1.59 | 0.03 | 1.61 | 5.6 | 7.46 | reflection seismic data | 5.55 | 7.4 | 5.72 | 7.61 |
| 26 | 199 | MQZ | Dugong | 5.6 | 7.46 | 1.69 | 0.03 | 1.71 | 5.63 | 7.5 | reflection seismic data | 5.72 | 7.61 | 5.87 | 7.79 |
| 26 | 199 | MQZ | Wobbegong | 5.63 | 7.5 | 1.79 | 0.35 | 1.81 | 5.98 | 7.89 | reflection seismic data | 5.87 | 7.79 | 6.21 | 8.17 |
| 26 | 199 | MQZ | volcanic | | | | | | | | layer absent | | | | |
| 26 | 199 | MQZ | Hammerhead | | | | | | | | interpretation uncertain | | | | |
| 26 | 199 | MQZ | Tiger | | | | | | | | interpretation uncertain | | | | |
| 26 | 199 | MQZ | White pointer | | | | | | | | interpretation uncertain | | | | |
| 26 | 199 | MQZ | Blue whale | | | | | | | | interpretation uncertain | | | | |
| 26 | 199 | MQZ | Bronze whaler | | | | | | | | interpretation uncertain | | | | |
| 26 | 199 | MQZ | Southern right | | | | | | | | interpretation uncertain | | | | |
| 26 | 199 | MQZ | Minke | | | | | | | | layer absent | | | | |
| 26 | 199 | MQZ | Sea Lion | | | | | | | | layer absent | | | | |
| 26 | 199 | MQZ | layer 1 | 5.98 | 7.89 | 1.99 | 0.5 | 2.01 | 6.49 | 8.39 | reflection seismic data | 6.21 | 8.17 | 6.34 | 8.29 |
| 26 | 199 | MQZ | Paleozoic ? | 6.49 | 8.39 | 3.49 | 0.49 | 3.51 | 6.98 | 8.68 | reflection seismic data | 6.34 | 8.29 | 6.67 | 8.49 |
| 26 | 199 | MQZ | layer 2 | 6.98 | 8.68 | 4.9 | 1.08 | 5 | 8.06 | 9.11 | reflection seismic data | 6.67 | 8.49 | 8.68 | 9.3 |
| 26 | 199 | MQZ | upper crust ? | 8.06 | 9.11 | 5.8 | 4.17 | 6 | 12.22 | 10.52 | primary refraction | 8.68 | 9.3 | 12.29 | 10.52 |

# Appendix 3C: Refraction Velocities from *Eltanin* Cruise 55 and *Vema* Cruise 33

Depths and velocities were calculated from refraction data obtained from sonobuoy instruments. Tables show depth (in km) and interval velocity (in km/s). Talwani et al. (1978) modelled the data from *Eltanin* Cruise 55 (i.e. 'EL' prefix) and König & Talwani (1977) modelled the data from *Vema* Cruise 33 (i.e. 'V' prefix).

EL41A-5

| Depth | Velocity | twt (s) |
|---|---|---|
| 0 | 1.5 | 0 |
| 5.54 | 1.5 | 7.39 |
| 5.54 | 2.43 | 7.39 |
| 6.66 | 2.43 | 8.31 |

EL53-41

| Depth | velocity | twt (s) |
|---|---|---|
| 0 | 1.5 | 0 |
| 5.56 | 1.5 | 7.41 |
| 5.56 | 2.44 | 7.41 |
| 6.4 | 2.44 | 8.1 |
| 6.4 | 2.56 | 8.1 |
| 7.38 | 2.56 | 8.87 |
| 7.38 | 2.9 | 8.87 |
| 7.9 | 2.9 | 9.23 |

EL53-42

| Depth | velocity | twt (s) |
|---|---|---|
| 0 | 1.5 | 0 |
| 5.55 | 1.5 | 7.40 |
| 5.55 | 2.1 | 7.40 |
| 6.64 | 2.1 | 8.44 |
| 6.64 | 3 | 8.44 |
| 7.14 | 3 | 8.77 |
| 7.14 | 3.6 | 8.77 |
| 7.92 | 3.6 | 9.20 |

EL53-43

| Depth | velocity | twt (s) |
|---|---|---|
| 0 | 1.5 | 0 |
| 5.55 | 1.5 | 7.4 |
| 5.55 | 1.87 | 7.4 |
| 6.51 | 1.87 | 8.43 |
| 6.51 | 2.86 | 8.43 |
| 7.27 | 2.86 | 8.96 |
| 7.27 | 3.6 | 8.96 |
| 7.91 | 3.6 | 9.31 |

EL53-44

| Depth | velocity | twt (s) |
|---|---|---|
| 0 | 1.5 | 0 |
| 5.55 | 1.5 | 7.4 |
| 5.55 | 1.63 | 7.4 |
| 6.27 | 1.63 | 8.28 |
| 6.27 | 3.1 | 8.28 |
| 7.03 | 3.1 | 8.77 |
| 7.03 | 3.6 | 8.77 |
| 8.25 | 3.6 | 9.45 |
| 8.25 | 5.8 | 9.45 |

EL53-46

| depth | velocity | twt (s) |
|---|---|---|
| 0 | 1.5 | 0 |
| 3.29 | 1.5 | 4.39 |
| 3.29 | 2 | 4.39 |
| 4.02 | 2 | 5.12 |
| 4.02 | 2.45 | 5.12 |
| 4.67 | 2.45 | 5.65 |
| 4.67 | 3 | 5.65 |

EL53-47

| depth | velocity | twt (s) |
|---|---|---|
| 0 | 1.5 | 0 |
| 2.64 | 1.5 | 3.52 |
| 2.64 | 2 | 3.52 |
| 3.92 | 2 | 4.8 |
| 3.92 | 2.45 | 4.8 |
| 4.35 | 2.45 | 5.15 |

| | | |
|---|---|---|
| 4.35 | 3.13 | 5.15 |

EL53-48

| Depth | velocity | twt (s) |
|---|---|---|
| 0 | 1.5 | 0 |
| 0.13 | 1.5 | 0.17 |
| 0.13 | 2 | 0.17 |
| 0.43 | 2 | 0.47 |
| 0.43 | 2.9 | 0.47 |
| 1.47 | 2.9 | 1.19 |
| 1.47 | 6.6 | 1.19 |

EL53-51

| depth | velocity | twt (s) |
|---|---|---|
| 0 | 1.5 | 0 |
| 3.46 | 1.5 | 4.61 |
| 3.46 | 2.58 | 4.61 |
| 4.45 | 2.58 | 5.38 |
| 4.45 | 3 | 5.38 |
| 5.63 | 3 | 6.17 |
| 5.63 | 4.9 | 6.17 |
| 6.26 | 4.9 | 6.42 |
| 6.26 | 5.8 | 6.42 |

V33-8

| depth | velocity | twt (s) |
|---|---|---|
| 0 | 1.5 | 0 |
| 5.59 | 1.5 | 7.45 |
| 5.59 | 1.8 | 7.45 |
| 6.05 | 1.8 | 7.96 |
| 6.05 | 4.8 | 7.96 |
| 7.92 | 4.8 | 8.74 |
| 7.92 | 7 | 8.74 |
| 12.06 | 7 | 9.93 |
| 12.06 | 8.3 | 9.93 |

V33-10A

| depth | velocity | twt (s) |
|---|---|---|
| 0 | 1.5 | 0 |
| 5.56 | 1.5 | 7.41 |
| 5.56 | 2 | 7.41 |
| 6.59 | 2 | 8.44 |
| 6.59 | 5 | 8.44 |
| 9.25 | 5 | 9.51 |

| | | |
|---|---|---|
| 9.25 | 6.9 | 9.51 |

V33-10B

| depth | velocity | twt (s) |
|---|---|---|
| 0 | 1.5 | 0 |
| 5.56 | 1.5 | 7.41 |
| 5.56 | 2 | 7.41 |
| 6.59 | 2 | 8.44 |
| 6.59 | 5 | 8.44 |
| 8.42 | 5 | 9.18 |
| 8.42 | 7.3 | 9.18 |

V33-11

| depth | velocity | twt (s) |
|---|---|---|
| 0 | 1.5 | 0 |
| 5 | 1.5 | 6.67 |
| 5 | 2 | 6.67 |
| 6.08 | 2 | 7.75 |
| 6.08 | 3.15 | 7.75 |
| 6.92 | 3.15 | 8.28 |
| 6.92 | 4.7 | 8.28 |
| 9.89 | 4.7 | 9.54 |
| 9.89 | 6.7 | 9.54 |
| 14.46 | 6.7 | 10.91 |
| 14.46 | 8.5 | 10.91 |

V33-12

| Depth | velocity | twt (s) |
|---|---|---|
| 0 | 1.5 | 0 |
| 5.05 | 1.5 | 6.73 |
| 5.05 | 2.2 | 6.73 |
| 6.94 | 2.2 | 8.45 |
| 6.94 | 3.25 | 8.45 |
| 7.36 | 3.25 | 8.71 |
| 7.36 | 5.4 | 8.71 |
| 10.47 | 5.4 | 9.86 |
| 10.47 | 6.7 | 9.86 |
| 13.02 | 6.7 | 10.62 |
| 13.02 | 8.1 | 10.62 |

V33-13

| depth | velocity | twt (s) |
|---|---|---|
| 0 | 1.5 | 0 |
| 4.03 | 1.5 | 5.37 |

| | | |
|---|---|---|
| 4.03 | 1.8 | 5.37 |
| 4.66 | 1.8 | 6.07 |
| 4.66 | 3 | 6.07 |
| 7 | 3 | 7.63 |
| 7 | 5.3 | 7.63 |
| 9.11 | 5.3 | 8.43 |
| 9.11 | 7.5 | 8.43 |
| 13.87 | 7.5 | 9.70 |
| 13.87 | 8.3 | 9.70 |

V33-14

| depth | velocity | twt (s) |
|---|---|---|
| 0 | 1.5 | 0 |
| 4.63 | 1.5 | 6.17 |
| 4.63 | 2.2 | 6.17 |
| 6.3 | 2.2 | 7.69 |
| 6.3 | 4.15 | 7.69 |
| 8.05 | 4.15 | 8.53 |
| 8.05 | 5.05 | 8.53 |
| 10.21 | 5.05 | 9.39 |
| 10.21 | 6.15 | 9.39 |
| 15.03 | 6.15 | 10.96 |
| 15.03 | 7.3 | 10.96 |

V33-15

| depth | velocity | twt (s) |
|---|---|---|
| 0 | 1.5 | 0 |
| 4.57 | 1.5 | 6.09 |
| 4.57 | 2 | 6.09 |
| 5.7 | 2 | 7.22 |
| 5.7 | 3.1 | 7.22 |
| 7.71 | 3.1 | 8.52 |
| 7.71 | 5.3 | 8.52 |
| 10.98 | 5.3 | 9.75 |
| 10.98 | 6.7 | 9.75 |
| 16.76 | 6.7 | 11.48 |
| 16.76 | 8.3 | 11.48 |

V33-16

| depth | velocity | twt (s) |
|---|---|---|
| 0 | 1.5 | 0 |
| 5.61 | 1.5 | 7.48 |
| 5.61 | 1.8 | 7.48 |
| 6.31 | 1.8 | 8.26 |
| 6.31 | 4.75 | 8.26 |
| 8.27 | 4.75 | 9.08 |
| 8.27 | 7.1 | 9.08 |
| 11.26 | 7.1 | 9.93 |
| 11.26 | 8.2 | 9.93 |

V33-18

| depth | velocity | twt (s) |
|---|---|---|
| 0 | 1.5 | 0 |
| 4.4 | 1.5 | 5.87 |
| 4.4 | 2.2 | 5.87 |
| 5.83 | 2.2 | 7.17 |
| 5.83 | 3.7 | 7.17 |
| 8.31 | 3.7 | 8.51 |
| 8.31 | 5.4 | 8.51 |
| 11.3 | 5.4 | 9.61 |
| 11.3 | 5.95 | 9.61 |
| 16.01 | 5.95 | 11.20 |
| 16.01 | 7.2 | 11.20 |

V33-19

| depth | velocity | twt (s) |
|---|---|---|
| 0 | 1.5 | 0 |
| 5.61 | 1.5 | 7.48 |
| 5.61 | 2 | 7.48 |
| 6.47 | 2 | 8.34 |
| 6.47 | 5 | 8.34 |
| 9.49 | 5 | 9.55 |
| 9.49 | 6.6 | 9.55 |
| 11.72 | 6.6 | 10.22 |
| 11.72 | 8.5 | 10.22 |

V33-21

| depth | velocity | twt (s) |
|---|---|---|
| 0 | 1.5 | 0 |
| 5 | 1.5 | 6.66 |
| 5 | 1.8 | 6.66 |
| 5.67 | 1.8 | 7.41 |
| 5.67 | 3.1 | 7.41 |
| 8.16 | 3.1 | 9.02 |
| 8.16 | 5.5 | 9.02 |
| 10.29 | 5.5 | 9.79 |
| 10.29 | 6.75 | 9.79 |
| 15.6 | 6.75 | 11.37 |
| 15.6 | 8.5 | 11.37 |

V33-32

| depth | velocity | twt (s) |
|---|---|---|
| 0 | 1.5 | 0 |
| 4.72 | 1.5 | 6.29 |
| 4.72 | 1.64 | 6.29 |
| 5.07 | 1.64 | 6.72 |
| 5.07 | 2.57 | 6.72 |
| 5.69 | 2.57 | 7.20 |
| 5.69 | 2.74 | 7.20 |
| 6.22 | 2.74 | 7.59 |
| 6.22 | 3.87 | 7.59 |
| 7.05 | 3.87 | 8.02 |
| 7.05 | 4.3 | 8.02 |
| 7.43 | 4.3 | 8.20 |
| 7.43 | 4.75 | 8.20 |
| 8.51 | 4.75 | 8.65 |
| 8.51 | 5.35 | 8.65 |
| 10.16 | 5.35 | 9.27 |
| 10.16 | 6 | 9.27 |

V33-33

| Depth | velocity | twt (s) |
|---|---|---|
| 0 | 1.5 | 0 |
| 4.59 | 1.5 | 6.12 |
| 4.59 | 1.93 | 6.12 |
| 5.14 | 1.93 | 6.69 |
| 5.14 | 2.06 | 6.69 |
| 5.63 | 2.06 | 7.17 |
| 5.63 | 2.7 | 7.17 |
| 6.07 | 2.7 | 7.49 |
| 6.07 | 3.66 | 7.49 |
| 6.75 | 3.66 | 7.86 |
| 6.75 | 3.71 | 7.86 |
| 7.62 | 3.71 | 8.33 |
| 7.62 | 5 | 8.33 |
| 8.8 | 5 | 8.80 |
| 8.8 | 6.15 | 8.80 |

V33-34

| depth | velocity | twt (s) |
|---|---|---|
| 0 | 1.5 | 0 |
| 4.68 | 1.5 | 6.24 |
| 4.68 | 2 | 6.24 |
| 5.21 | 2 | 6.77 |
| 5.21 | 2.07 | 6.77 |
| 5.6 | 2.07 | 7.15 |
| 5.6 | 3.34 | 7.15 |
| 6.47 | 3.34 | 7.67 |
| 6.47 | 3.7 | 7.67 |
| 7.47 | 3.7 | 8.21 |
| 7.47 | 4.45 | 8.21 |
| 8.08 | 4.45 | 8.48 |
| 8.08 | 5.1 | 8.48 |
| 9.89 | 5.1 | 9.19 |
| 9.89 | 5.45 | 9.19 |
| 11.67 | 5.45 | 9.85 |
| 11.67 | 6.7 | 9.85 |

V33-35

| depth | Velocity | twt (s) |
|---|---|---|
| 0 | 1.5 | 0 |
| 5.6 | 1.5 | 7.47 |
| 5.6 | 2.53 | 7.47 |
| 7.73 | 2.53 | 9.15 |
| 7.73 | 4 | 9.15 |
| 10.33 | 4 | 10.45 |
| 10.33 | 5.3 | 10.45 |

V33-36

| depth | Velocity | twt (s) |
|---|---|---|
| 0 | 1.5 | 0 |
| 5.1 | 1.5 | 6.8 |
| 5.1 | 2.03 | 6.8 |
| 5.63 | 2.03 | 7.32 |
| 5.63 | 2.81 | 7.32 |
| 6.26 | 2.81 | 7.77 |
| 6.26 | 3.35 | 7.77 |
| 7.05 | 3.35 | 8.24 |
| 7.05 | 4 | 8.24 |
| 7.22 | 4 | 8.33 |
| 7.22 | 5.25 | 8.33 |
| 13.23 | 5.25 | 10.62 |
| 13.23 | 7.4 | 10.62 |
| 15.91 | 7.4 | 11.34 |
| 15.91 | 8.3 | 11.34 |

V33-37

| depth | Velocity | twt (s) |
|---|---|---|
| 0 | 1.5 | 0 |
| 3.86 | 1.5 | 5.15 |

| | | |
|---|---|---|
| 3.86 | 1.8 | 5.15 |
| 4.82 | 1.8 | 6.21 |
| 4.82 | 2.85 | 6.21 |
| 5.8 | 2.85 | 6.90 |
| 5.8 | 3.45 | 6.90 |
| 6.57 | 3.45 | 7.35 |
| 6.57 | 5 | 7.35 |
| 11.51 | 5 | 9.32 |
| 11.51 | 6 | 9.32 |
| 18.79 | 6 | 11.75 |
| 18.79 | 7.2 | 11.75 |

V33-38

| depth | velocity | twt (s) |
|---|---|---|
| 0 | 1.5 | 0 |
| 1.59 | 1.5 | 2.12 |
| 1.59 | 1.75 | 2.12 |
| 2.16 | 1.75 | 2.77 |
| 2.16 | 2.43 | 2.77 |
| 3.1 | 2.43 | 3.55 |
| 3.1 | 2.89 | 3.55 |
| 3.7 | 2.89 | 3.96 |
| 3.7 | 3.41 | 3.96 |
| 4.32 | 3.41 | 4.32 |
| 4.32 | 3.77 | 4.32 |
| 10.08 | 3.77 | 7.38 |
| 10.08 | 6 | 7.38 |

V33-39

| Depth | velocity | twt (s) |
|---|---|---|
| 0 | 1.5 | 0 |
| 2.67 | 1.5 | 3.56 |
| 2.67 | 2 | 3.56 |
| 3.29 | 2 | 4.18 |
| 3.29 | 3.6 | 4.18 |
| 8.59 | 3.6 | 7.12 |
| 8.59 | 5.4 | 7.12 |
| 17.26 | 5.4 | 10.34 |
| 17.26 | 7.2 | 10.34 |

V33-40

| Depth | velocity | twt (s) |
|---|---|---|
| 0 | 1.5 | 0 |
| 5.03 | 1.5 | 6.71 |
| 5.03 | 2.1 | 6.71 |
| 6.35 | 2.1 | 7.96 |
| 6.35 | 3.45 | 7.96 |
| 9.53 | 3.45 | 9.81 |
| 9.53 | 5.2 | 9.81 |
| 12.2 | 5.2 | 10.83 |

# Appendix 4: GAB Geological Sample Stations

**Note:**

1. Column 'Site' lists sample station sites according to BMR survey number/geological sample station number. Abbreviations used include: DR – dredge, GC – gravity core, and VC – vibrocore.
2. Column 'Depth' lists water depth in metres, dredges are also dragged through a depth range.
3. Columns 'latitude' and 'longitude' refer to the starting position of the dredge drag.
4. BMR survey 102 vibrocore stations occasionally used grab-sampling techniques as well.

**References:**

*For the D77-11 sample to the south of the Naturaliste Plateau*
Nicholls, I.A., Ferguson, J., Jones, H., Marks, G.P. & Mutter, J.C., 1981. Ultramafic blocks from the ocean floor SW of Australia. *Earth and Planetary Science Letters*, 56, 362–374.

*For BMR research cuises 10 and 11 samples (Survey 66)*
Davies, H.L., Clarke, J.D.A., Stagg, H.M.J., Shafik, S., McGowran, B., Alley, N.F. & Willcox, J.B., 1989. Maastrichtian and younger sediments from the Great Australian Bight. *Bureau of Mineral Resources, Geology and Geophysics, Report 288.*

*For BMR Survey 102 samples*
Feary, D.A., 1993. Geological sampling in the Great Australian Bight: Scientific post-cruise report - R/V *Rig Seismic* Cruise 102. *AGSO Record, 1993/18.*

| Site | Position | Latitude (S) | Longitude (E) | Depth | Sample Description |
|---|---|---|---|---|---|
| D77-11 | abyssal plain, Diamantina Zone | -36.6333 | 112.2667 | 4100 | Lherzolite block; clinopyroxenite block; serpentinite block; breccia block |
| 102DR001 | abyssal plain | -36.8575 | 118.7698 | 5090 | 100% Mn nodules, mostly spherical |
| 102DR002 | Eucla Shelf edge | -33.3297 | 128.026 | 250-180 | Quaternary medium to coarse sand |
| 102DR003 | Nullarbor Canyon, Ceduna Terrace | -35.2793 | 130.7517 | 4180-3660 | 90% Camp.-Maast. mudstone with Mn coating; 10% siltstone |

| | | | | | |
|---|---|---|---|---|---|
| 102DR004 | lower slope, central Ceduna Terrace | -35.725 | 131.4933 | 4680 | Unsuccessful |
| 102DR005 | Pearson Canyon, Ceduna Terrace | -36.2788 | 134.2118 | 5206-4376 | 90% L. Maast. mudstone with Mn coating; 10% L. Maast. siltstone |
| 102DR006 | Whidbey Canyon, Ceduna Terrace | -36.149 | 134.7372 | 3815-3694 | Minor mud recovered |
| 102DR007 | Whidbey Canyon, Ceduna Terrace | -36.1497 | 134.7372 | 4380-3660 | 5% ooze; 5% calcarenite/calcisiltite; 5% mudstone; 70% dolomite; 20% claystone |
| 102DR008 | Topgallant Canyon, Ceduna Terrace | -36.2217 | 134.9683 | 4550-3700 | Unsuccessful |
| 102DR009 | abyssal plain | -37.7812 | 132.333 | 5550-4940 | 10% Mn nodules; 30% Mn-rich mudstones; 50% grainstone/packstone; 10% basalt |
| 102DR010 | abyssal plain | -39.9213 | 131.9932 | 5567-5241 | 75% igneous rock - ?serpentinised gabbro; 10% conglomerate; 15% altered basalts |
| 102DR011 | abyssal plain | -39.7653 | 119.767 | 5240-5050 | 90% spherical to sub-spherical Mn nodules; 10% basalt |
| 102DR012 | abyssal plain | -37.48 | 119.6667 | 5300-3960 | 100% spherical Mn nodules |
| 102DR013 | abyssal plain | -37.2436 | 118.1558 | 4480-3950 | 5% igneous boulder; 10% mafic rock; 40% basalt; 10% gabbro; 25% altered rock; 10% Mn |
| 102GC001 | Eyre Terrace | -34.1665 | 128.0245 | 3615 | Quaternary nanno-foram ooze and sandy turbidite |
| 102GC002 | Eyre Terrace | -34.0832 | 128.025 | 3114 | Quaternary nanno-foram and foram-nanno ooze |
| 102GC003 | Eyre Terrace | -34.0001 | 128.0247 | 2755 | Quaternary nanno-foram and foram-nanno ooze |
| 102GC004 | Eyre Terrace | -33.9168 | 128.0252 | 2282 | Quaternary nanno-foram and foram-nanno ooze |
| 102GC005 | Eyre Terrace | -33.833 | 128.0258 | 1787 | Quaternary foram-nanno ooze |
| 102GC006 | Eyre Terrace | -33.7498 | 128.0253 | 1427 | Quaternary nanno-foram ooze |
| 102GC007 | Eyre Terrace | -33.667 | 128.0242 | 1178 | Quaternary nanno-foram ooze and two sandy turbidites |
| 102GC008 | Eyre Terrace | -33.5836 | 128.0253 | 913 | Quaternary nanno-foram ooze with four thin turbidites and shelf-derived skeletal debris |
| 102GC009 | Eyre Terrace | -33.5 | 128.0252 | 769 | Quaternary nanno-foram ooze with one thin turbidite and shelf-derived debris |
| 102GC010 | Eyre Terrace | -33.4165 | 128.0258 | 527 | Quaternary foram-nanno ooze |
| 102GC011 | Eyre Terrace | -33.4168 | 128.0252 | 529 | Foram-nanno ooze |
| 102GC012 | western Ceduna Terrace | -31.5238 | 131.0085 | 498 | No recovery |
| 102GC013 | western Ceduna Terrace | -33.8243 | 130.8035 | 1008 | Quaternary nanno-foram ooze and pockets of sandy debris |
| 102GC014 | western Ceduna Terrace | -34.3748 | 130.4178 | 1504 | Quaternary nanno-foram and foram-nanno ooze |
| 102GC015 | western Ceduna Terrace | -34.5872 | 130.2608 | 2003 | Quaternary nanno-foram ooze |
| 102GC016 | western Ceduna Terrace | -34.7528 | 130.141 | 2495 | Quaternary nanno-foram and foram-nanno ooze |

| | | | | | |
|---|---|---|---|---|---|
| 102GC017 | western Ceduna Terrace | -34.8908 | 130.0555 | 3001 | Quaternary foram-nanno ooze |
| 102GC018 | western Ceduna Terrace | -34.9553 | 130.0072 | 3504 | Quaternary foram-nanno ooze |
| 102GC019 | lower slope, western Ceduna Terrace | -34.9242 | 129.7875 | 3902 | Quaternary nanno-foram ooze and silty clay |
| 102GC020 | lower slope, western Ceduna Terrace | -34.924 | 129.7867 | 3902 | No recovery |
| 102GC021 | lower slope, western Ceduna Terrace | -34.924 | 129.7862 | 3900 | Quaternary foram-nanno ooze, silty clay and clay |
| 102GC022 | central Ceduna Terrace | -34.0358 | 129.8892 | 1458 | Quaternary foram-nanno ooze |
| 102GC023 | central Ceduna Terrace | -34.0357 | 129.8898 | 1465 | No recovery |
| 102GC024 | central Ceduna Terrace | -34.0368 | 129.8893 | 1404 | Fe/Mn rock fragments and skeletal debris |
| 102GC025 | central Ceduna Terrace | -34.0365 | 129.8888 | 1453 | Fe/Mn rock fragments |
| 102GC026 | Nullarbor Canyon, Ceduna Terrace | -35.376 | 130.7405 | 4568 | Quaternary foram-nanno ooze and silty clay |
| 102GC027 | lower slope, central Ceduna Terrace | -35.7537 | 131.5008 | 4536 | Silty clay |
| 102GC028 | Fowlers Canyon, Ceduna Terrace | -36.2278 | 133.2905 | 4960 | No recovery |
| 102GC029 | Fowlers Canyon, Ceduna Terrace | -36.2278 | 133.2895 | 4930 | Foram-nanno ooze and silty clay |
| 102GC030 | Fowlers Canyon, Ceduna Terrace | -36.0765 | 133.403 | 3804 | Quaternary foram-nanno and nanno-foram ooze |
| 102GC031 | Fowlers Canyon, Ceduna Terrace | -36.098 | 133.3692 | 3994 | No recovery |
| 102GC032 | Fowlers Canyon, Ceduna Terrace | -36.0967 | 133.3707 | 4014 | Quaternary foram-nanno ooze and silty clay |
| 102GC033 | Fowlers Canyon, Ceduna Terrace | -36.114 | 133.3462 | 4360 | No recovery |
| 102GC034 | Fowlers Canyon, Ceduna Terrace | -36.1145 | 133.3463 | 4378 | Quaternary foram-nanno ooze and silty clay |
| 102GC035 | Pearson Canyon, Ceduna Terrace | -36.2763 | 134.1848 | 5219 | Quaternary foram-nanno ooze, bryozoan sand and silty clay |
| 102GC036 | Whidbey Canyon, Ceduna Terrace | -36.0857 | 134.7993 | 3320 | Quaternary nanno-foram and foram-nanno ooze |
| 102GC037 | Whidbey Canyon, Ceduna Terrace | -36.0858 | 134.7783 | 3792 | No recovery |
| 102GC038 | abyssal plain | -37.2648 | 118.3521 | 5339 | ? |
| 102VC001 | Eucla Shelf transect | -33.262 | 128.0248 | 277 | Minor recovery - bioclastic grains |
| 102VC002 | Eucla Shelf transect | -33.2748 | 128.0255 | 184 | Rhodolith gravel overlain and bioclastic sand |
| 102VC003 | Eucla Shelf transect | -33.2747 | 128.0255 | 184 | Rhodolith gravel overlain and bioclastic sand |
| 102VC004 | Eucla Shelf transect | -33.2505 | 128.025 | 152 | Rhodolith gravel and sand |
| 102VC005 | Eucla Shelf transect | -33.0833 | 128.025 | 113 | Bioclastic sand |
| 102VC006 | Eucla Shelf transect | -32.9167 | 128.025 | 80 | Bioclastic sand, skeletal fragments and limestone clasts |
| 102VC007 | Eucla Shelf transect | -32.75 | 128.025 | 67 | Bioclastic sand |
| 102VC008 | Eucla Shelf transect | -32.5833 | 128.025 | 69 | Bioclastic sand |
| 102VC009 | Eucla Shelf transect | -32.4167 | 128.025 | 58 | Bioclastic sand |

| | | | | | |
|---|---|---|---|---|---|
| 102VC010 | Eucla Shelf transect | -32.25 | 128.025 | 31 | Bioclastic sand and dolomitic limestone |
| 102VC011 | Eucla Shelf transect | -32.1667 | 128.0253 | 22 | Bioclastic sand and dolomitic limestone |
| 066GC001 | Ceduna Terrace (BMR 65/15) | -33.7431 | 132.1554 | 186 | ? |
| 066GC002 | Ceduna Terrace (BMR 65/15) | -33.84 | 132.0783 | 591 | Pelagic calcareous ooze |
| 066GC003 | Ceduna Terrace (BMR 65/15) | -33.8512 | 132.0885 | 600 | Pelagic calcareous ooze |
| 066GC004 | Ceduna Terrace (BMR 65/15) | -33.9303 | 132.0407 | 701 | Pelagic calcareous ooze |
| 066GC005 | Ceduna Terrace (BMR 65/02) | -34.0384 | 130.6914 | 1134 | Pelagic calcareous ooze and several sandy horizons |
| 066GC006 | Ceduna Terrace (BMR 65/02) | -34.5241 | 129.6803 | 3135 | ? |
| 066GC007 | Ceduna Terrace (BMR 65/02) | -34.5906 | 129.5286 | 3662 | Several beds of reworked sand, some ooze |
| 066GC008 | Eyre Terrace (BMR 65/06) | -33.665 | 127.7034 | 1151 | Pelagic calcareous ooze and one turbidite horizon |
| 066GC009 | Eyre Terrace (BMR 65/06) | -33.4989 | 127.5953 | 757 | ? |
| 066GC010 | Ceduna Terrace (BMR 65/15) | -35.2778 | 131.1816 | 2643 | Pelagic calcareous ooze and alternating colour bands |
| 066GC011 | Ceduna Terrace (BMR 65/15) | -35.2026 | 131.2266 | 2326 | Pelagic calcareous ooze |
| 066GC012 | Ceduna Terrace (BMR 65/15) | -35.1536 | 131.2704 | 2010 | Pelagic calcareous ooze |
| 066GC013 | Ceduna Terrace (BMR 65/15) | -34.9941 | 131.359 | 1734 | Pelagic calcareous ooze |
| 066GC014 | Ceduna Terrace (BMR 65/15) | -34.8356 | 131.4331 | 1498 | Colour-banded pelagic calcareous ooze, one horizon larger planktic forams |
| 066GC015 | Ceduna Terrace (BMR 65/15) | -34.6954 | 131.5509 | 1376 | Pelagic calcareous ooze |
| 066GC016 | Ceduna Terrace (BMR 65/15) | -34.5421 | 131.6545 | 1253 | Pelagic calcareous ooze |
| 066GC017 | Ceduna Terrace (BMR 65/15) | -34.4042 | 131.7349 | 1186 | Pelagic calcareous ooze |
| 066GC018 | Ceduna Terrace (BMR 65/15) | -34.2706 | 131.8181 | 1247 | Pelagic calcareous ooze |
| 066GC019 | Ceduna Canyon | -35.472 | 132.9174 | 2396 | Sequence of terrigenous siltstone, mudstone and gravel overlain by pelagic calcareous ooze |
| 066GC020 | canyon, eastern Ceduna Terrace slope | -35.6957 | 133.3127 | 2810 | Shell hash, quartz sand, and rock fragments overlain by pelagic calcareous ooze |
| 066GC021 | Canyon, eastern Ceduna Terrace slope | -35.6881 | 133.3311 | 2717 | Pelagic calcareous ooze with one horizon cross-bedded quartz and foram sand |
| 066GC022 | Canyon, eastern Ceduna Terrace slope | -35.6997 | 133.3538 | 2316 | Pelagic calcareous ooze with one turbidite horizon of echinoid detritus |
| 066DR001 | upper slope, Eyre Terrace | -33.9333 | 128.6383 | 3280-2950 | Tert limestone; Maast siltstone, sandstone; Paleocene phosphate; ? basalt |
| 066DR002 | upper slope, Eyre Terrace | -34.0387 | 126.7342 | 2500-2070 | Precambrian granodiorite; Eocene mudstone |

| | | | | | |
|---|---|---|---|---|---|
| 066DR003 | upper slope, Eyre Terrace | -33.9758 | 128.6087 | 3535-3390 | L. Cretaceous mudstone, sandstone, conglomerate; Tertiary carbonate; ? basalt |
| 066DR004 | eastern Eyre Terrace | -34.1585 | 129.1063 | 3332-3095 | ?E. Tertiary siliceous wackestone |
| 066DR005 | eastern Eyre Terrace | -35.266 | 130.7755 | 3800-3200 | Unsuccessful |
| 066DR006 | eastern Ceduna Terrace | -35.5682 | 132.9127 | 2620-2015 | Oligocene pelagic wackestone |
| 066DR007 | eastern Ceduna Terrace | -35.6996 | 133.3256 | 2720-2200 | L. Cretaceous - E. Tertiary mudstone/siltstone; Miocene siltstone/wackestone |
| 066DR008 | eastern Ceduna Terrace | -35.6787 | 134.4325 | 2826-2244 | L. Paleocene - M. Eocene siltstone/mudstone; E.-M. Eocene wackestone |
| 066DR009 | upper slope, Duntroon Sub-basin | -36.0016 | 134.8299 | 3680-2982 | Pliocene mudstone and wackestone |
| 066DR010 | upper slope, Duntroon Sub-basin | -35.9896 | 134.8432 | 3614-2925 | M. Eocene and E. Miocene wackestone |
| 066DR011 | upper slope, Duntroon sub-basin | -35.8274 | 135.1583 | 3200-2141 | L. Cretaceous siltstone; E. Eocene sandstone; M.-L. Oligocene wackestone |
| 066DR012 | upper slope, Duntroon Sub-basin | -35.9134 | 135.0905 | 3670-2720 | L. Paleocene and M. Eocene mudstone; L. Eocene and E. Oligocene wackestone |
| 066DR013 | upper slope, Duntroon Sub-basin | -35.9744 | 135.2278 | | Unsuccessful |
| 066DR014 | upper slope, Duntroon Sub-basin | -35.9727 | 135.2259 | 3064-2627 | E. Eocene organic-rich mudstone; M.-L. Eocene and E. Oligocene wackestone |
| 066DR015 | upper slope, Duntroon Sub-basin | -36.3344 | 135.669 | 3394-2494 | M. Oligocene and E. Miocene lime mudstone |
| 066DR016 | upper slope, Duntroon Sub-basin | -36.4017 | 135.855 | 3432-3302 | ?Oligocene dolomitic packstone and siliceous wackestone |

# Appendix 5: GAB Heatflow Data

The following data are taken from Willcox, Stagg, Davies et al. (1988).

| Stn | Latitude | Longitude | WD | N | Temp | Rec | K | G | Q |
|---|---|---|---|---|---|---|---|---|---|
| HF01 | 33 51.069S | 132 05.308E | 600 | 3 | 3.21 | | | | |
| | | | | | 3.46 | | | | |
| HF02 | 33 55.820S | 132 02.441E | 701 | 3 | 6.87 | 2.15 | 0.8 | 448 | 358* |
| HF03 | 34 01.774S | 131 58.218E | 879 | 3 | 4.83 | 2.15 | 0.8 | 152 | 122 |
| HF04 | 34 07.345S | 131 54.699E | 1092 | 0 | 3.47 | | | | |
| HF05 | 34 12.998S | 131 51.533E | 1195 | 1 | 3.15 | | | | |
| HF06 | 34 22.711S | 131 45.743E | 1178 | 1 | 3.27 | | | | |
| HF07 | 34 32.843S | 131 39.159E | 1250 | 2 | 2.95 | | | | |
| HF08 | 34 02.212S | 130 40.060E | 1151 | 3 | 3.23 | 2.47 | | | |
| HF09 | 34 07.822S | 130 27.228E | 1302 | 2 | 3.3 | 2.47 | | | |
| HF10 | 34 15.932S | 130 12.405E | 1676 | 3 | 2.56 | 2.47 | 0.83 | 55 | 46 |
| HF11 | 34 24.056S | 129 57.746E | 2175 | 1 | 2.19 | | | | |
| HF12 | 33 39.901S | 127 42.206E | 1063 | 3 | 3.8 | 1.86 | | | |
| HF13 | 35 16.668S | 131 10.897E | 2643 | 2 | 1.93 | 2.34 | 0.96 | 65 | 62 |
| HF14 | 35 12.156S | 131 13.597E | 2326 | 3 | 2.12 | 1 | 0.89 | 68 | 61 |
| HF15 | 35 09.216S | 131 16.225E | 2010 | 4 | 2.33 | 1.67 | 0.87 | 68 | 59 |
| HF16 | 34 59.643S | 131 21.541E | 1734 | 3 | 2.54 | 1.6 | 0.95 | 101 | 96 |
| HF17 | 34 50.137S | 131 25.983E | 1498 | 4 | 2.67 | 2.18 | 0.87 | 75 | 65 |
| HF18 | 34 41.721S | 131 33.056E | 1376 | 4 | 2.86 | 2.07 | 0.94 | 47 | 44 |
| HF19 | 34 32.528S | 131 39.272E | 1253 | 3 | 2.97 | 0.91 | 0.9 | 126 | |
| HF20 | 34 24.251S | 131 44.095E | 1186 | 3 | 3.13 | 2.13 | 0.93 | 84 | 78 |
| HF21 | 34 16.234S | 131 49.083E | 1247 | 1 | 2.99 | 1.25 | | | |

Column headings as follows:

Stn - heatflow station number
Latitude, Longitude - station coordinate
WD - water depth in metres
N - number of thermistors that penetrated into sediment
Temp - bottom water temperature in $C^o$
Rec - core recovery in metres
K - thermal conductivity in W/m/K
G - thermal gradient in $C^o$/km
Q - heatflow in $mW/m^2$

* This heatflow value was treated as highly suspect.

## Appendix 6: Interpreted Seismic Horizons

Note 1: first set of horizons refers to horizons used for sediments, generally in deep-water areas (i.e. ~>3000 m on the lower continental slope) and defined for the purpose of this study. Second set of horizons refers to horizons defined in the Southern Margin Frontiers Project, and in the Eyre and Ceduna Sub-basins. Third set of horizons refers to horizons used for volcanogenic complexes including a few other specific horizons, and defined for the purpose of this study.

Note 2: abbreviation AAB stands for Australian–Antarctic Basin.

| Seismic horizon | Colour of horizon | Horizon details | Type section/location |
|---|---|---|---|
| *1128.1* | Blue | Pliocene, interpreted at ODP Site 1128 | Line 65/04, Figure 12b |
| *1128.2* | Dark blue | Miocene, interpreted at ODP Site 1128 | Line 65/04, Figure 12b |
| *1128.3* | Aqua | Early Oligocene, interpreted at ODP Site 1128 | Line 65/04, Figure 12b |
| *1128.4* | Blue | Base Oligocene, interpreted at ODP Site 1128 | Line 65/04, Figure 12b |
| *ter2* | Light blue | ?Near base Cainozoic – younger horizon | Line 199/06, Figure 12a |
| *ter1* | Light blue | ?Near base Cainozoic – older horizon | Line 199/06, Figure 12a |
| *lmio* | Green | ?Late Miocene, horizon in AAB, ?equivalent to 1128.2 | Line 199/06, Figure 12a |
| *eoli* | olive green | ?Early Oligocene, horizon in AAB | Line 199/06, Figure 12a |
| *leoc* | Aqua | ?Late Eocene, horizon in AAB | Line 199/06, Figure 12a |
| *meo2* | Blue | ?Middle Eocene – younger horizon, AAB | Line 199/06, Figure 12a |
| *meo1* | Light blue | ?Middle Eocene – older horizon, AAB | Line 199/06, Figure 12a |
| *Dugong* | Light green | Base Dugong supersequence | Line 199/08, Plate 3 |
| *Wobbegong* | Pink | Base Wobbegong supersequence | Line 199/08, Plate 3 |
| *Hammerhead* | Green | Base Hammerhead supersequence | Line 199/05, Figure 13 |
| *Tiger* | Brown | Base Tiger supersequence | Line 199/05, Figure 13 |
| *White pointer* | Orange | Base White Pointer supersequence | Line 199/09, Plate 3 |
| *Blue whale* | Blue | Base Blue Whale supersequence | Line 199/09, Plate 3 |
| *Bronze whaler* | Yellow | Base Bronze Whaler supersequence | Line 199/09, Plate 3 |
| *Southern right* | Light blue | Base Southern Right supersequence | Line 199/09, Plate 3 |
| *Minke* | Pink | Base Minke supersequence | Line 199/09, Plate 3 |
| *t_pr* | olive green | Top basal progradational sequence within Hammerhead supersequence | Line 199/07, Figure 14a |
| *Moho* | Red | Top ?Moho | Lines 199/03, -/04, -/05; Plate 3 |

| | | | |
|---|---|---|---|
| *tran* | Purple | Top transitional crust | Line 199/05, Figure 13 |
| *ocea* | Red | Top oceanic crust | Line 199/07, Plate 4 |
| *ovol* | Brown | Top ?volcaniclastics/flows overlying oceanic crust | Line 199/02, Plate 3 |
| *buil* | Pink | Top volcanic buildup | Line 199/03 |
| *oflo* | Pink | Top ?volcanic flows on oceanic basement | Line 199/01, Plate 3 |
| *intr* | orange | Top of intrusions in continental crust | Line 199/01, Plate 3 |
| *brid* | pink | Top basement ridge | Line 199/05, Figure 13 |
| *lcru* | yellow | Top lower continental crust | Line 199/05, Figure 13 |

# 12. LIST OF TABLES



# 13. LIST OF FIGURES

(after Sayers et al. 2001).

Figure 15. Crustal provinces of the deep-water central Great Australian Bight. Purple lines – track lines from Survey 199, black line – ?transfer/transform fault zone, blue contours and labels (m) – isobaths.

Figure 16. (a) Preferred spreading rate model for the Southern Margin after Tikku & Cande (1999). (b–e) Line drawings of seismic profiles showing observed gravity/magnetic data over the COT, with magnetic anomaly identifications superimposed based on the model of Tikku & Cande (1999) above. LC – lower crust; Pz – Palaeozoic; J – Jurassic; K – Cretaceous (equivalent pre-rift and syn-rift); LK – Late Cretaceous (equivalent late syn-rift); heavy, intermediate and light stipple represent post-rift sediments; 'v' pattern – oceanic crust; hinge pattern – basement ridge (altered mantle, serpentinised mantle, associated igneous rocks, altered sediments), filled triangle symbol denotes the COB, v? – possible volcanic flows. Figure revised from Sayers et al. (2001).

Figure 17. Profile of 1-D depth-velocity models across oceanic crust. 6.20 – example of P-wave velocity in km/s, * – poorly determined velocity, ( ) – assumed velocity, TU – thickness uncertain. Labels at top of models represent both the survey name and sonobuoy number (i.e. V33 – *Vema* Cruise 33, EL – *Eltanin* Cruise 55, 199 – Survey 199).

Figure 18. Profile of 1-D depth-velocity models across the continent-ocean transition. 6.20 – example of P-wave velocity in km/s, * – poorly determined velocity, ( ) – assumed velocity, TU – thickness uncertain. Labels at top of models represent both the survey name and sonobuoy number (i.e. V33 – *Vema* Cruise 33, EL – *Eltanin* Cruise 55, 199 – Survey 199). Note that *Vema* Cruise 33 and *Eltanin* Cruise 55 do not differentiate between pre- and post-breakup sediments.

Figure 19. Profile of 1-D depth-velocity models across the basement ridge. 6.20 – example of P-wave velocity in km/s, * – poorly determined velocity, ( ) – assumed velocity, TU – thickness uncertain. Labels at top of models represent both the survey name and sonobuoy number (i.e. V33 – *Vema* Cruise 33, EL – *Eltanin* Cruise 55, 199 – Survey 199).

Figure 20. Profile of 1-D depth-velocity models across thinned continental crust. 6.20 – example of P-wave velocity in km/s, * – poorly determined velocity, ( ) – assumed velocity, TU – thickness uncertain. Labels at top of models represent both the survey name and sonobuoy number (i.e. V33 – *Vema* Cruise 33, EL – *Eltanin* Cruise 55, 199 – Survey 199). Note that *Vema* Cruise 33 and *Eltanin* Cruise 55 do not differentiate between pre- and post-breakup sediments.

Figure 21. (a) ?volcanics outcropping at the seabed. (b) volcanic buildups on oceanic crust. (c–d) ?volcanics in continent-ocean transition (COT) province. Dashed black line represents arbitary boundary between oceanic crust and COT. lmio – ?late Miocene, eoli – ?early Oligocene, leoc – ?late Eocene, meo2 – ?Middle Eocene, younger horizon; meo1 – ?Middle Eocene, older horizon; ter2 - ?near base Cainozoic, younger horizon; ter1 – ?near base Cainozoic, older horizon; tran – top transitional crust, ocea – top oceanic crust,

Figure 22. Seismic character of pre-breakup sediments in the continent–ocean transition compared with those over extended continental crust. Abbreviations: K – Cretaceous, UK – Upper Cretaceous, LC – lower crust, 'v' symbol represents oceanic crust, bar symbol represents basement ridge, ter2 – ?near base Cainozoic, younger horizon; ter1 – ?near base Cainozoic, older horizon; tran – top transitional crust, brid – top basement ridge, tran – top transitional crust, lcru – top lower continental crust.

Figure 23. Characterisation of the lower crust and overlying sedimentary section beneath the lower continental slope, based on seismic reflection data and refraction-based velocities/depth.

Figure 24. Possible flatspot in toe-thrusts beneath the continental slope.

Figure 25.(a) Sketch (not to scale) to illustrate one of the hypotheses discussed in this report. The model (from Whitmarsh & Miles, 1995) includes A, unthinned continental crust; B, continental crust thinned by tectonic extension with upper crust normal faults; C, a transitional crust consisting of blocks of faulted continental crust and a high density of intrusives (black) which are oriented parallel to the seafloor spreading anomalies; and D, oceanic crust produced by seafloor spreading. Crosses indicate outcrops of mantle ultramafic rocks (peridotite ridge). (b) Model at the point just after continental breakup where the top of the asthenosphere is shallow enough to allow igneous intrusion of the continental crust to occur over a broad zone. Dotted region represents serpentinised peridotite. Figure from Whitmarsh & Miles (1995) (c) Summary E–W cross sections along two transects off west Iberia, based on multichannel seismic reflection profiles of Murillas et al. (1990) and seismic refraction results of Whitmarsh et al., and Horsefield (1992), PR = peridotite ridge. Figure from Whitmarsh & Sawyer (1996). (d) Section across the southern Iberia Abyssal Plain, based on seismic refraction lines of Whitmarsh et al. (1990), gravity model of Whitmarsh et al. (1993) and on multichannel seismic reflection profile LG-12 (Beslier et al., 1993). Figure from Whitmarsh & Sawyer (1996).

Figure 26. (a) Interpretations of the depth section between Sites 900 and 901, Iberia Margin (from Krawczyk et al., 1996). The eastern basement

high is capped by a seismic transparent layer of prerift/pretilting sediments. Farther to the west, different tilted blocks are imaged. They are bound by fault structures (i.e. listric fault L) and a detachment 'H', which developed during different phases of rifting. 'H' developed during the synrift I phase accommodating top-to-the-west motion, and was subsequently cut and rotated by 'L' during the synrift II stage. Backrotation of 'H' first during synrift I and subsequently during synrift II explains its current orientation. 'H' terminates at the top of the basement high 500 m east of the drilled Site 900. Wedge-shaped sedimentary sequences are either of early synrift/prerift or of synrift II age. B and C. This figure assumes the eastward-dipping part of 'H' cutting across 'L' at about 12 km depth by analogy to the Galicia Margin (e.g. Boillot et al. 1997). (b) This sketch summarises and extends interpretations of (a) to the west: deep lithospheric levels were tectonically unroofed as a result of conjugate, lithospheric shear zone activity during rifting (after Beslier et al. 1995). Figure from Krawczyk et al. (1996). (c) Laboratory model of Brun & Beslier (1996), reprinted with permission from Elsevier; Bc = brittle crust (sand), Dc = ductile crust (silicone); Bm = brittle mantle (sand); Dm = ductile mantle (silicone).

Figure 27. (a) Seismic profile on line 199/05 showing interpretation of sedimentary sequences and crust from the outer Ceduna Sub-basin, across the COT, COB and onto the oceanic crust. Interpretation is based on seismic reflection data and refraction modelling. 2 – Turonian; 3 – early Campanian; 4 – Mid-Eocene. J? – Possible Jurassic; LC – lower crust. Dashed sub-horizontal line represents a possible sequence boundary roughly equivalent to the top Jurassic. Sonobuoy refraction model velocities shown as vertical strips, positioned at one end of the shot range for display purposes. (b) Potential field model for line 199/05. Magnetic anomaly picks are based on Tikku & Cande (1999). Upper and lower values in the boxes are density ($t/m^3$) and magnetic susceptibility (cgs), respectively, for the associated layer. The normal polarity bodies used to model magnetic anomalies over oceanic crust have been placed where the data demands a change in magnetic properties. The bodies integrate a number of magnetic polarity changes associated with the slow-spreading crust. UK – Upper Cretaceous, K – Cretaceous. Hachured area represents an area of probable, altered mantle interpreted from modelled refraction velocities of 7.2–7.6 km/s. Figure from Sayers et al. (2001).

Figure 28. Reconstruction diagram for the continent-ocean transition and general breakup model using a 4-layer lithosphere (i.e. ductile and brittle crust and mantle, similar to the model of Brun & Beslier (1996)). (a) Upper and lower crustal extension, décollement faulting in mobile shales of the Ceduna Sub-basin, uplift. (b) Lower crustal extension, hot rising ductile mantle, partial unroofing of mantle and

gabbro intrusions. (c) Breakup, slow spreading oceanic crust and formation of oceanic lithospheric mantle, intrusions into lower crust. UK – Upper Cretaceous (equivalent Tiger supersequence), K – Cretaceous (equivalent supersequences White Pointer to Minke), J – Jurassic, LC – lower crust; 1 – pre-Tiger supersequences, 2 – Tiger supersequence. Figure from Sayers et al. (2001).

# 14. LIST OF PLATES

Plate 1. Generalised crustal provinces and data control.

Plate 2. Bathymetry, wells, sample stations, heat-flow stations and sonobuoys.

Plate 3. Interpreted seismic sections (Survey 199).

Plate 4. Interpreted seismic sections (Survey 199), uninterpreted seismic sections (Survey 65).

Plate 5. Generalised geology – ODP Site 1128.

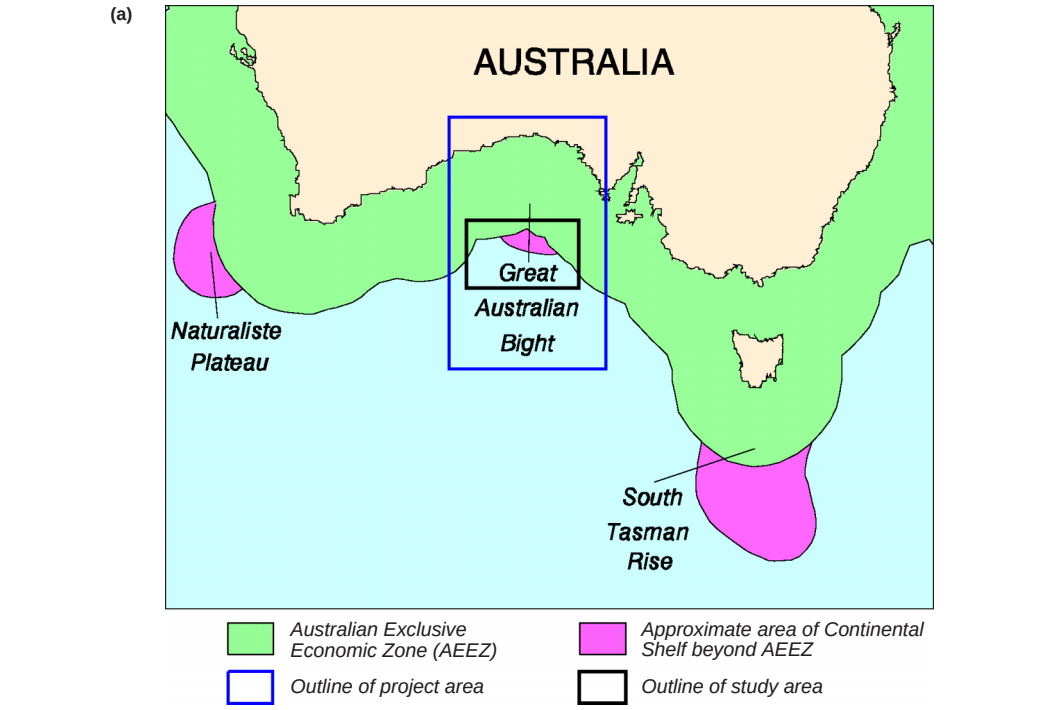


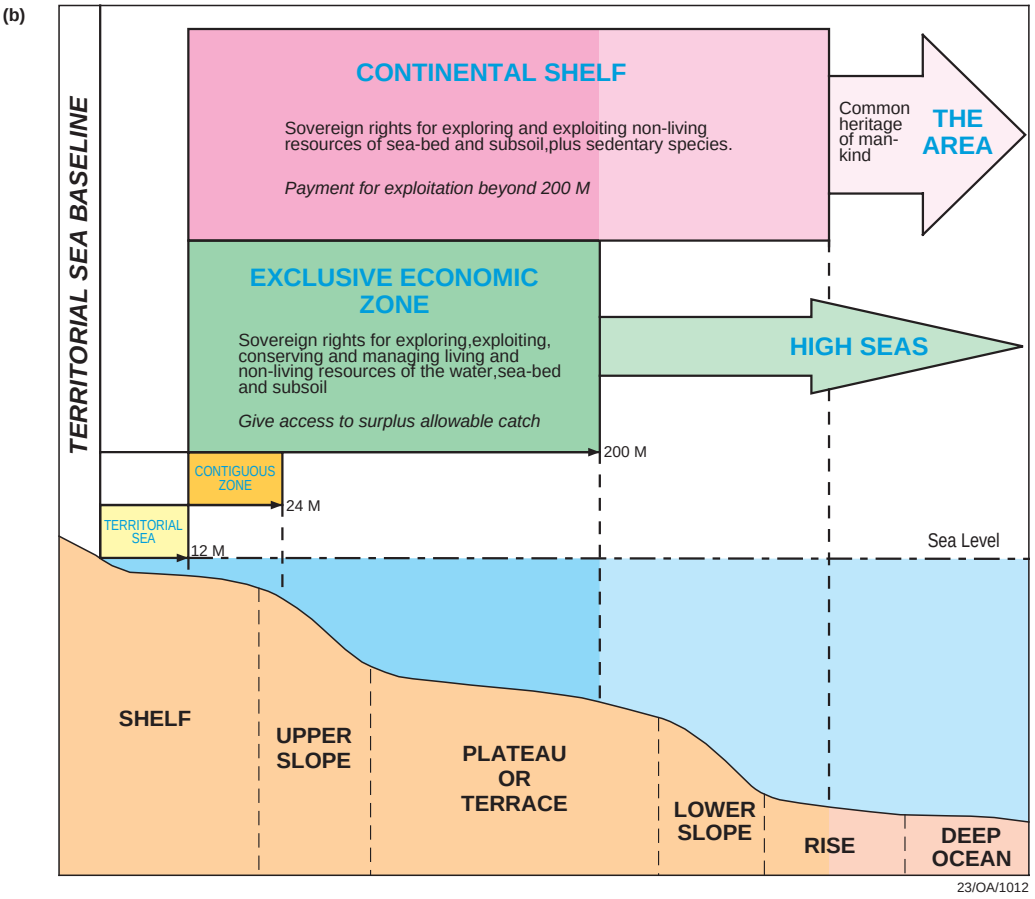


**Figure 1.** (a) Marine jurisdictional zones off southern Australia (after Symonds et al., 1998a). (b) Visual representation of marine jurisdictional zones contained in the 1982 Convention on the Law of the Sea. See Appendix 1 for detailed explanations.

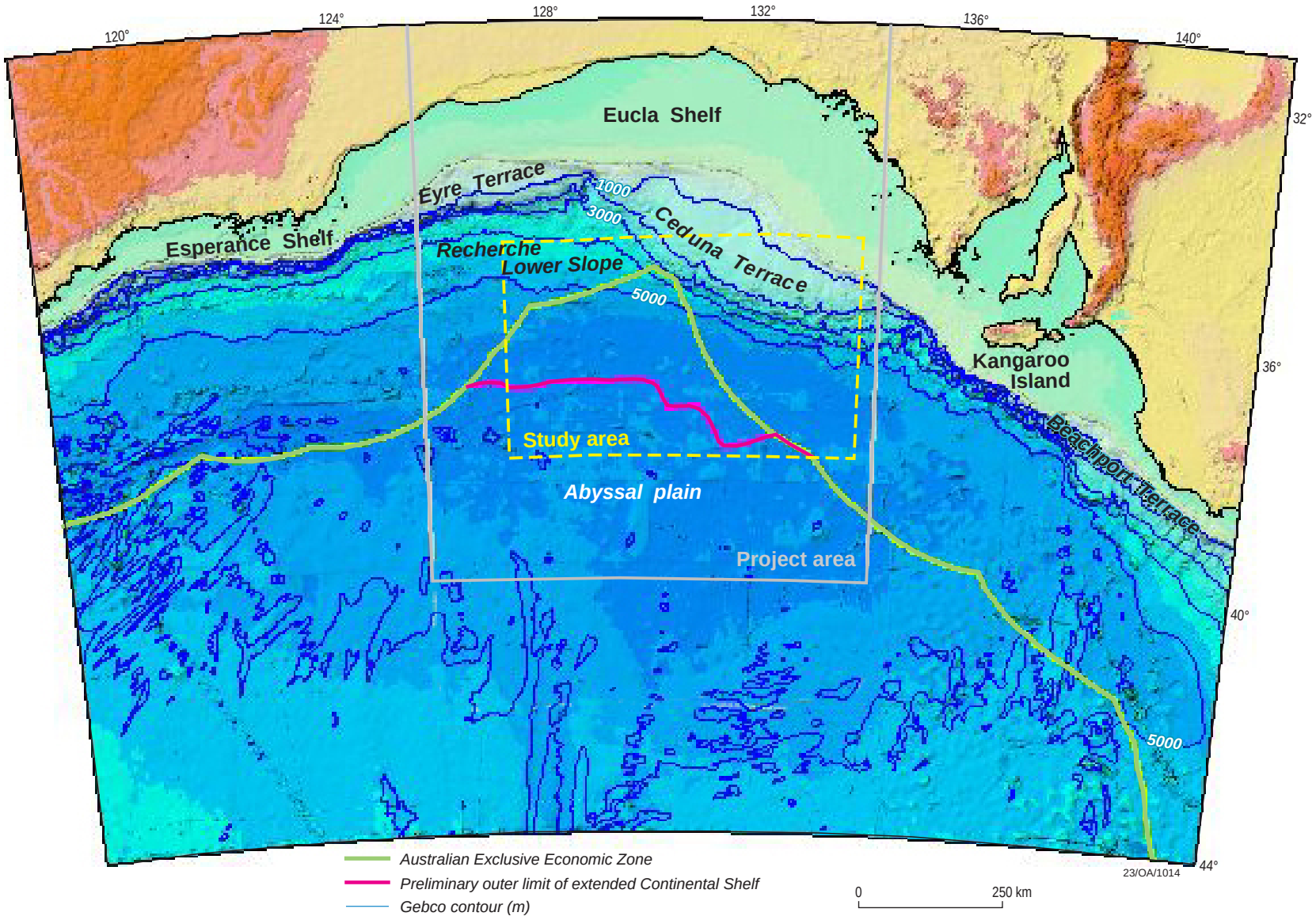


**Figure 2.** Physiography of the central Great Australian Bight study and project areas. Bluish shading - deep water, greenish shading - shallow water. Blue contours and labels (m) - isobaths. Green line represents the Australia Exclusive Economic Zone (AEEZ), pink line represents the preliminary boundary of extended Continental Shelf off the central Great Australian Bight. The latter line is not necessarily indicative or representative of the final outer limit of the Continental Shelf that might be used by Australia in any submission it makes to the Commission on the Limits of the Continental Shelf.

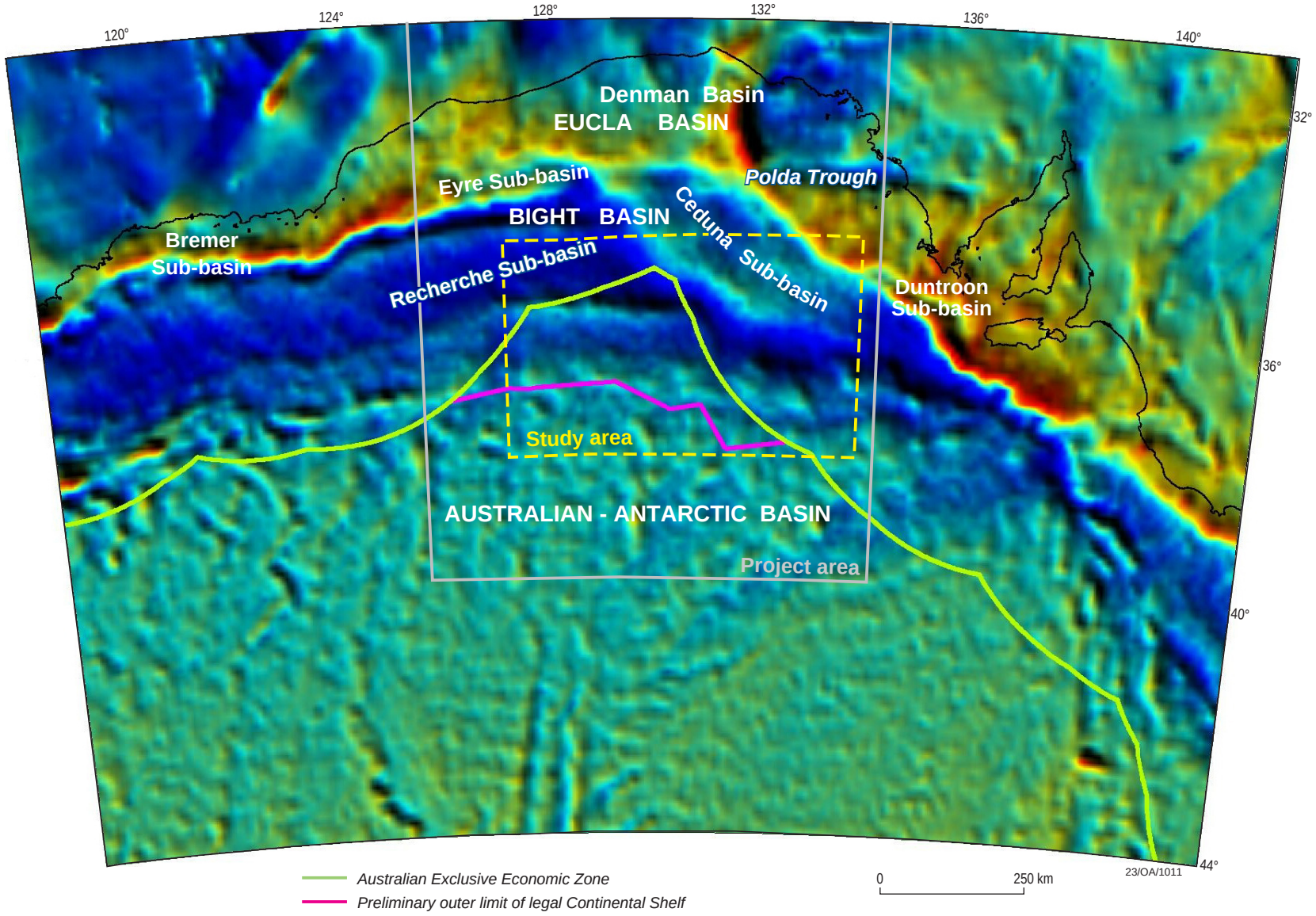


**Figure 3.** Regional setting of the central Great Australian Bight study and project areas. The backdrop image is the Free Air Anomaly satellite gravity where blues represent gravity lows and reds represent gravity highs. Green line represents the Australia Exclusive Economic Zone (AEEZ), pink line represents the preliminary boundary of extended Continental Shelf off the central Great Australian Bight. The latter line is not necessarily indicative or representative of the final outer limit of the Continental Shelf that might be used by Australia in any submission it makes to the Commission on the Limits of the Continental Shelf.

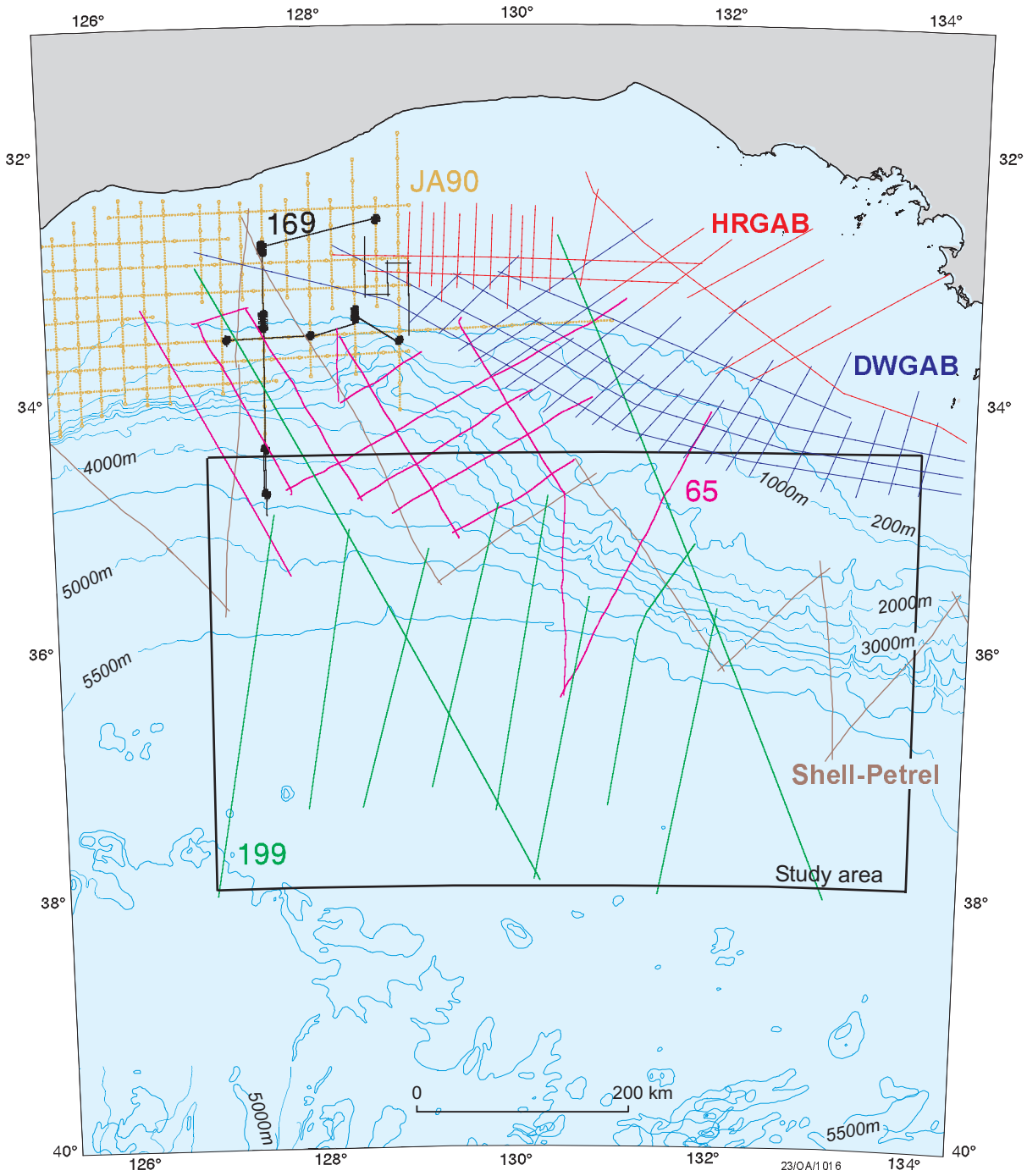


**Figure 4.** Seismic survey track chart and isobaths. Blue contours & labels (m) - isobaths; straight, coloured lines represent different seismic surveys, numbers represent survey names.

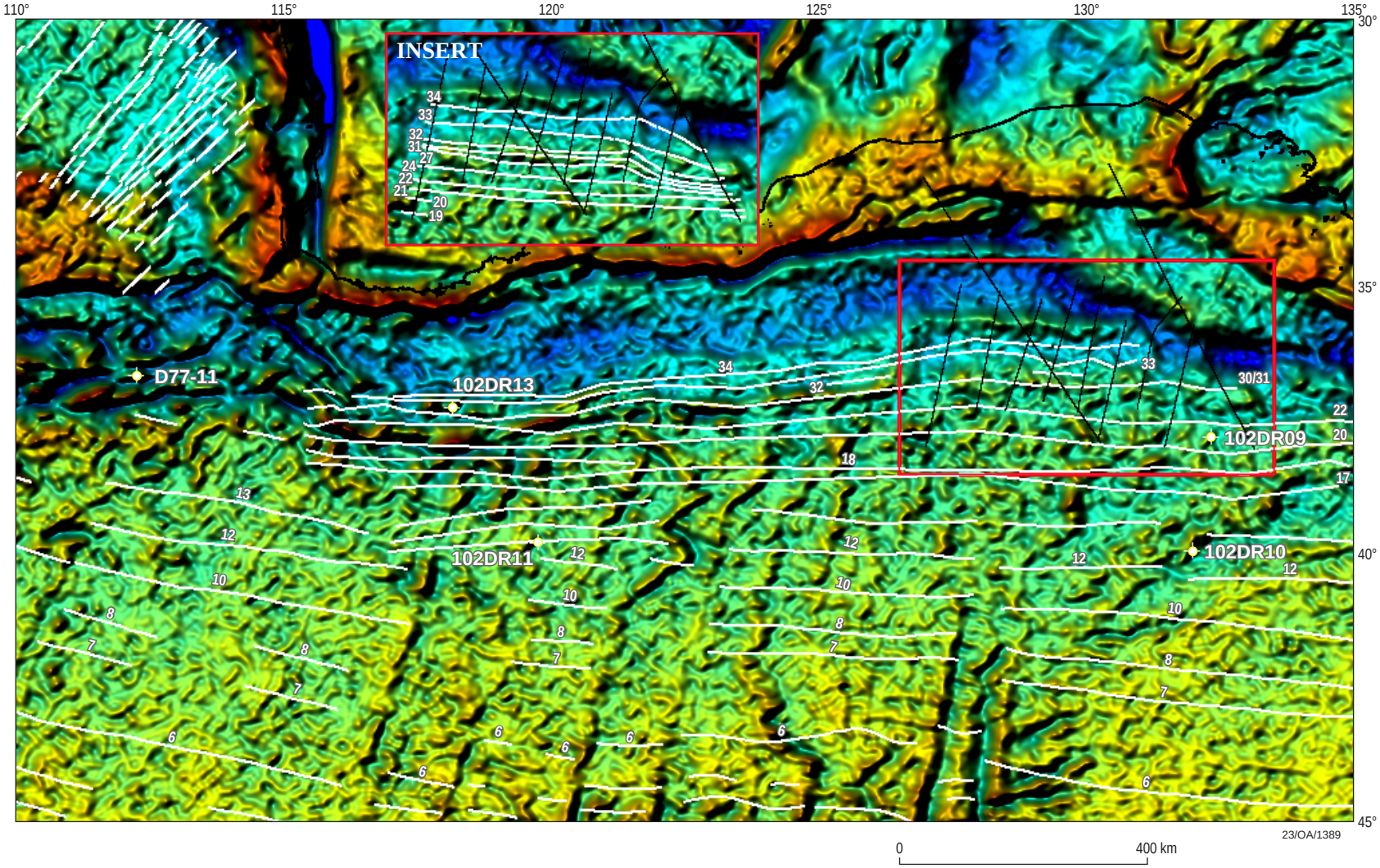


**Figure 5.** Magnetic lineations superimposed on a free air anomaly satellite gravity image that was enhanced using ER-Mapper. Magnetic lineations in main image are from Cande & Mutter (1982) and re-interpreted lineations (see inset) from Tikku & Cande (1999). Circles - dredge sample site, D77-11 - lherzolites and serpentinite, 102DR13 - ?gabbro and basalt, 102DR9 & -11 - basalt, 102DR10 - altered basalts and ?serpentinized gabbro. Black lines represent seismic tracks of Survey 199.

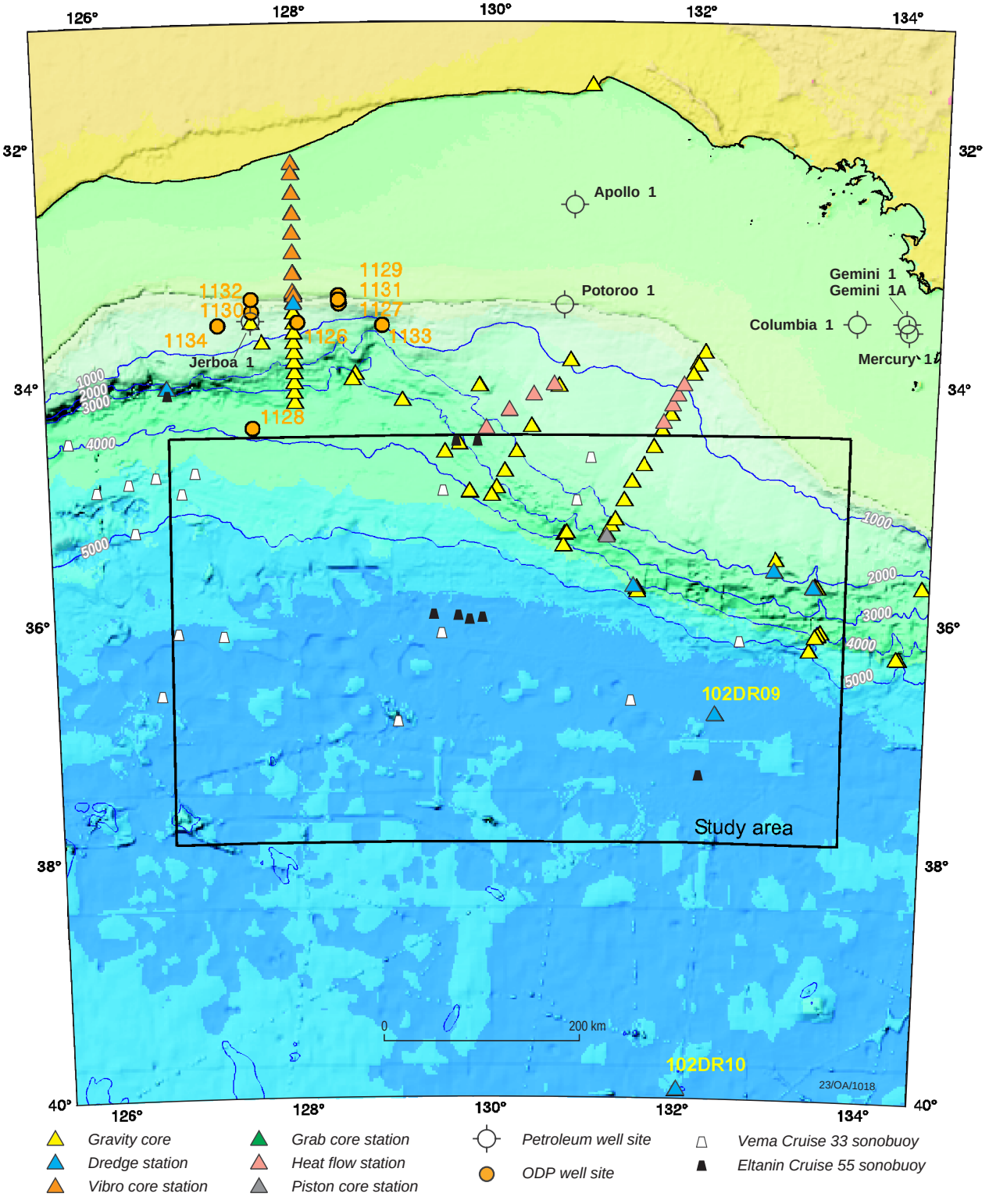


**Figure 6.** Wells, sample stations and bathymetry. Greenish shading - shallow water, bluish shading - deep water, blue contours & labels - isobaths (m).

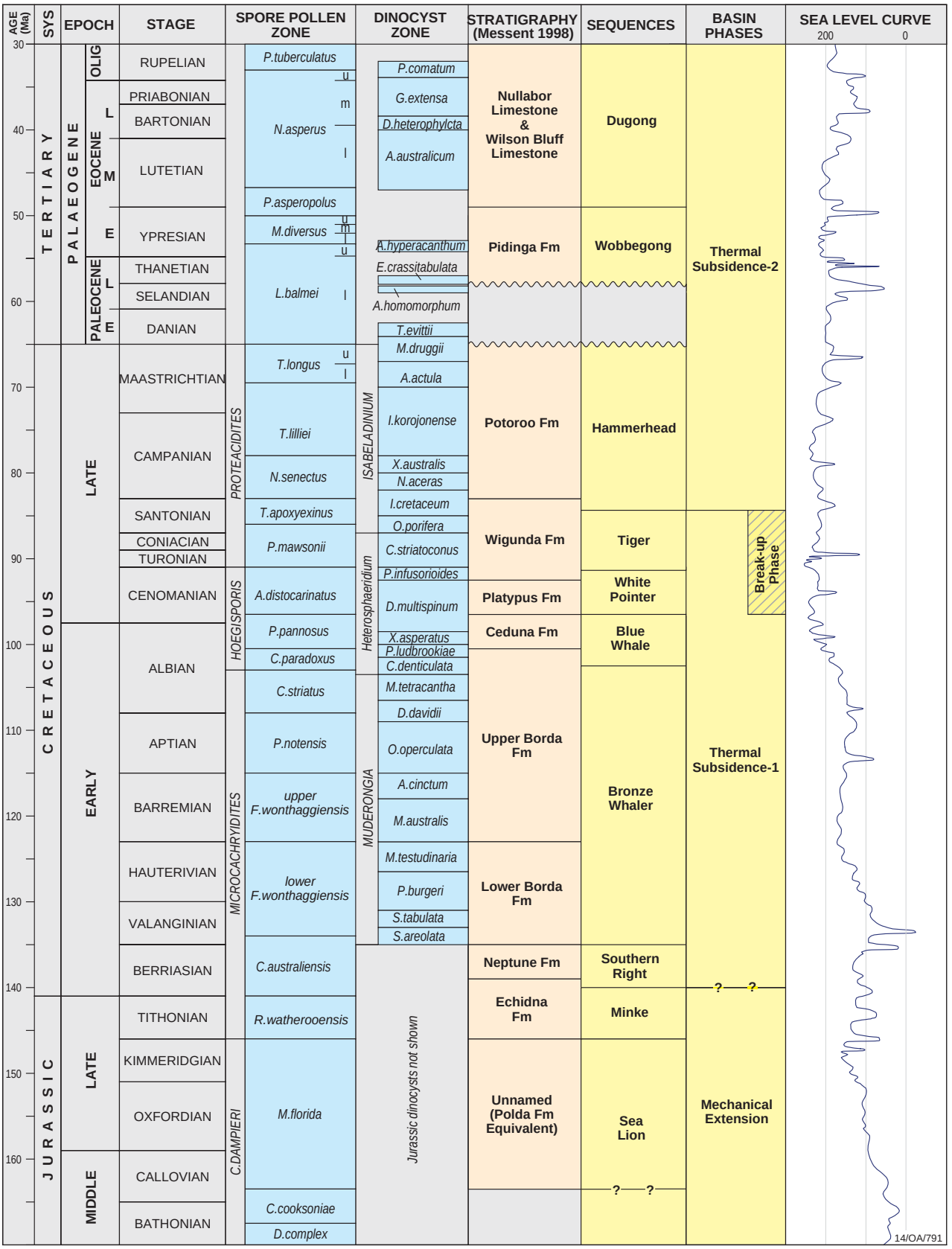


**Figure 7.** Sequence stratigraphy scheme for the Eyre, Ceduna and Recherche Sub-basins (after Totterdell et al, 2000).

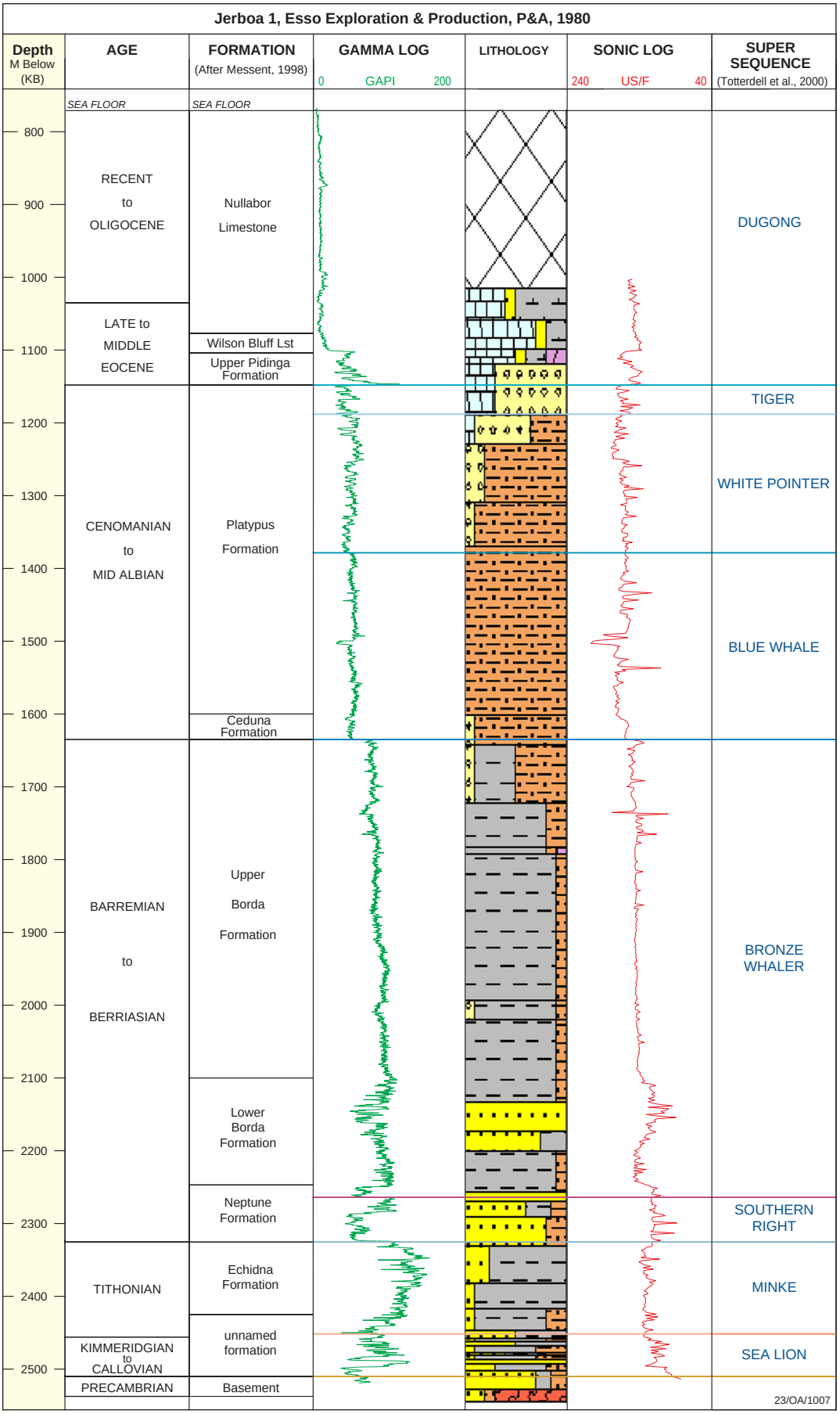


**Fig 8.** Composite log for Jerboa 1, Eyre Sub-basin.

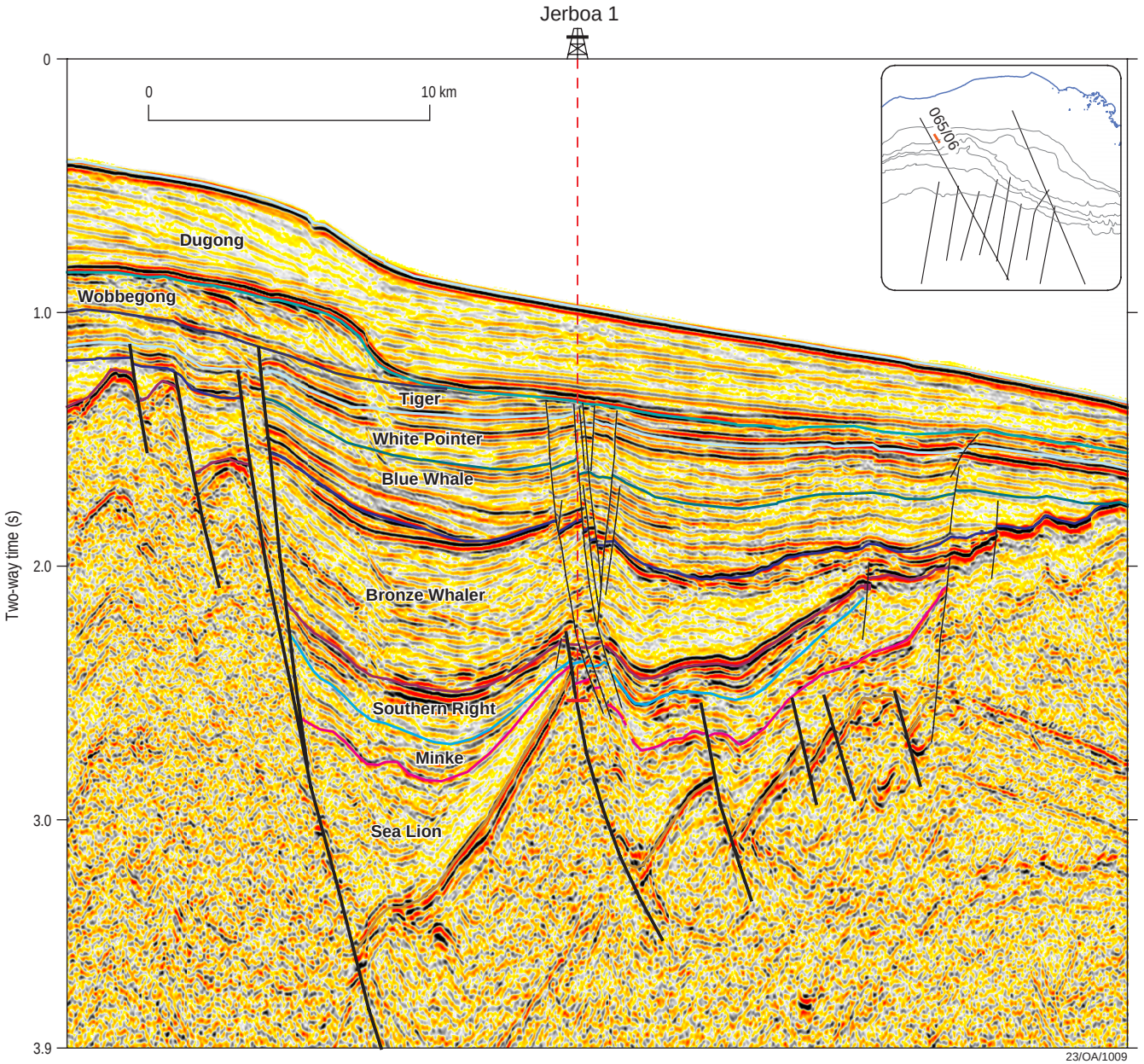


**Figure 9.** Portion of seismic line 65/06, showing the distribution and geometry of sequences in the vicinity of Jerboa 1, Eyre Sub-basin.

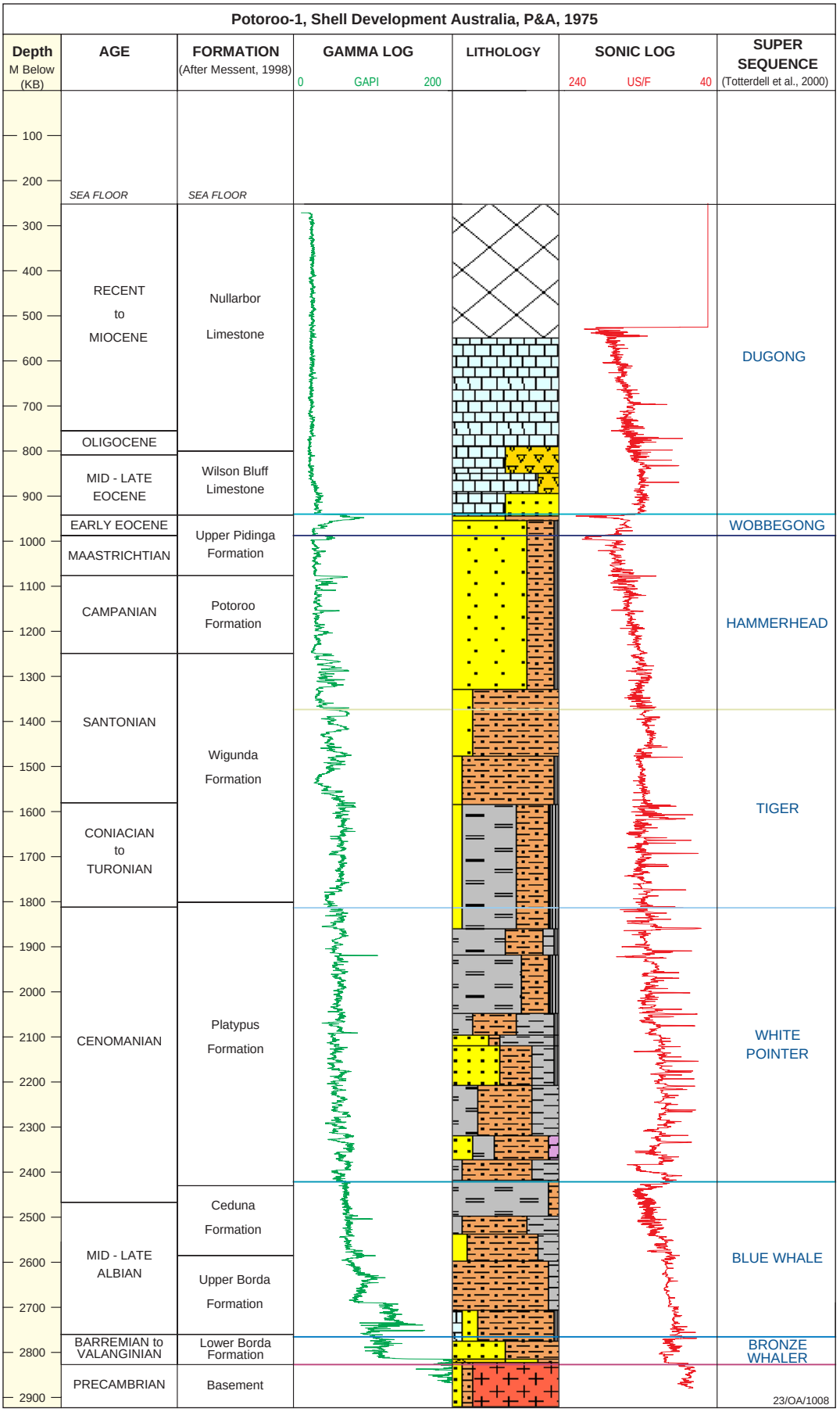


**Figure 10.** Composite log for Potoroo-1, Ceduna Sub-basin.

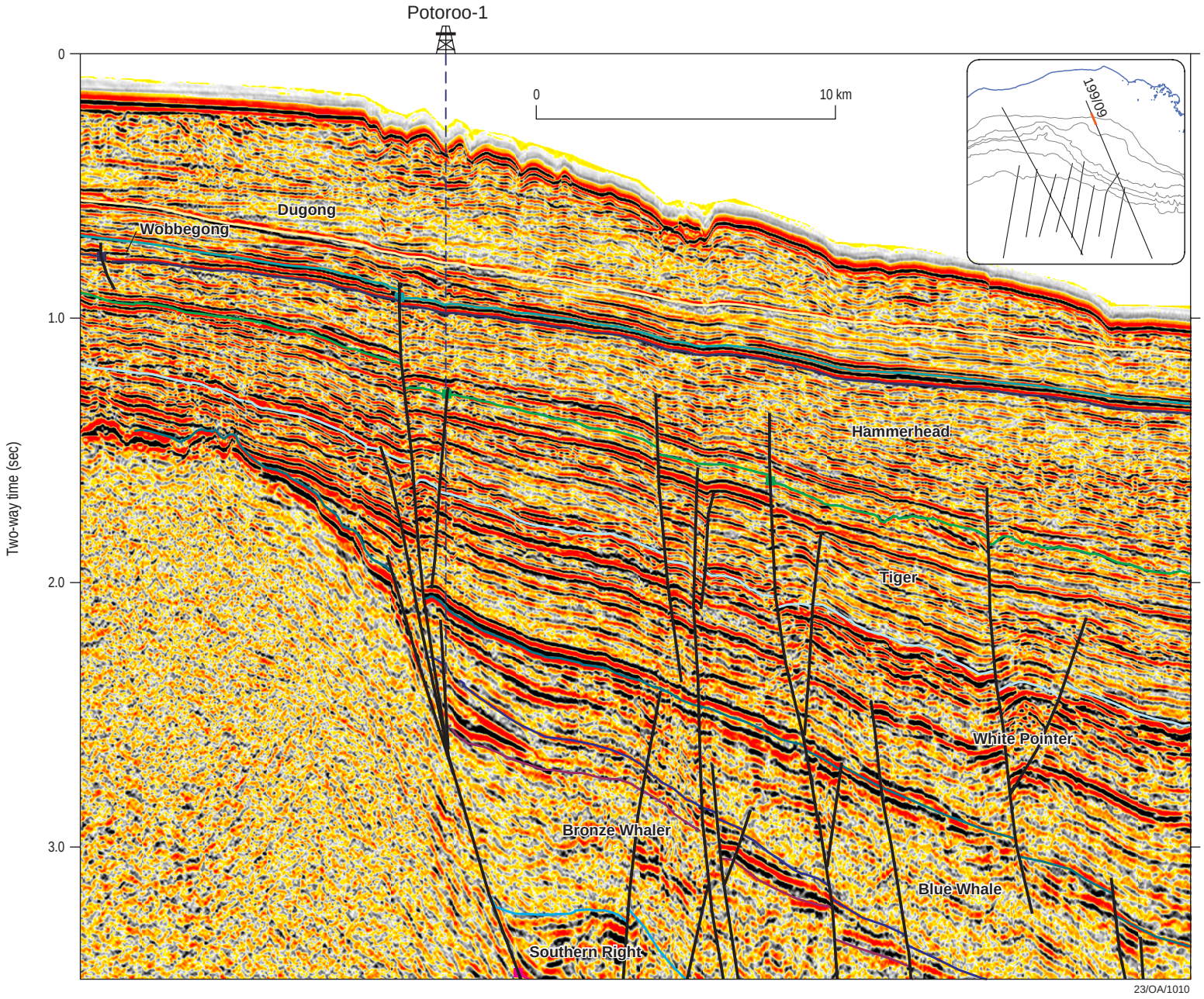


**Figure 11.** Portion of seismic line 199/09, showing the distribution and geometry of sequences in the vicinity of Potoroo-1, Ceduna Sub-basin.

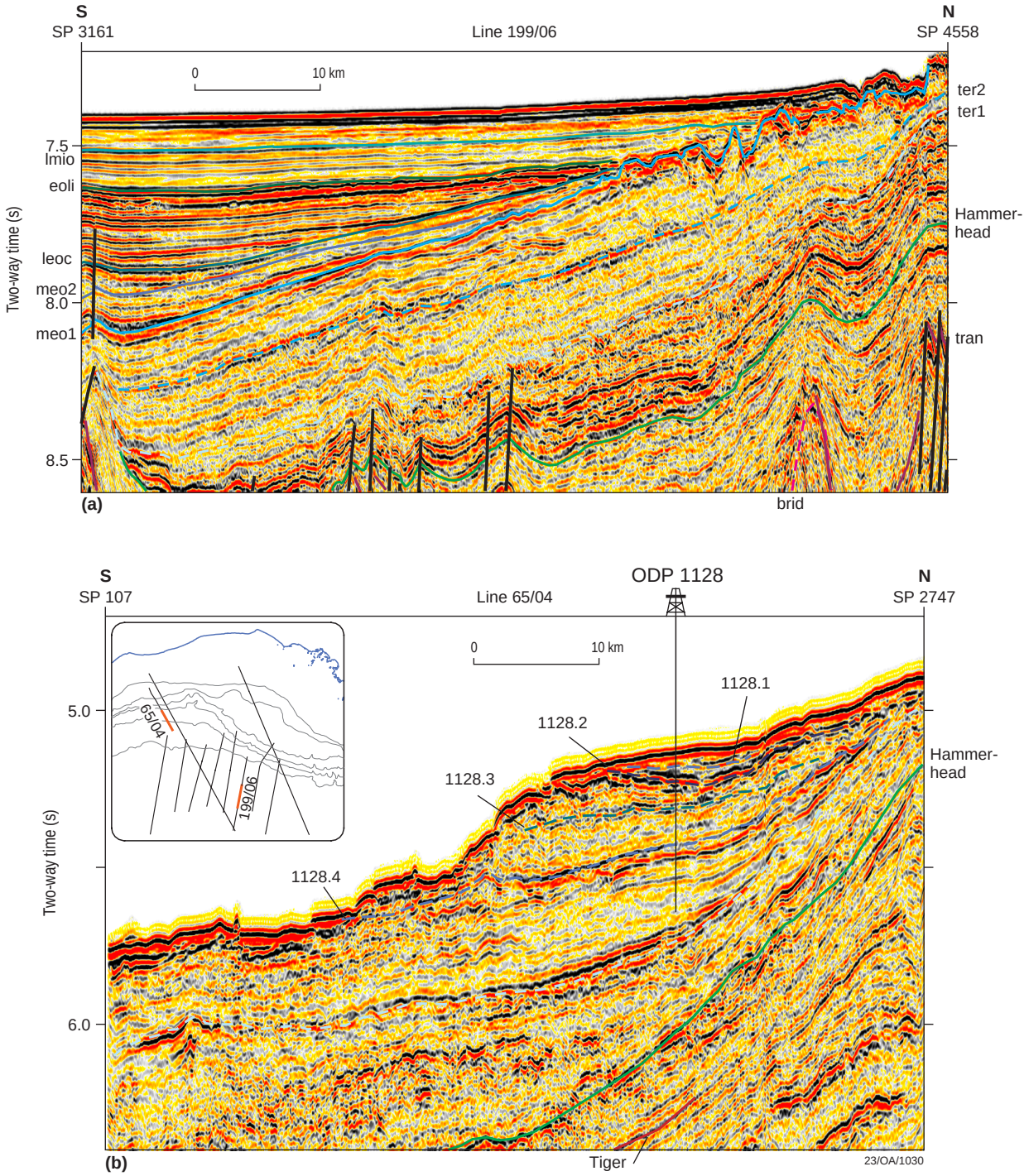


**Figure 12.** (a) Portion of seismic line 199/06 showing sediments of the Australian-Antarctic Basin (i.e. post meo1) overlying post-breakup sediments belonging to the Hammerhead and younger sequences. (b) Seismic horizons identified at ODP Site 1128, located on the continental slope. lmio - ?late Miocene, eoli - ?early Oligocene, leoc - ?late Eocene, meo2 - ?Middle Eocene, younger horizon; meo1 - ?Middle Eocene, older horizon; ter2 - ?near base Cainozoic, younger horizon; ter1 - ?near base Cainozoic, older horizon; brid - top basement ridge, tran - top transitional crust, 1128.1 - Pliocene, 1128.2 - Miocene, 1128.3 - early Oligocene, 1128.4 - base Oligocene.

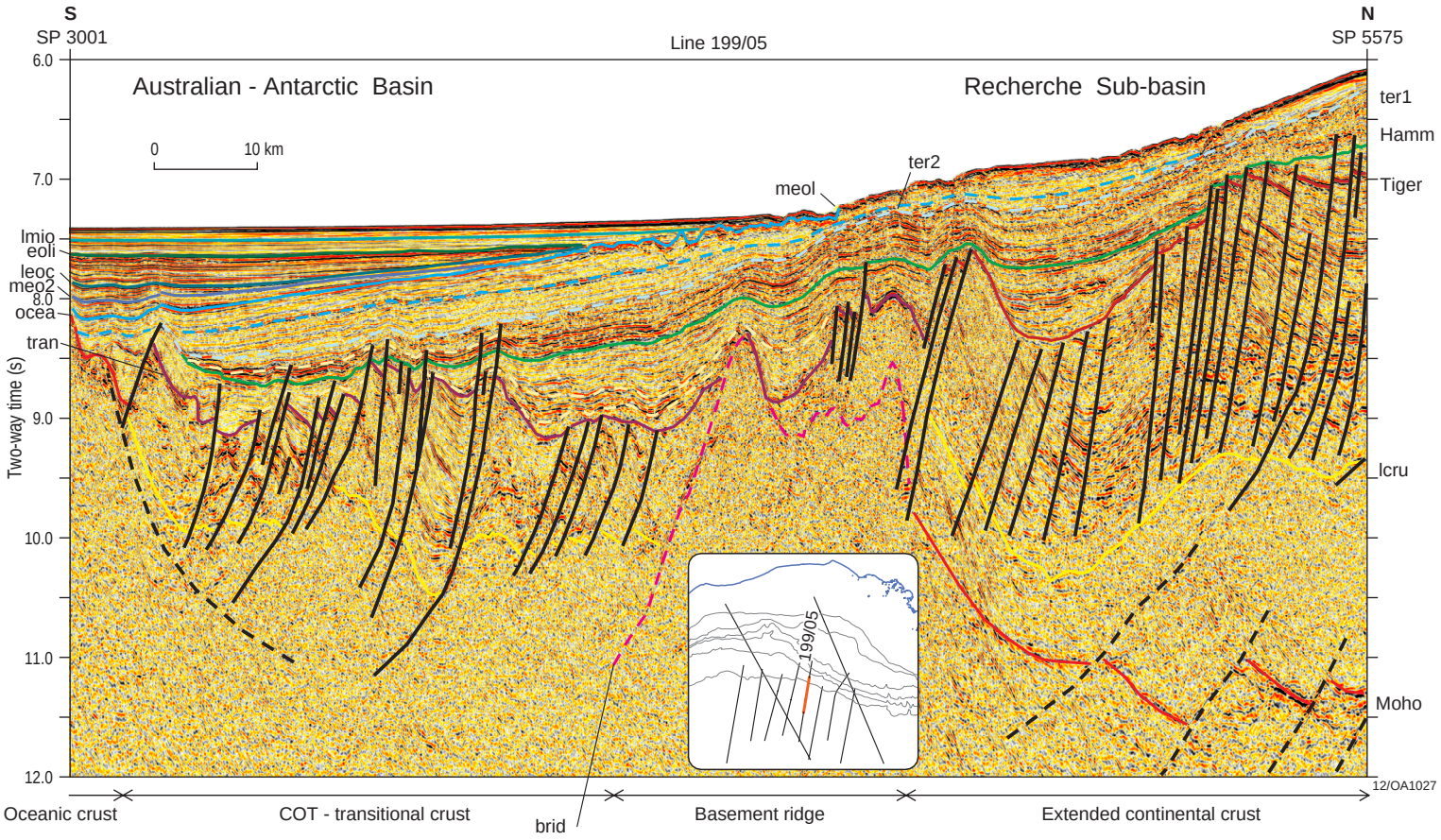


**Figure 13.** Interpretation of sediments and crust across the continent-ocean transition zone, based on seismic reflection and refraction data. Dashed black lines - faulted mantle and crust. lmio - ?late Miocene, eoli - ?early Oligocene, leoc - ?late Eocene, meo2 - ?Middle Eocene, younger horizon; meo1 - ?Middle Eocene, older horizon; ter2 - ?near base Cainozoic, younger horizon; ter1 - ?near base Cainozoic, older horizon; Hamm - base Hammerhead sequence, brid - top basement ridge, tran - top transitional crust, lcru - top lower continental crust.

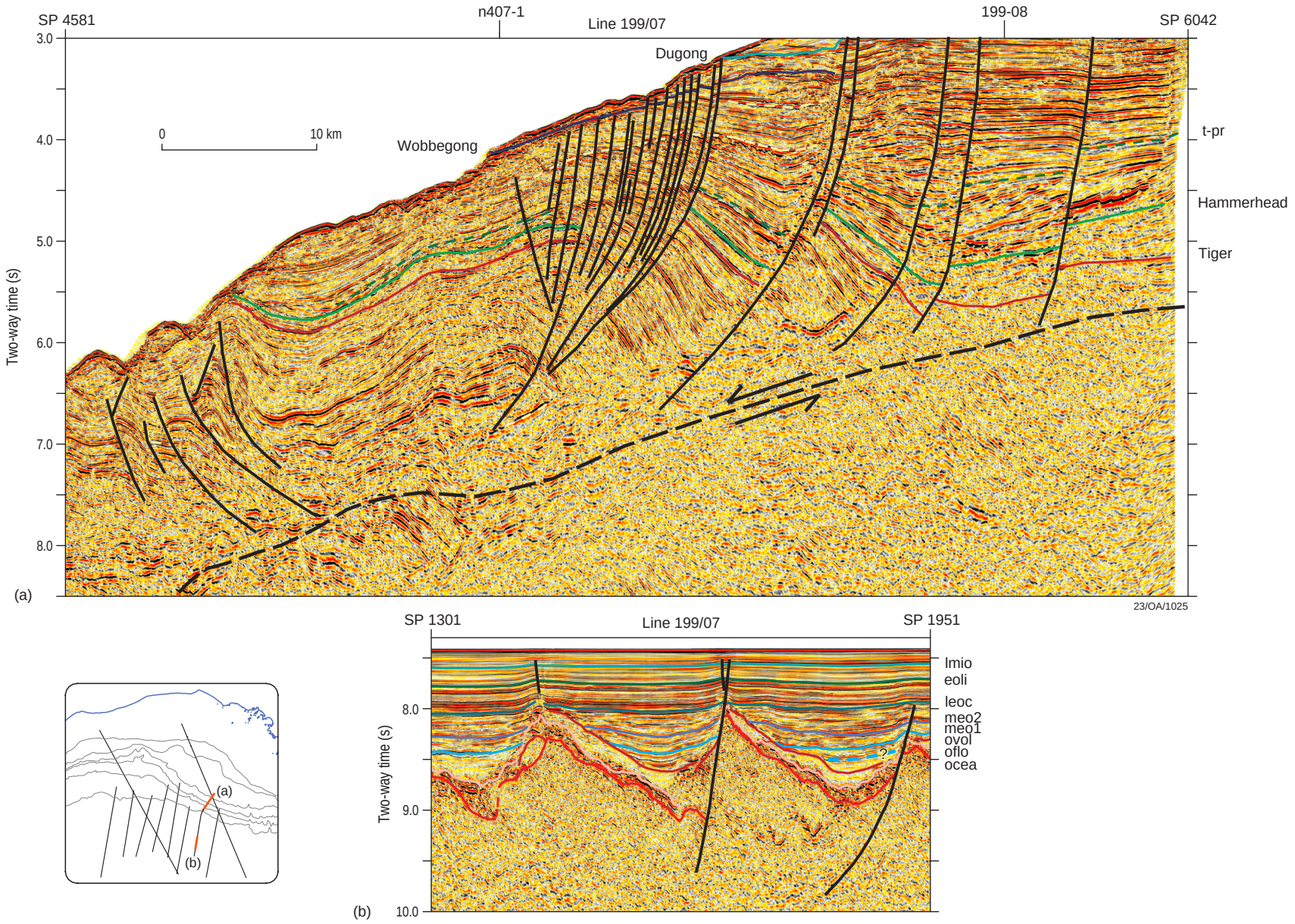


**Figure 14.** (a) ?décollement (dashed line) under the Ceduna Terrace and slope. (b) ?rifting in oceanic crust. lmio - ?late Miocene, eoli - ?early Oligocene, leoc - ?late Eocene, meo2 - ?Middle Eocene, younger horizon; meo1 - ?Middle Eocene, older horizon; t-pr - top basal progradational sequence within Hammerhead supersequence, ovol - top ?volcaniclastics/flows overlying oceanic crust, oflo - top flows on oceanic crust, ocea - top oceanic crust (after Sayers et al, 2001).

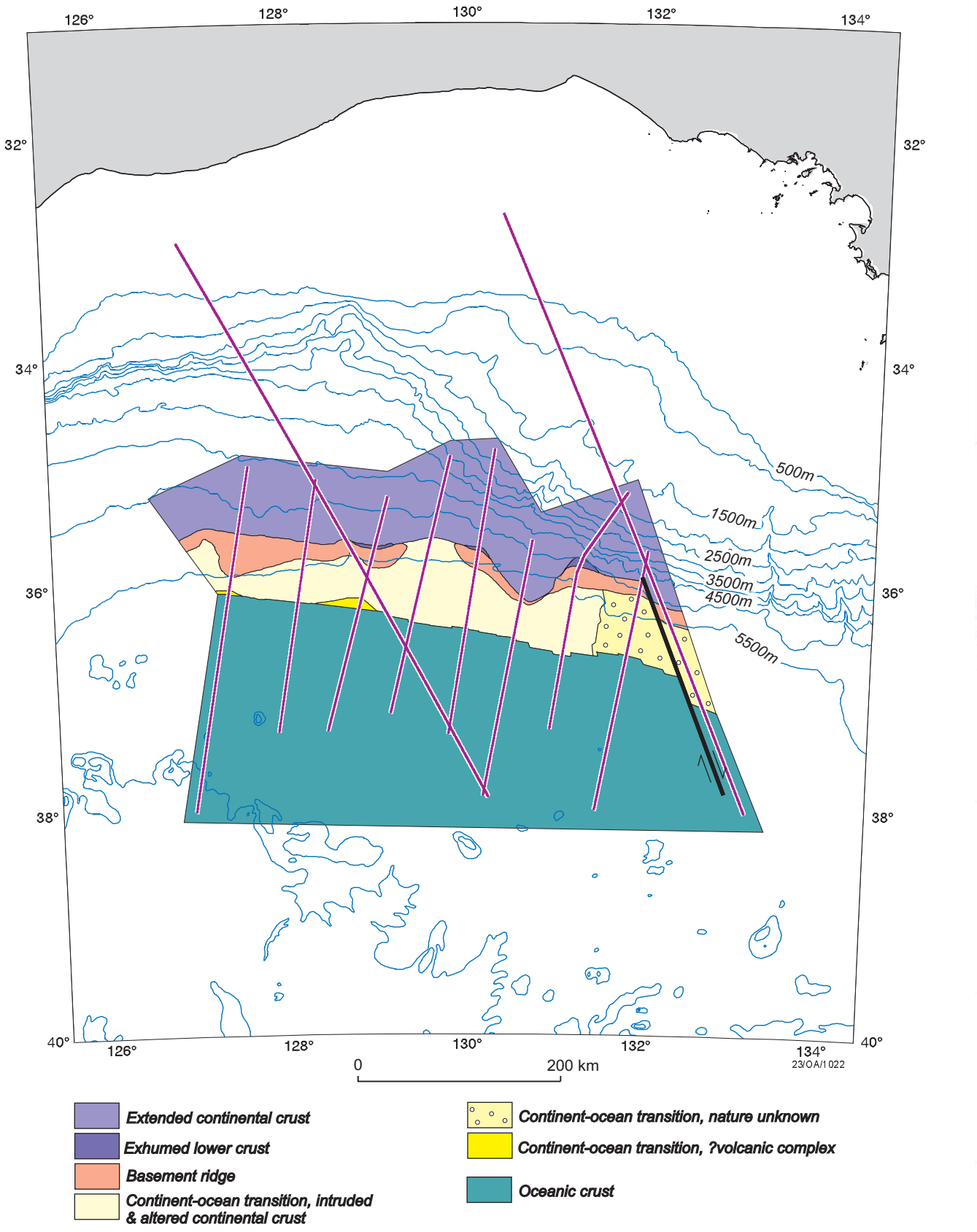


**Figure 15.** Crustal provinces of the deep-water central Great Australian Bight. Purple lines - track lines from Survey 199, black line - ?transfer/transform fault zone, blue contours and labels (m) - isobaths.

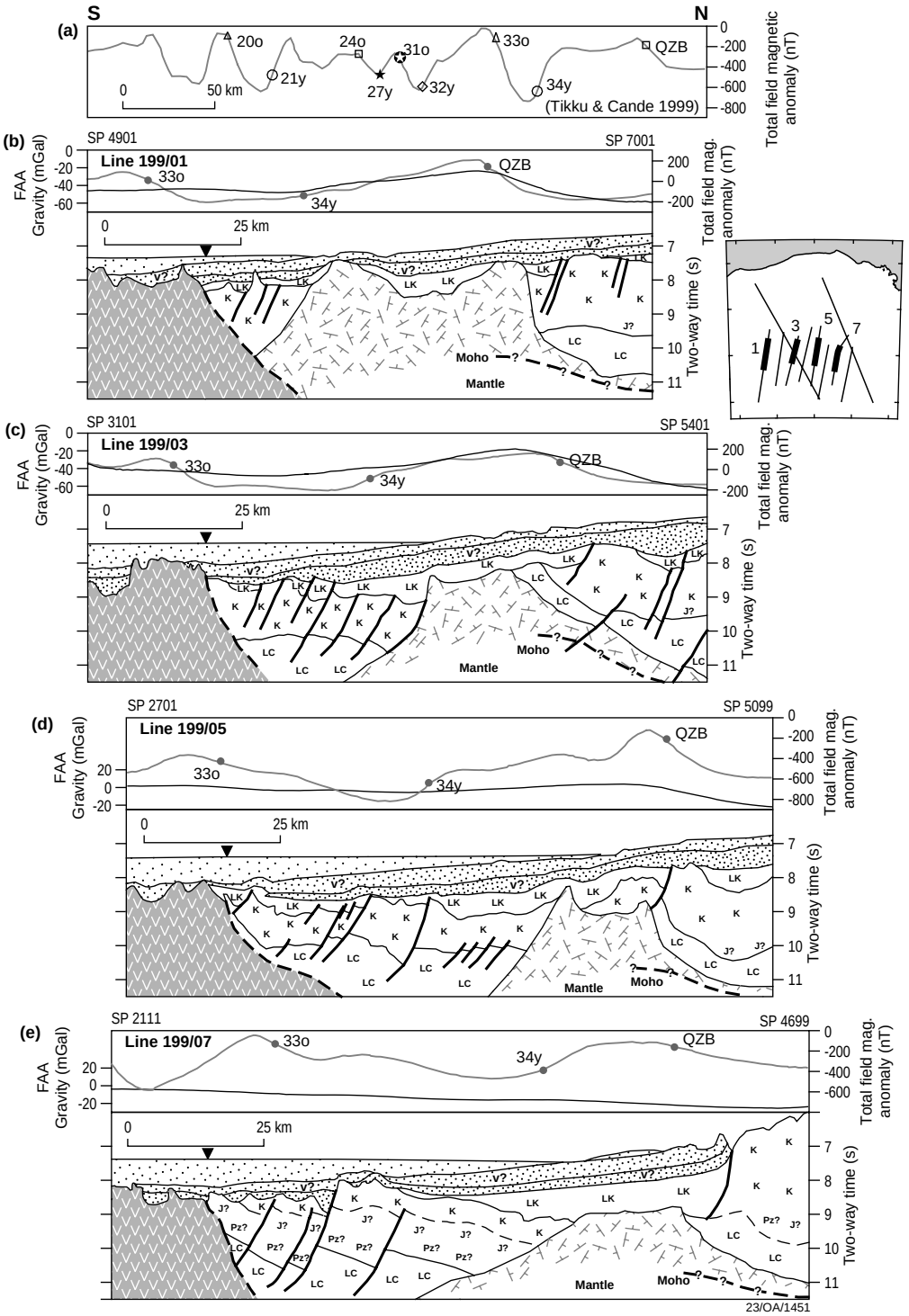


**Figure 16.** a) Preferred spreading rate model for the Southern Margin after Tikku & Cande (1999). (b-e) Line drawings of seismic profiles showing observed gravity/magnetic data over the COT, with magnetic anomaly identifications superimposed, based on the model of Tikku & Cande (1999) above. LC - lower crust; Pz - Palaeozoic; J - Jurassic; K - Cretaceous (equivalent pre-rift and syn-rift); LK - Late Cretaceous (equivalent late syn-rift); heavy, intermediate and light stipple represent post-rift sediments; 'v' pattern - oceanic crust; hinge pattern - basement ridge (altered mantle, serpentinized mantle, associated igneous rocks, altered sediments), filled triangle symbol denotes the COB, v? - possible volcanic flows. Figure revised from Sayers et al. (2001).

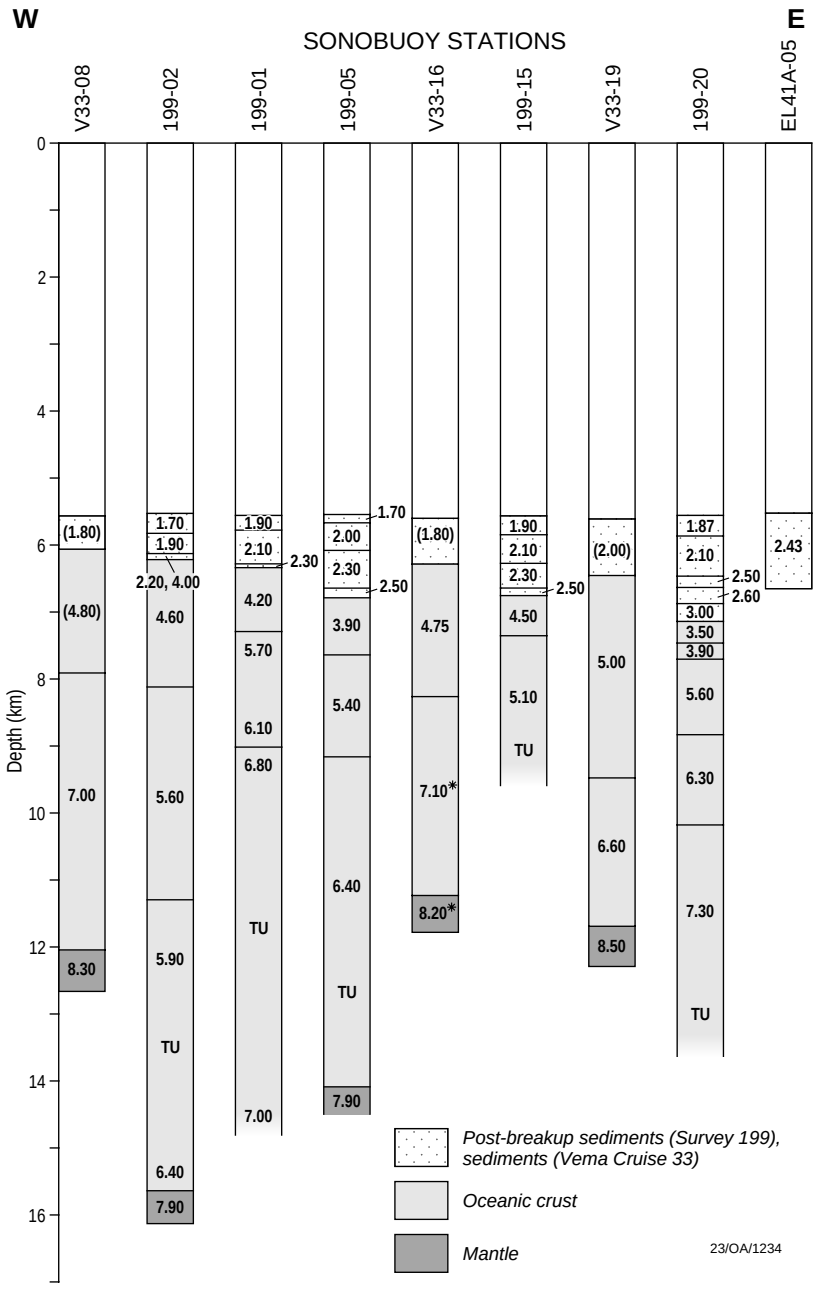


**Figure 17.** Profile of 1-D depth-velocity models across oceanic crust. 6.20 - example of P-wave velocity in km/s, * - poorly determined velocity, ( ) - assumed velocity, TU - thickness uncertain. Labels at top of models represent both the survey name and sonobuoy number (i.e. V33 - *Vema* Cruise 33, EL - *Eltanin* Cruise 55, 199 - Survey 199).

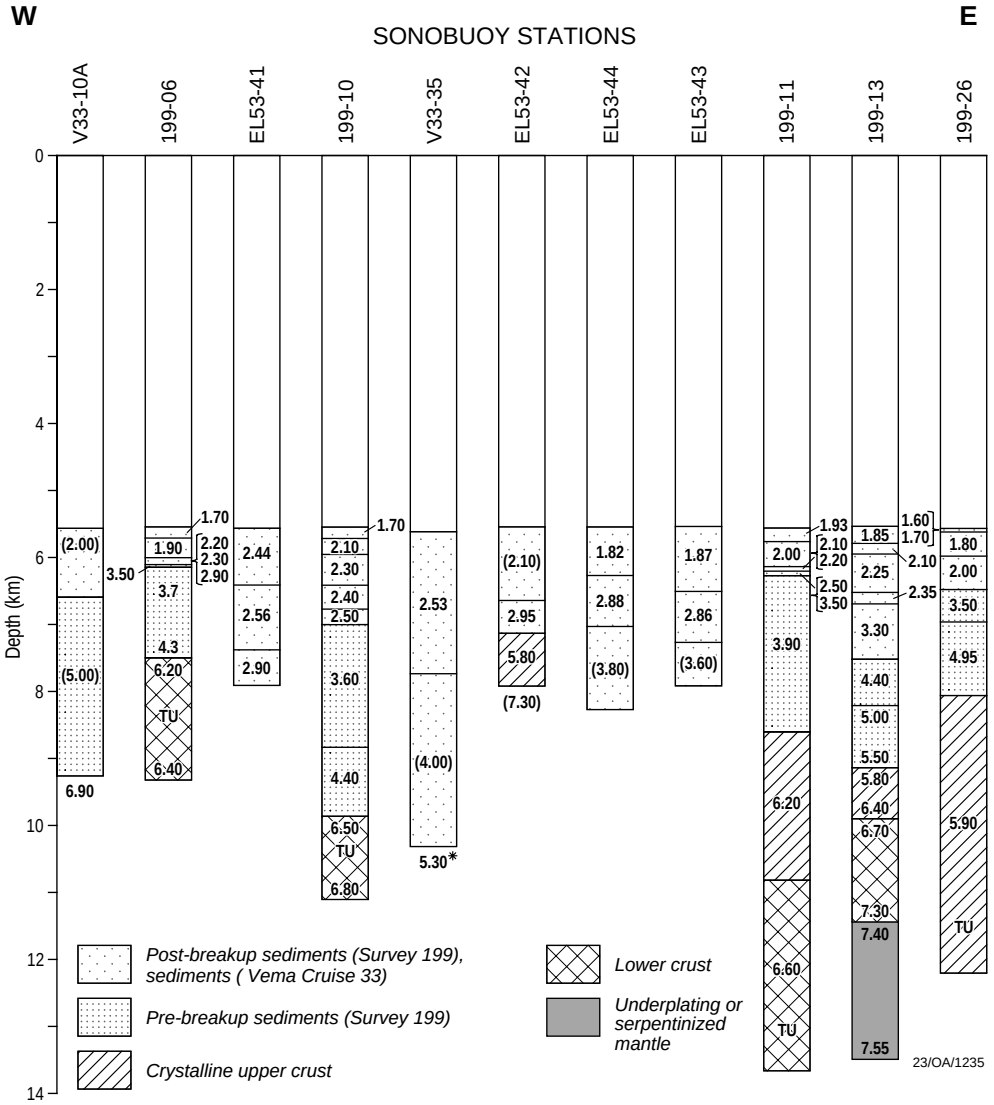


**Figure 18.** Profile of 1-D depth-velocity models across the continent-ocean transition. 6.20 - example of P-wave velocity in km/s, * - poorly determined velocity, ( ) - assumed velocity, TU - thickness uncertain. Labels at top of models represent both the survey name and sonobuoy number (i.e. V33 - *Vema* Cruise 33, EL - *Eltanin* Cruise 55, 199 - Survey 199). Note that *Vema* Cruise 33 and *Eltanin* Cruise 55 do not differentiate between pre- and post-breakup sediments.

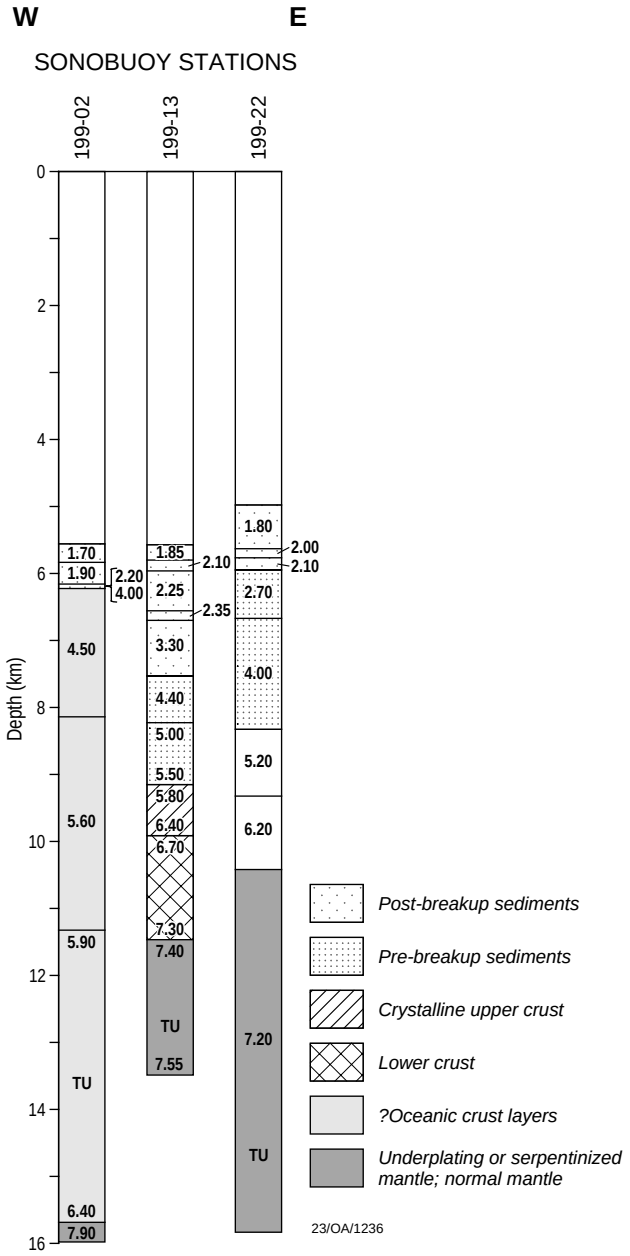


**Figure 19.** Profile of 1-D depth-velocity models across the basement ridge. 6.20 - example of P-wave velocity in km/s, * - poorly determined velocity, ( ) - assumed velocity, TU - thickness uncertain. Labels at top of models represent both the survey name and sonobuoy number (i.e. V33 - *Vema* Cruise 33, EL - *Eltanin* Cruise 55, 199 - Survey 199).

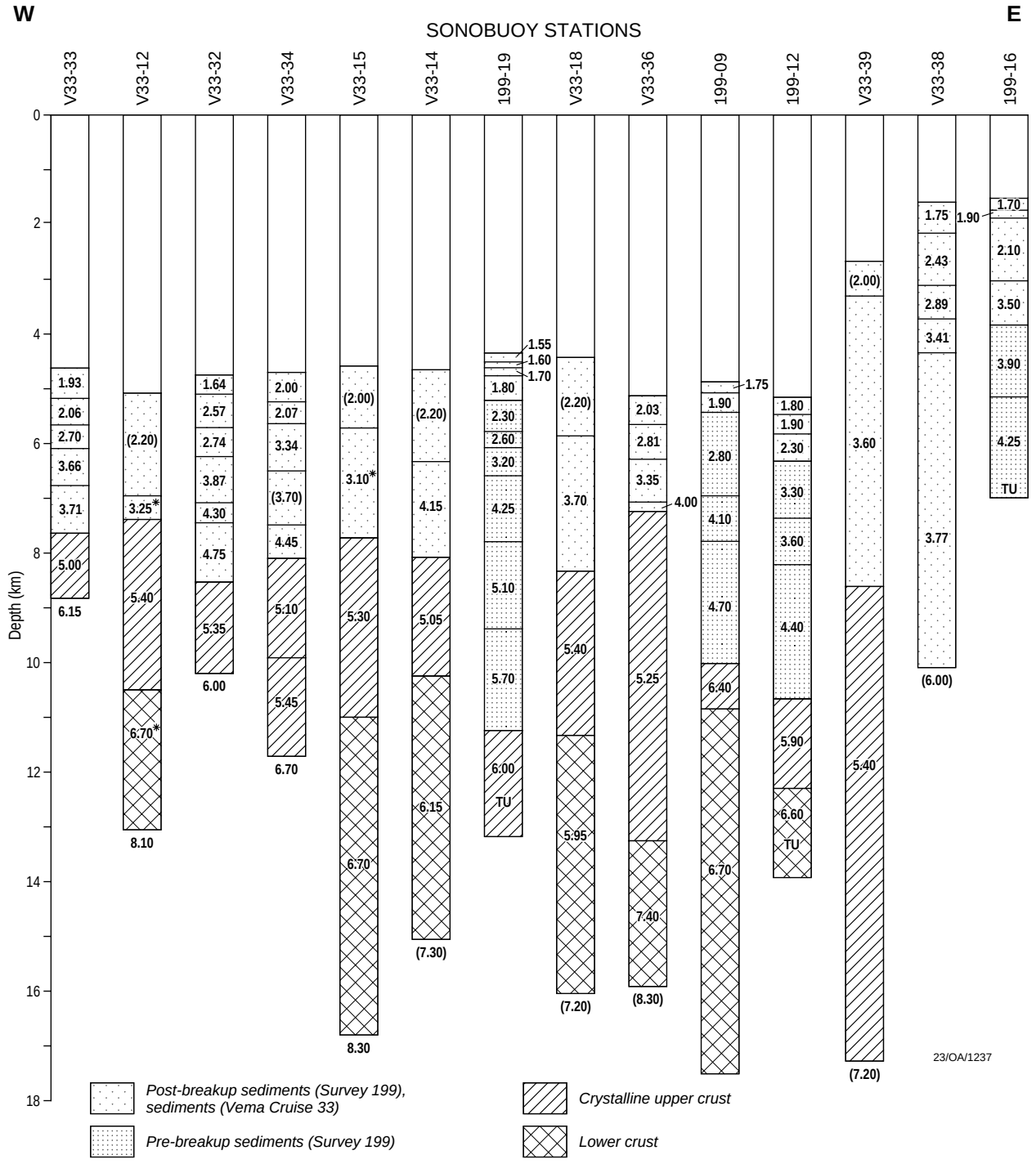


**Figure 20.** Profile of 1-D depth-velocity models across thinned continental crust. 6.20 - example of P-wave velocity in km/s, * - poorly determined velocity, ( ) - assumed velocity, TU - thickness uncertain. Labels at top of models represent both the survey name and sonobuoy number (i.e. V33 - *Vema* Cruise 33, EL - *Eltanin* Cruise 55, 199 - Survey 199). Note that *Vema* Cruise 33 and *Eltanin* Cruise 55 do not differentiate between pre- and post-breakup sediments.

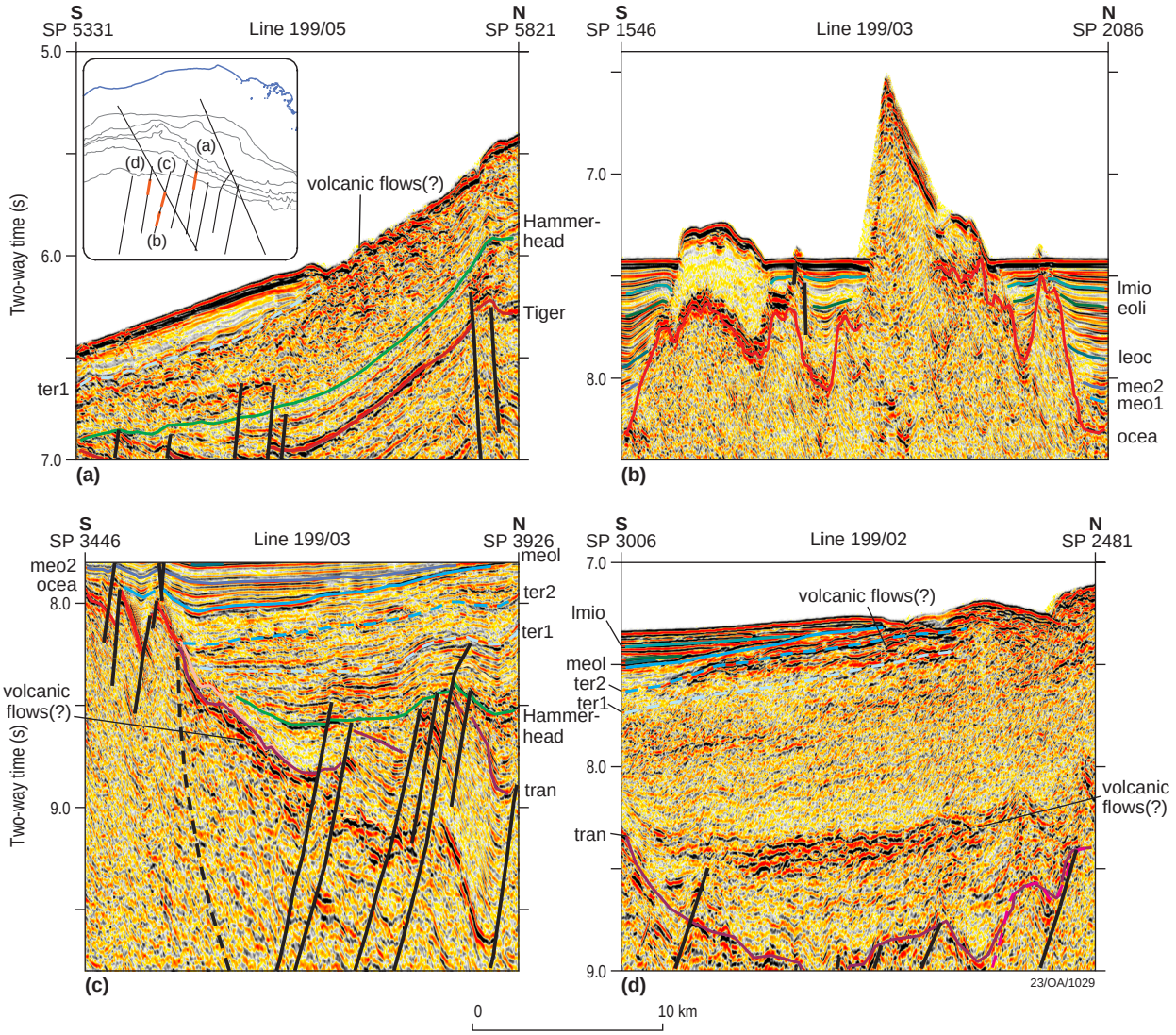


**Figure 21.** (a) ?volcanics outcropping at the seabed. (b) volcanic buildups on oceanic crust. (c-d) ?volcanics in continent-ocean transition (COT) province. Dashed black line represents arbitary boundary between oceanic crust and COT. lmio - ?late Miocene, eoli - ?early Oligocene, leoc - ?late Eocene, meo2 - ?Middle Eocene, younger horizon; meo1 - ?Middle Eocene, older horizon; ter2 - ?near base Cainozoic, younger horizon; ter1 - ?near base Cainozoic, older horizon; tran - top transitional crust, ocea - top oceanic crust.

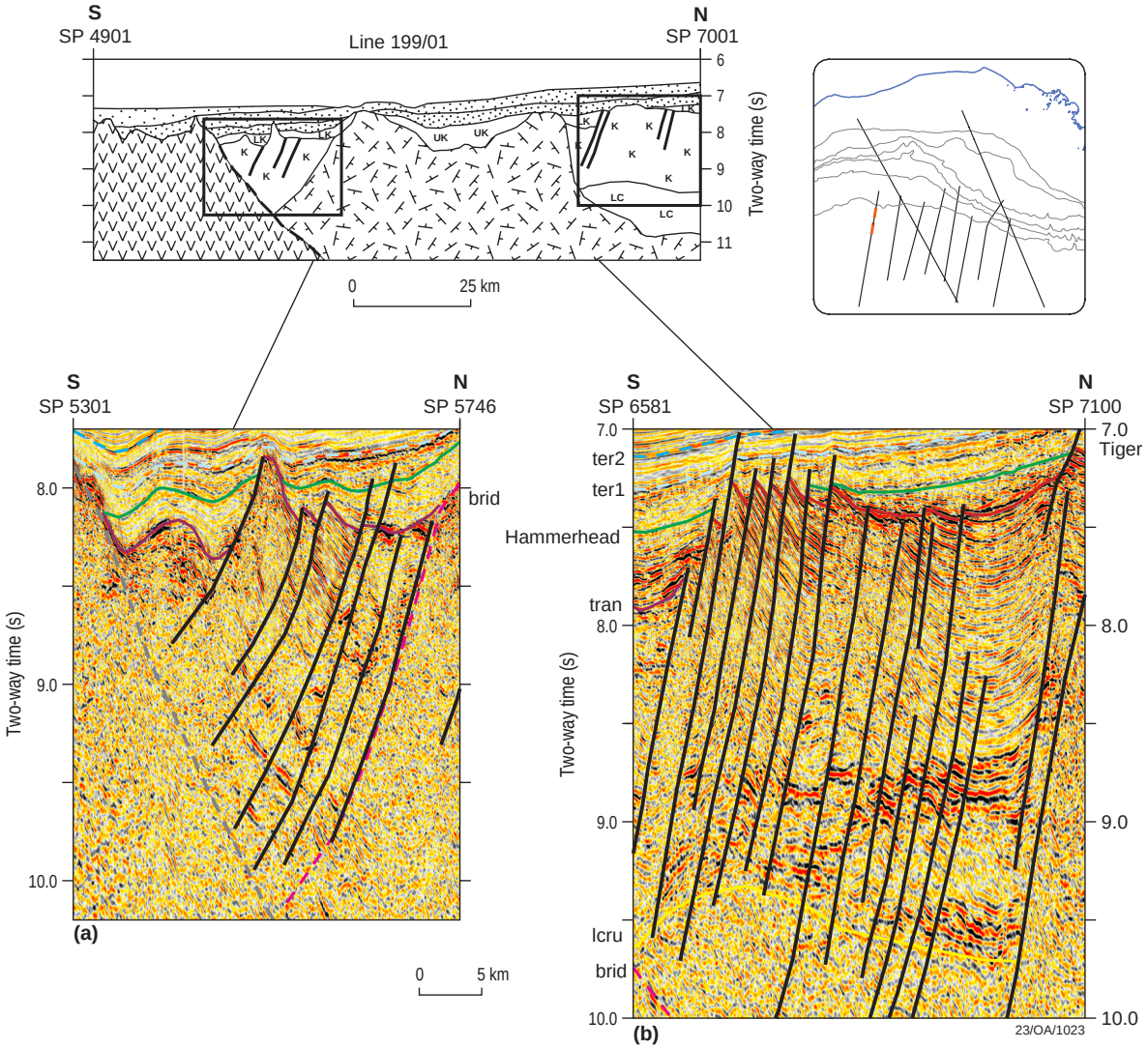


**Figure 22.** Seismic character of pre-breakup sediments in the continent-ocean transition compared with those over extended continental crust. Abbreviations: K - Cretaceous, UK - Upper Cretaceous, LC - lower crust,'v' symbol represents oceanic crust, bar symbol represents basement ridge, ter2 - ?near base Cainozoic, younger horizon; ter1 - ?near base Cainozoic, older horizon; tran - top transitional crust, brid - top basement ridge, tran - top transitional crust, lcru - top lower continental crust.

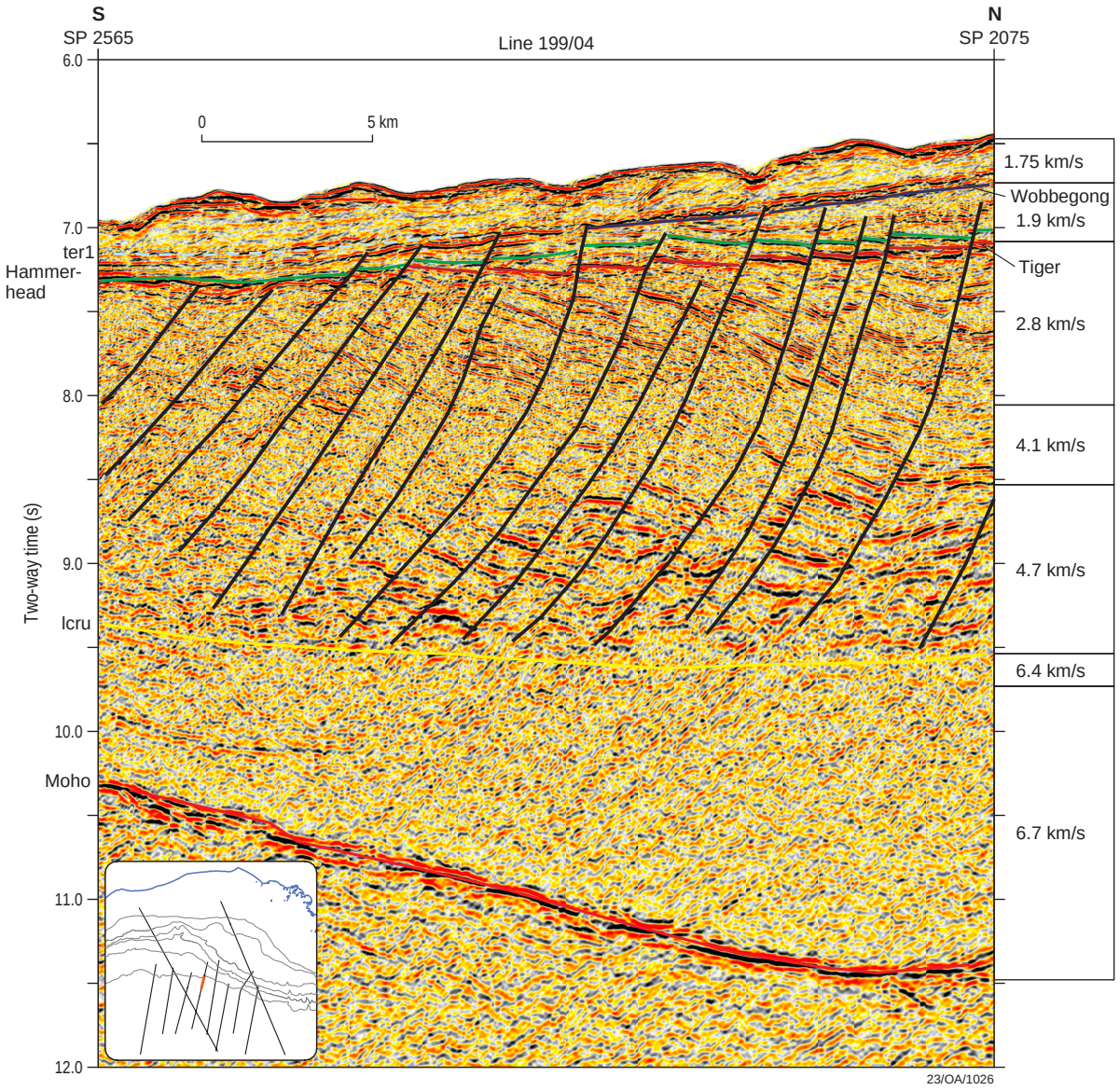


**Figure 23.** Characterisation of the lower crust and overlying sedimentary section beneath the lower continental slope, based on seismic reflection data and refraction-based velocities/depth.

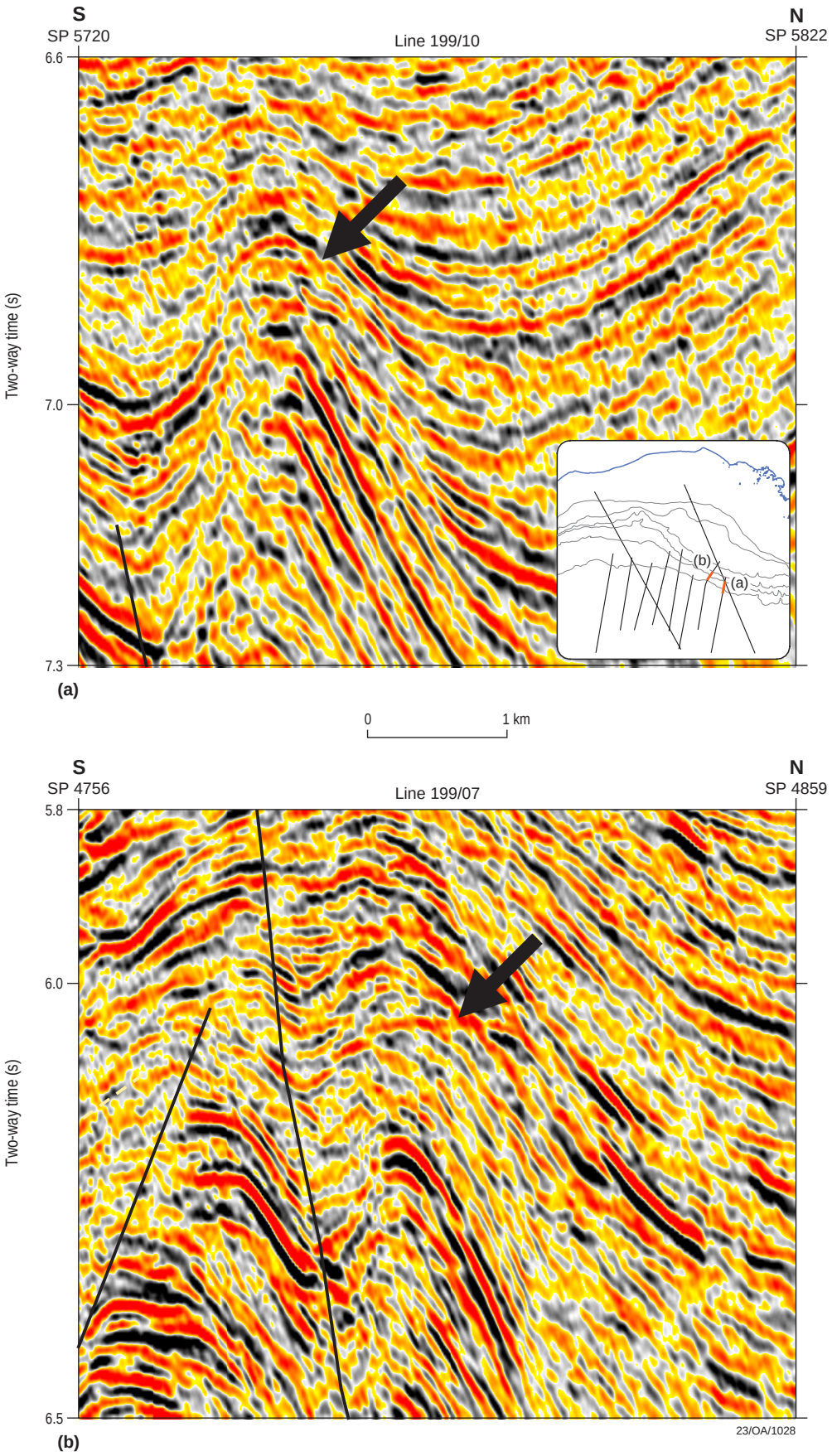


**Figure 24.** Possible flatspot in toe-thrusts beneath the continental slope.

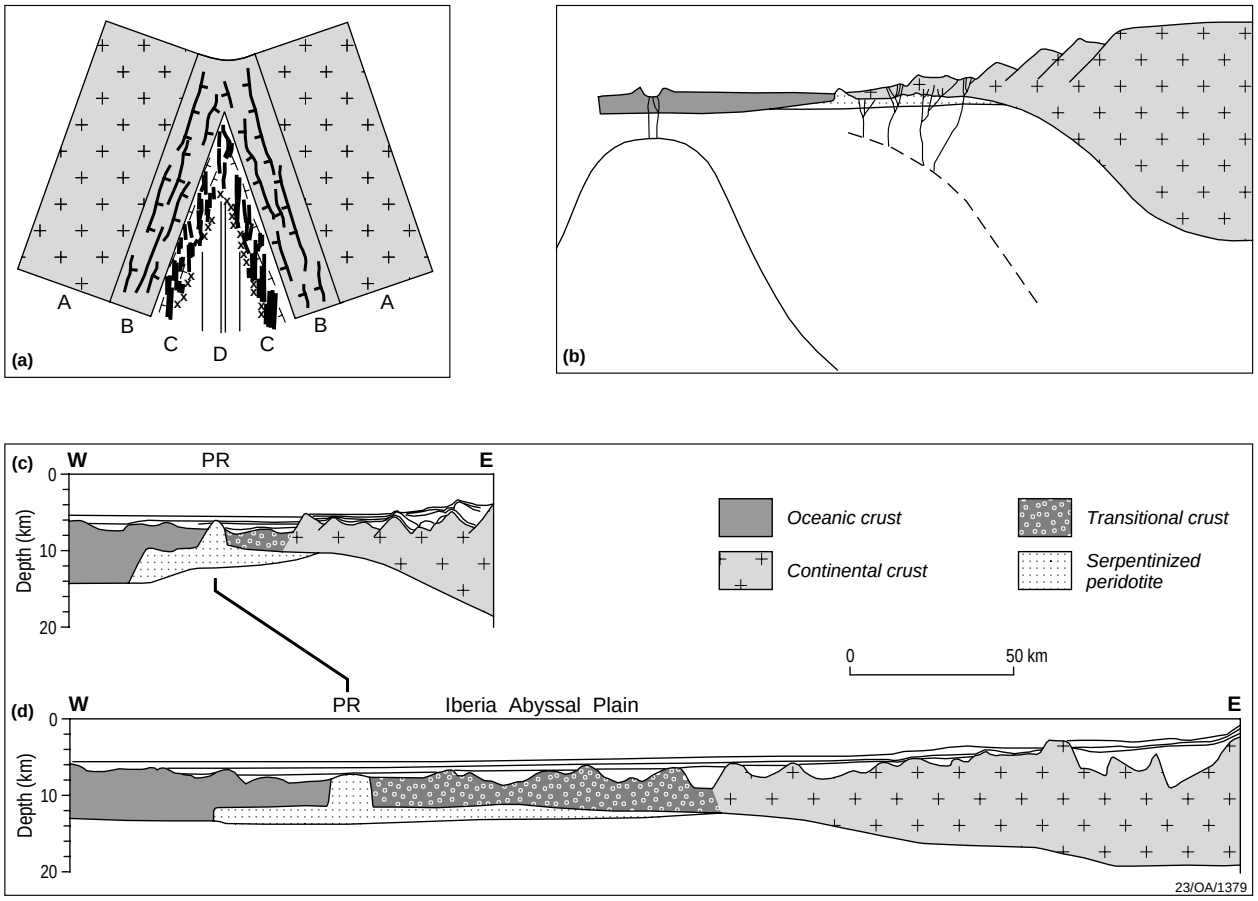


**Figure 25.** (a) Sketch (not to scale) to illustrate one of the hypotheses discussed in this report. The model (from Whitmarsh & Miles, 1995) includes A, unthinned continental crust; B, continental crust thinned by tectonic extension with upper crust normal faults; C, a transitional crust consisting of blocks of faulted continental crust and a high density of intrusives (black) which are oriented parallel to the seafloor spreading anomalies; and D, oceanic crust produced by seafloor spreading. Crosses indicate outcrops of mantle ultramafic rocks (peridotite ridge). (b) Model at the point just after continental breakup where the top of the asthenosphere is shallow enough to allow igneous intrusion of the continental crust to occur over a broad zone. Dotted region represents serpentinized peridotite. Figure from Whitmarsh & Miles (1995). (c) Summary E-W cross sections along two transects off west Iberia, based on multichannel seismic reflection profiles of Murillas et al. (1990) and seismic refraction results of Whitmarsh et al., and Horsefield (1992), PR = peridotite ridge. Figure from Whitmarsh & Sawyer (1996). (d) Section across the southern Iberia Abyssal Plain, based on seismic refraction lines of Whitmarsh et al. (1990), gravity model of Whitmarsh et al. (1993) and on multichannel seismic reflection profile LG-12 (Beslier et al., 1993). Figure from Whitmarsh & Sawyer (1996).

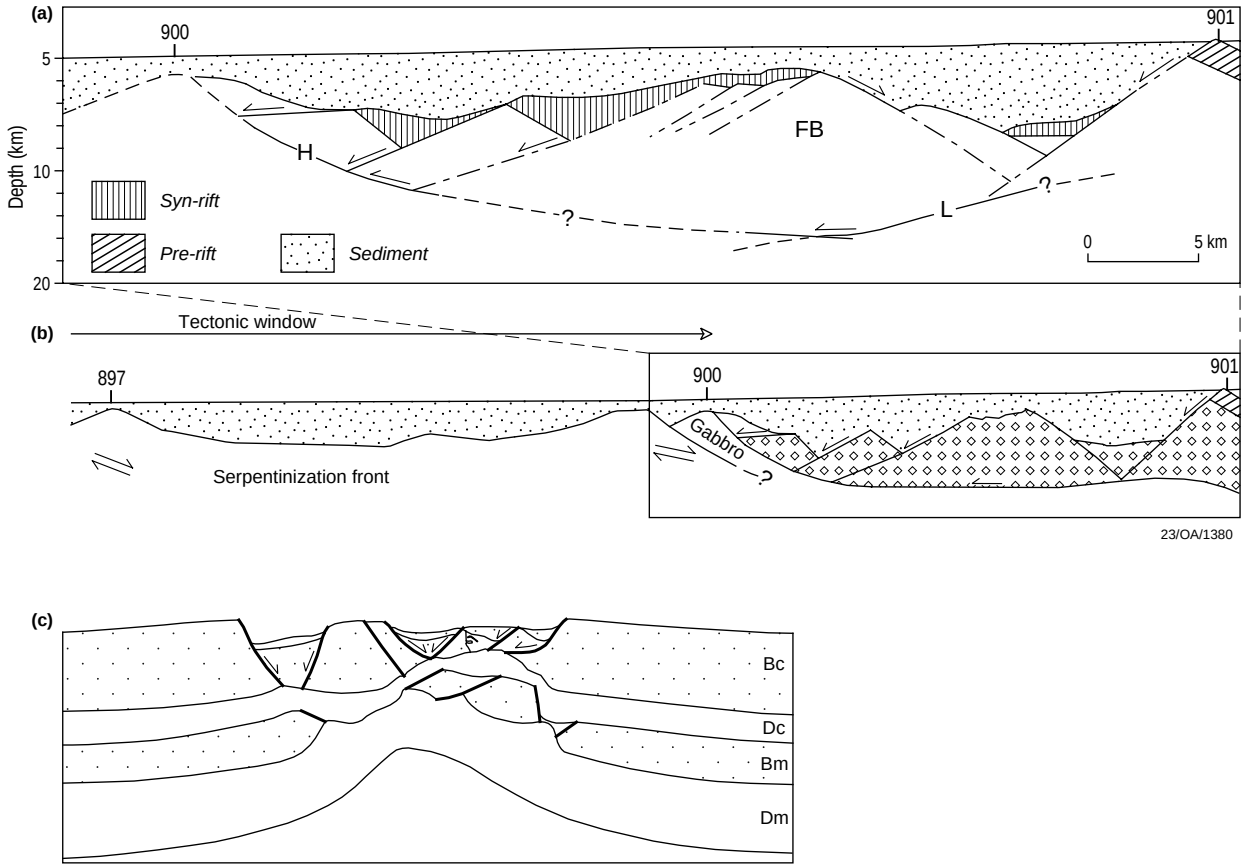





**Figure 26.** (a) Interpretations of the depth section between Sites 900 and 901, Iberia Margin (from Krawczyk et al., 1996). The eastern basement high is capped by a seismic transparent layer of prerift/pretilting sediments. Farther to the west, different tilted blocks are imaged. They are bound by fault structures (i.e. listric fault L) and a detachment 'H', which developed during different phases of rifting. 'H' developed during the synrift I phase accommodating top-to-the-west motion, and was subsequently cut and rotated by 'L' during the synrift II stage. Backrotation of 'H' first during synrift I and subsequently during synrift II explains its current orientation. 'H' terminates at the top of the basement high 500 m east of the drilled Site 900. Wedge-shaped sedimentary sequences are either of early synrift/prerift or of synrift II age. B and C. This figure assumes the eastward-dipping part of 'H' cutting across 'L' at about 12 km depth by analogy to the Galicia Margin (e.g. Boillot et al., 1997). (b) This sketch summarises and extends interpretations of (a) to the west: deep lithospheric levels were tectonically unroofed as a result of conjugate, lithospheric shear zone activity during rifting (after Beslier et al. 1995). Figure from Krawczyk et al. (1996). (c) Laboratory model of Brun & Beslier (1996), reprinted with permission from Elsevier; Bc = brittle crust (sand), Dc = ductile crust (silicone); Bm = brittle mantle (sand); Dm = ductile mantle (silicone).

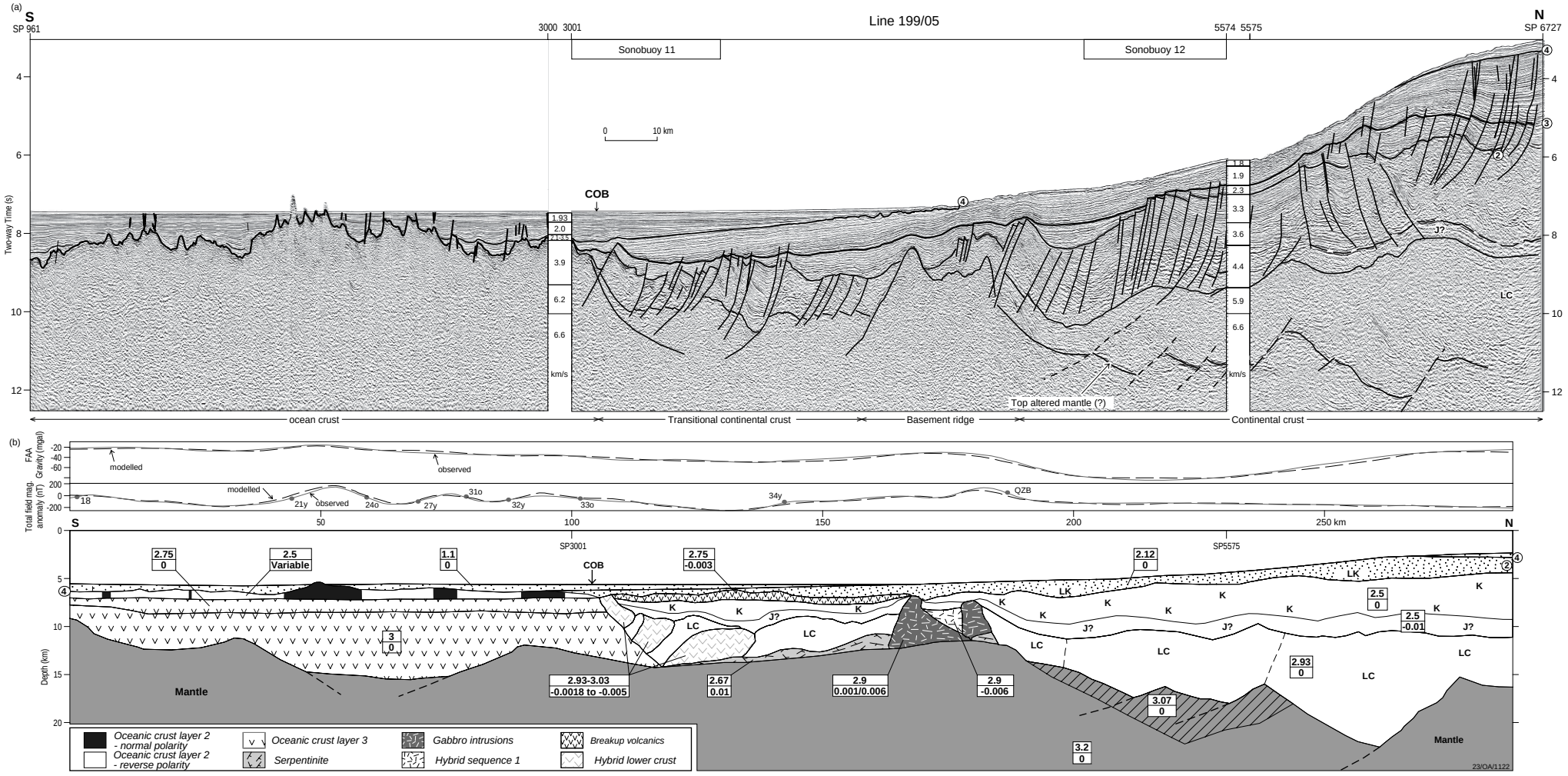


**Figure 27.** (a) Seismic profile on line 199/05 showing interpretation of sedimentary sequences and crust from the outer Ceduna Sub-basin, across the COT, COB and onto the oceanic crust. Interpretation is based on seismic reflection data and refraction modelling. 2 - Turonian; 3 - early Campanian; 4 - Mid-Eocene. J? - Possible Jurassic; LC - lower crust. Dashed sub-horizontal line represents a possible sequence boundary roughly equivalent to the top Jurassic. Sonobuoy refraction model velocities shown as vertical strips, positioned at one end of the shot range for display purposes. (b) Potential field model for line 199/05. Magnetic anomaly picks are based on Tikku & Cande (1999). Upper and lower values in the boxes are density ($t/m^3$) and magnetic susceptibility (cgs), respectively, for the associated layer. The normal polarity bodies used to model magnetic anomalies over oceanic crust have been placed where the data demands a change in magnetic properties. The bodies integrate a number of magnetic polarity changes associated with the slow-spreading crust. UK - Upper Cretaceous, K - Cretaceous. Hachured area represents an area of probable, altered mantle interpreted from modelled refraction velocities of 7.2-7.6 km/s. Figure from Sayers et al. (2001).

A high resolution A3 plot file of this figure suitable for large size □ plotters can be found in the Plot files sub-directory as .PS or .JPEG on □

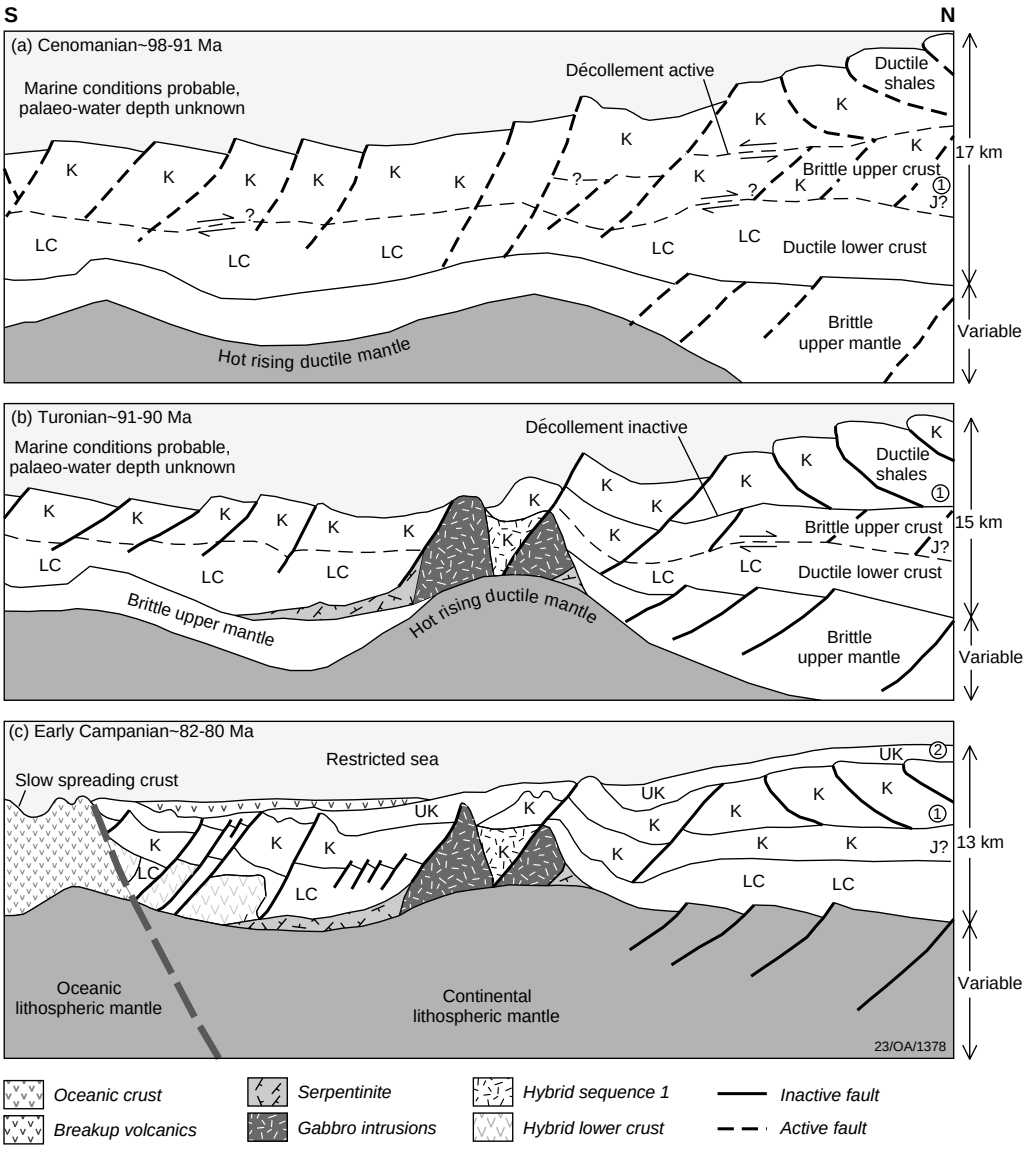


**Figure 28.** Reconstruction diagram for the continent-ocean transition and general breakup model using a 4-layer lithosphere (i.e. ductile and brittle crust and mantle, similar to the model of Brun & Beslier (1996). (a) Upper and lower crustal extension, décollement faulting in mobile shales of the Ceduna Sub-basin, uplift. (b) Lower crustal extension, hot rising ductile mantle, partial unroofing of mantle and gabbro intrusions. (c) Breakup, slow spreading oceanic crust and formation of oceanic lithospheric mantle, intrusions into lower crust. UK - Upper Cretaceous (equivalent Tiger supersequence), K - Cretaceous (equivalent supersequences White Pointer to Minke), J - Jurassic, LC - lower crust; 1 - pre-Tiger super-sequences, 2 - Tiger supersequence. Figure from Sayers et al. (2001).

A high resolution A3 plot file of this figure suitable for large size plotters can be found in the Plot files sub-directory as .PS or .JPEG on this CD

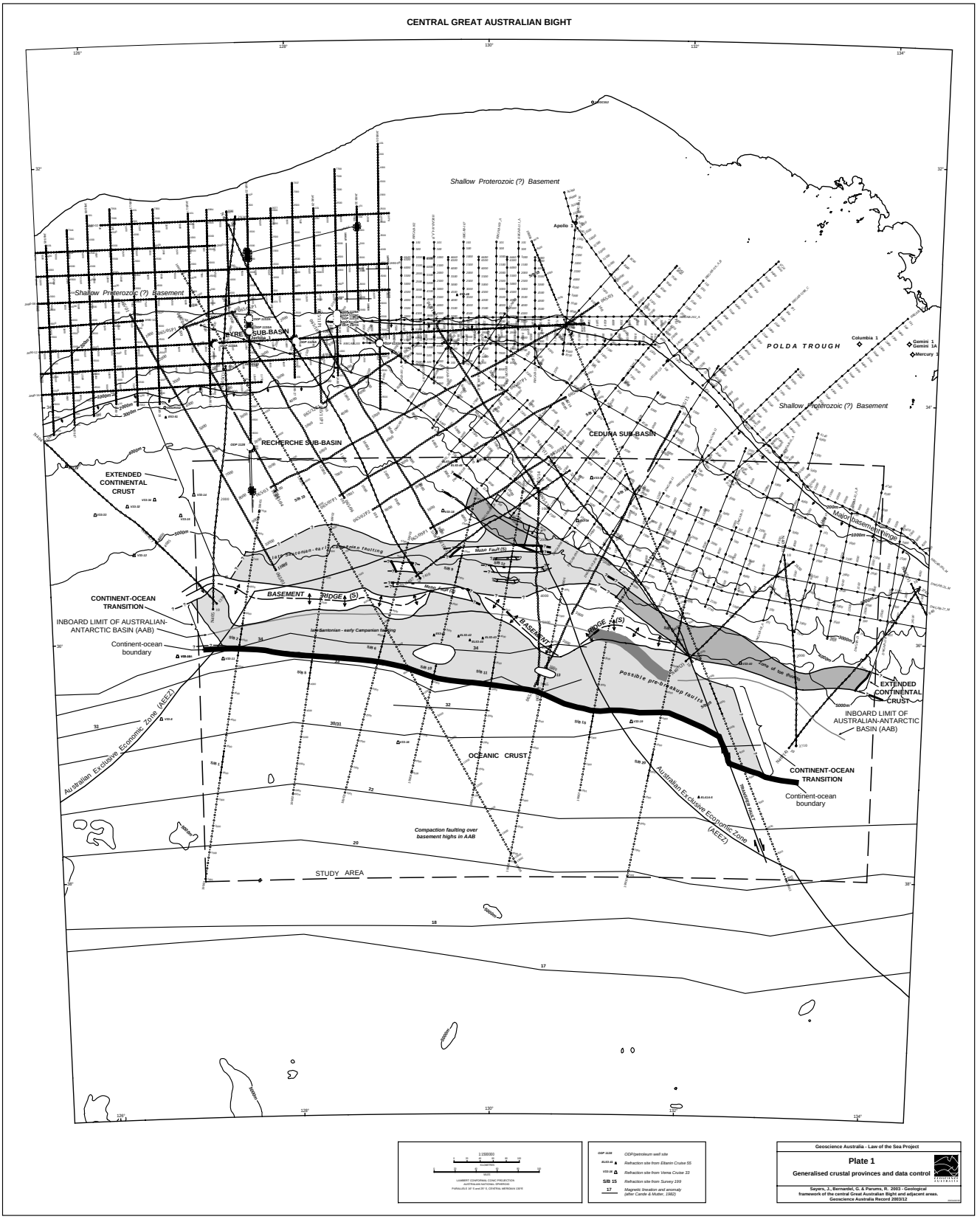

A high resolution A3 plot file of this figure is suitable for large size plotters can be found in the Plot files sub-directory as .PS or .JPEG on this CD

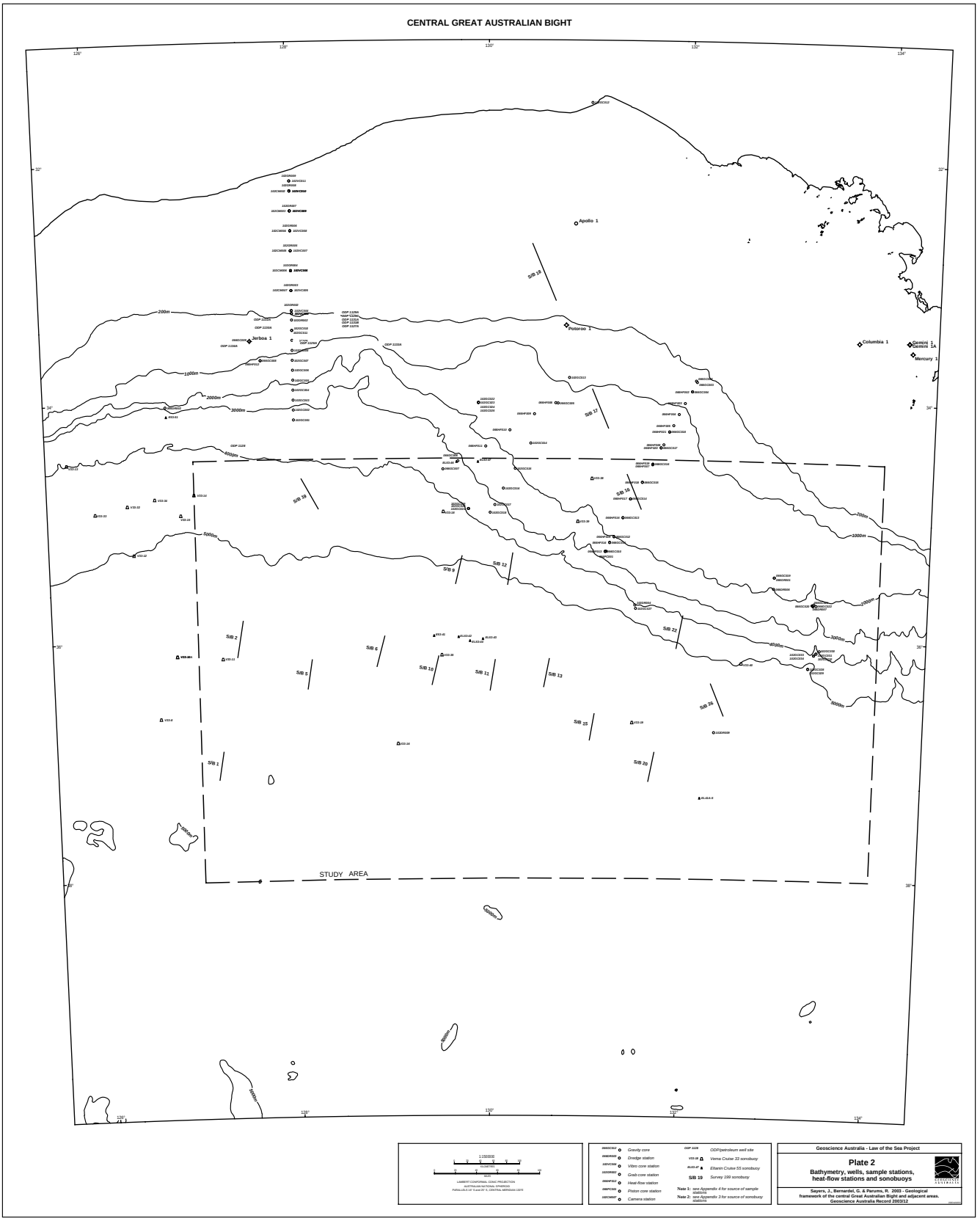

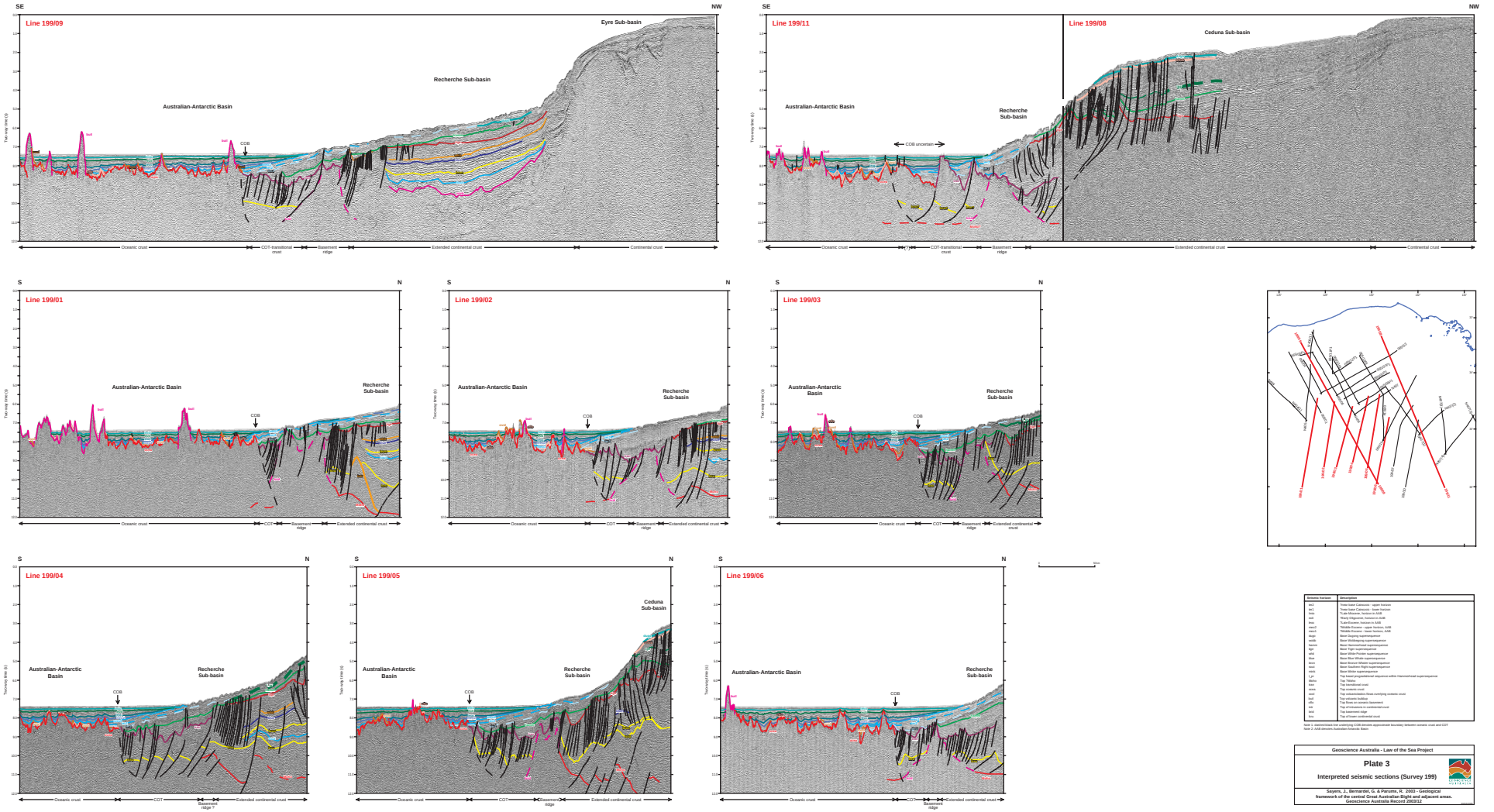


A high resolution A3 plot file of this figure suitable for large size □ plotters can be found in the Plot files sub-directory as .PS or .JPEG on □

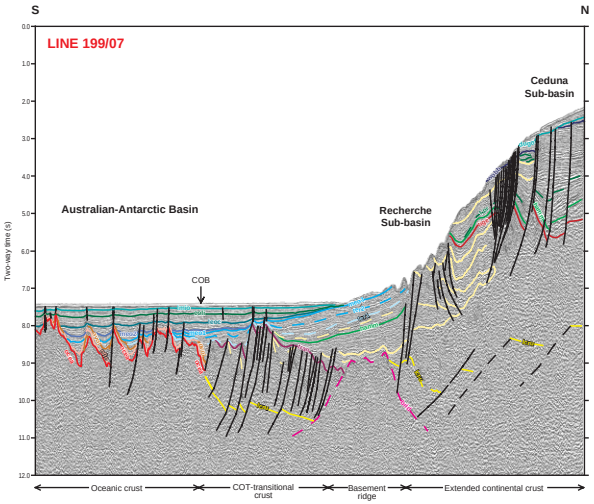


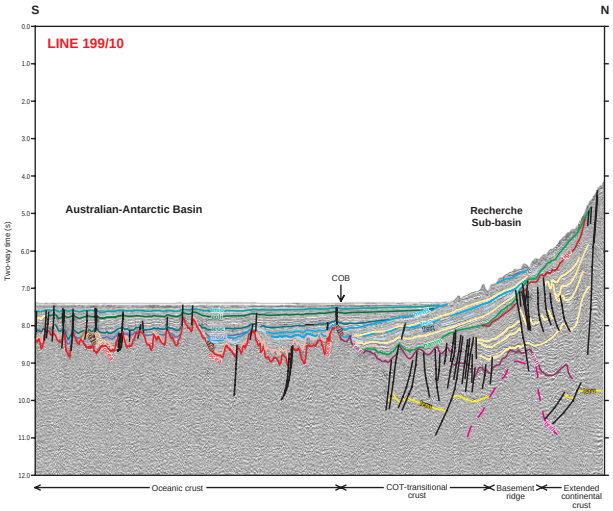


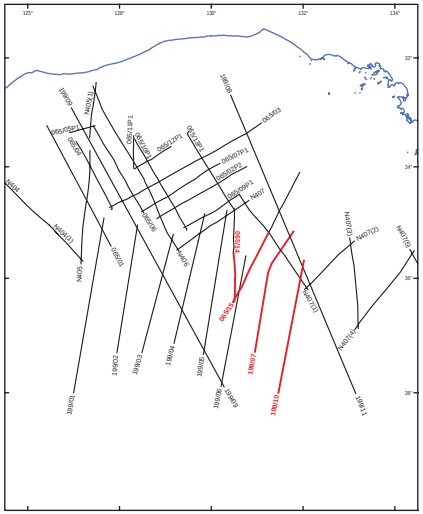


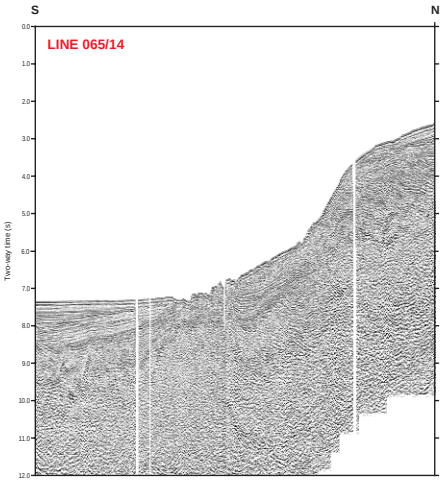


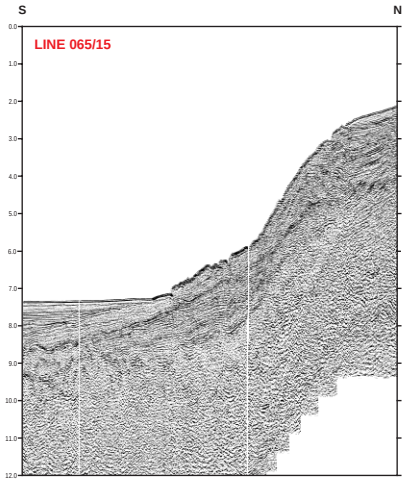


0 50km

| Seismic horizon | Description |
|---|---|
| ter2 | ?near base Cainozoic - upper horizon |
| ter1 | ?near base Cainozoic - lower horizon |
| lmio | ?Late Miocene, horizon in AAB |
| eoli | ?Early Oligocene, horizon in AAB |
| leoc | ?Late Eocene, horizon in AAB |
| meo2 | ?Middle Eocene - upper horizon, AAB |
| meo1 | ?Middle Eocene - lower horizon, AAB |
| dugo | Base Dugong supersequence |
| wobb | Base Wobbegong supersequence |
| hamm | Base Hammerhead supersequence |
| tige | Base Tiger supersequence |
| t_pr | Top basal progradational sequence within Hammerhead supersequence |
| tran | Top transitional crust |
| ocea | Top oceanic crust |
| ovol | Top volcaniclastic flows overlying oceanic crust |
| ofbs | Top flows on oceanic basement |
| brid | Top basement ridge |
| lcru | Top of lower continental crust |

Note 1: AAB denotes Australian-Antarctic Basin

Geoscience Australia - Law of the Sea Project

**Plate 4**

**Interpreted seismic sections (Survey 199).**
**Uninterpreted seismic sections (Survey 65)**

Sayers, J., Bernardel, G. & Parums, R. 2003 - Geological framework of the central Great Australian Bight and adjacent areas. Geoscience Australia Record 2003/12

A high resolution A3 plot file of this figure suitable for large size □ plotters can be found in the Plot files sub-directory as .PS or .JPEG on □

# ODP 1128

Area: Offshore Great Australian Bight

Latitude: 34°23.4563S

Longitude: 127°35.4554E

Water Depth: 3874.3 m

TD = 452.6 m

Datum: Sea Floor (sf)

GEOSCIENCE AUSTRALIA

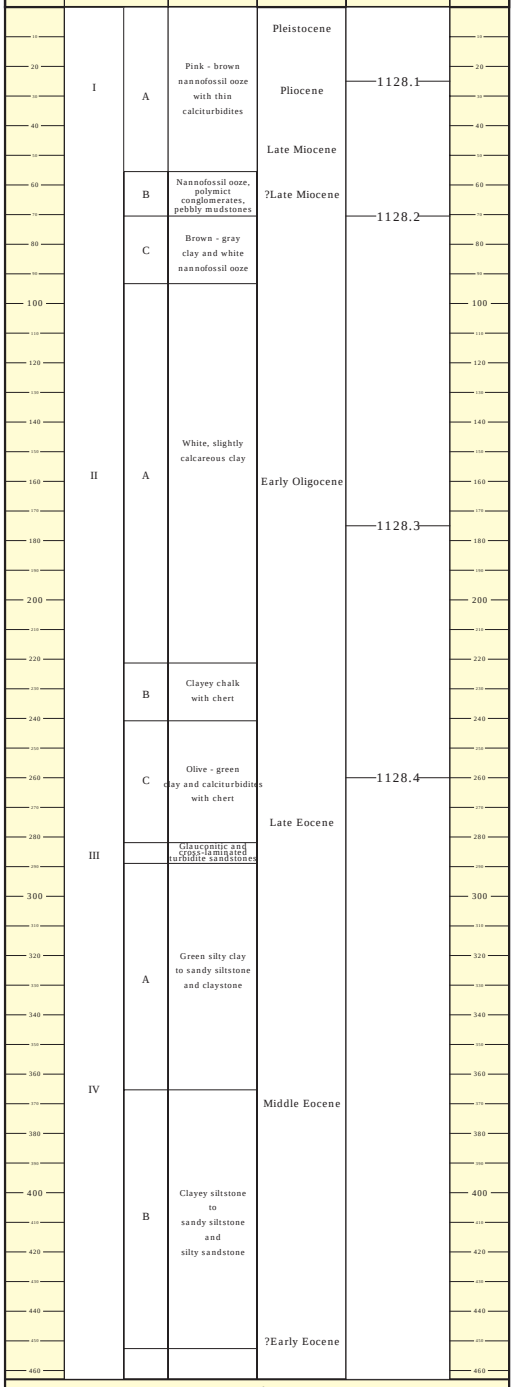


## Data Sources

Latitude, Longitude, Water Depth, Total Depth, Lithology, Lithology Unit and Age derived from Feary et al., 1999.



Well Composite produced by Peter Butler and Chris Lawson for the Law of the Sea Project. Date: 18-May-2000

**Geoscience Australia - Law of the Sea Project**

## Plate 5

**Generalised geology - ODP Site 1128**


**Sayers, J., Bernardel, G. & Parums, R. 2003 - Geological framework of the central Great Australian Bight and adjacent areas. Geoscience Australia Record 2003/12**


23DA1026

A high resolution A3 plot file of this figure suitable for large size plotters can be found in the Plot files sub-directory as .PS or .JPEG on this CD

**Instructions for the CD-ROM**

# Geological framework of the central Great Australian Bight and adjacent areas

**This CD-ROM contains the above-titled document as GeoscienceAustraliaRecord2003_12.pdf**

**To view this document on PC, install the Adobe Acrobat Reader v4.0 located in the Acrobat\Win_NT sub-directory on this CD, double click on the file Acrd4enu.exe and follow the installation prompts.**

**Once the reader is installed, go to the Record directory, double click on the GeoscienceAustraliaRecord2003_12.pdf to launch the document.**

**Please note:**
**Additional readers for Macintosh and Unix are also supplied on this CD**
**For Macintosh use, Acrobat\Macintosh\ar405eng.bin**
**For Unix use, Acrobat\Unix\sunsparc-rs-405.tar.gz**

**Directories on this CD**

**Acrobat directory:**
**Sub-directories of Adobe Acrobat Reader installation files for Win_NT, Macintosh, Unix and Help, which includes © Acrobat copyright, Adobe Acrobat Reader Guide and information on Adobe.**

**Plot files directory:**
**With sub-directories containing PostScript (.PS) and Joint Photographic Experts Group (.JPG) plot files of the A0, A1 and A3 plates used in this Record. These are all suitable for plotting to large format plotters.**

**Record directory:**
**GeoscienceAustraliaRecord2003_12.pdf**

If you have problems printing the pdf file, it may be that your Acrobat Driver is not the latest version. It may be necessary to install the updated Acrobat Driver from the Adobe Web site

Here is the link for the ADOBE Universal Postscript Windows Driver Installer 1.0.6 - English
<http://www.adobe.com/support/downloads/detail.jsp?ftpID=1500>

And for the Mac users ... the link for the Adobe PostScript printer driver 8.8 for Macintosh - English
<http://www.adobe.com/support/downloads/detail.jsp?ftpID=1494>